Numerical Modelling of Non-equilibrium Reactive Transport in Acid Mine Drainage

Thesis submitted to the
Indian Institute of Technology Guwahati
for the award of the degree
of

DOCTOR OF PHILOSOPHY

by
R.SOMESWARAN

Department of Civil Engineering
Indian Institute of Technology Guwahati
Guwahati – 781039, Assam, India

February 2019

Department of Civil Engineering
Indian Institute of Technology Guwahati
Assam-781039

CERTIFICATE

It is hereby certified that the work contained in this thesis entitled **"Numerical Modelling of Non-equilibrium Reactive Transport in Acid Mine Drainage"** submitted by **R. Someswaran** (Roll No. 09610411) for the award of the degree of Doctor of Philosophy, has been carried out in the Department of Civil Engineering, Indian Institute of Technology Guwahati under my supervision and this work has not been submitted elsewhere for the award of any other degree or diploma.

This thesis in my opinion, has reached the standard fulfilling the requirements for the award of the degree of Doctor of Philosophy in accordance with the regulations of the institute.

Dr. Suresh A. Kartha
Associate Professor
Department of Civil Engineering
IIT Guwahati, India-781039

ACKNOWLEDGEMENTS

I express my sincere thanks to my research supervisor **Dr. Suresh A. Kartha** for his valuable guidance towards the completion of my research work. His continuous support towards research had given me enough freedom to think, plan and execute my ideas towards my work, which has provided a good basis for the present thesis. I would like to thank him for spending his precious time for discussion by which i have gained knowledge in terms of research. Certain characters I observed and learned from my supervisor are; plan it and do it, routinely and wisely spending the time for work until getting the result, always documenting the work, way of approaching problem and identifying the problem base. I believe these attitude and characters will always remain with me throughout my life.

Besides my supervisor, I would like to thank my doctoral committee members, **Prof. Subashisa Dutta, Prof. Gautam Barua,** Department of Civil Engineering and **Prof. Anoop K. Dass,** Department of Mechanical Engineering, for their valuable time, suggestions and effort which made my thesis successful. I would like to thank **Prof. Sreedeep S., Dr. Tadikonda Venkata Bharat,** Department of Civil Engineering **and Dr. Vinayak Narayan Kulkarni,** Department of Mechanical Engineering for their presence and suggestions during my annual review presentations. I am also grateful to my present and former **HOD's** and **Staffs** of Department of Civil Engineering for providing me the necessary facilities. I would also like to extend my thanks to the thesis reviewers **Dr Brijesh Kumar Yadav,** Department of Hydrology, IIT Roorkee and **Prof. Graham Sander**, School of Architecture, Building and Civil Engineering, Loughborough University for their constructive and insightful comments. I would like to thank the Viva voce examiners **Dr Brijesh Kumar Yadav,** Department of Hydrology, IIT Roorkee, **Prof. Rajib Kumar Bhattacharjya, Dr Sreeja P.,** Department of Civil Engineering and **Dr Dipankar Narayan Basu,** Department of Mechanical Engineering for their comments and discussions.

I was fortunate enough to get excellent and close friends **Dr. S. Gowrisankar**, **Dr. V. Satheeshkumar, Dr. A. Muthuraja,** seniors **Dr. J. Anandkumar, Dr. Pranab Jyoti Barman** and junior **Debraj Biswas,** I express my sincere thanks for their friendly support and helping nature during my stay in IITG, also would like to thank Subsurface Hydrology lab mates for their friendly approach and support. As a human we evolve by learning from

our surroundings, in that way I would like to thank all my **seniors**, **juniors, friends** from whom I learnt technical and life lessons as well and also would like to thank **IITG mess workers, shopkeepers, cleaners and other people** who made my stay, inside the IITG campus as well as in Assam, comfortable. Finally, I express my gratitude and sincere thanks to my beloved **parents D. Ravi, R. Renuka,** and **younger brother R. Vinoth kumar** without their love and sacrifice it would not have been possible to me to made it to this level. And I express my thanks to my **sisters Samaya Pradeep, Subhasini Satheesh, brother in laws Mr. Pradeep, Mr. Satheesh, brothers Mr. Barath and Mr. Thulasitharan, cousin Mr. Karthikeyan and to relatives** for their love and affection. Last but not least I would like to pay my sincere thanks to **dearest friend Dr. G. Senthilmurugan, wife S. V. Narmatha** for showering their love, care, sacrifice and encouragement which have made it possible for me to come so for.

February, 2019 **R. Someswaran**

ABSTRACT

Acid Mine Drainage (AMD) or acid rock drainage is the effluent acidic water that drains from the mining sites (active and abandoned) to the surrounding environment. In most cases, acidic mine waters are formed due to oxidation of iron sulphides (FeS_2, known as pyrite) that are present along with the metal ores and coal seams. Pyrite oxidation reaction adds acidity to the surface water that leads to the dissolution of heavy metals and its consequent transport towards groundwater zone. Contaminants in groundwater can be analyzed by a field study, laboratory observations, and mathematical modeling. The main aim of this research is to study the transport processes of dissolved species of AMD through the variably saturated subsurface zone under physical non-equilibrium conditions by using a numerical model. Occurrence of physical non-equilibrium is due to the difference in flow velocities between the water in the pores and the water that is adsorbed on the solid particles (a small layer) or due to the water that becomes stagnant at the dead end pores. The velocity of mobile pore water is high with respect to the stagnant water (where velocity is negligible). The mass transfer between these two water regions retard the contaminant transport and the immobile water zones may act as sinks/sources of contaminants and it can cause non-ideal conditions in solute transport. This research conceptualizes the liquid zones in the porous subsurface medium to have mobile and immobile zones. Though many research works are available on the concepts on mobile and immobile liquid zones for contaminant transport, this research, in addition emphasizes the use of mass transfer of water as well as contaminants simultaneously between the mobile and immobile regions that are rarely studied.

The conventional computational models of earlier years on solute transport use the simple advection diffusion equation to simulate the contaminant movement in subsurface. However, the presence of complexities in fluid flow as well as mass transfer due to the velocity differences and existence of dead end pores in the subsurface medium affect the simulated results from the advection diffusion equation. The study of non-equilibrium transport has importance in remediating the contaminated region by taking in to account the non-equilibrium concept in simulations for predictions. To study the AMD (ferrous ion) transport near to the field reality, mathematical models are useful tools. FEMWATER is an open source code available in the USGS website and is chosen for the modeling in this research. The FEMWATER model, developed by Yeh (1990) and upgraded by Robert Strobl for USEPA, is a 3D finite element, saturated/unsaturated, flow and transport model.

FEMWATER code contains two separate modules; one for flow called 3DFEMWATER; and another for solute transport called 3DLEWASTE.The flow module 3DFEMWATER was modified to accommodate liquid mass transfer between the mobile and immobile regions and the transport module, 3DLEWASTE was modified to handle the non-equilibrium solute mass transport. Two approaches of physical non-equilibrium transport were followed, i) Single porosity Flow and Non-Equilibrium Transport (SFNET) simulation (first type non-equilibrium), and ii) Dual porosity Flow and Non-Equilibrium Transport simulation (DFNET) (second type non-equilibrium). Transport processes due to ion exchange reaction is newly added to the source code of the model. The ion exchange module is able to handle multi-components, however, without any interactions between the components. Following the modification of the FEMWATER model and its validation with simple cases, a parameter analysis study was done and then FEMWATER was applied to a hypothetical domain to study the impact of physical non-equilibrium on the AMD (ferrous ion) reactive transport. Models were applied to study conservative and reactive solute transport properties in homogeneous and heterogeneous medium along with a set of assumptions like constant inflow of water, constant temperature at 25^0C, neutral pH, domain is free of contaminants at initial time, single specie transport and equilibrium reaction taking place only in mobile water region

Difference in contaminant (ferrous ion) spreading patterns are observed between the advection-dispersion model and physical non-equilibrium models, which is evident from the advancement of the solute front in the direction of water flow. A difference in contaminant spreading pattern is also observed between first and second type non-equilibrium models. In c*onventional physical non-equilibrium transport models (first type non-equilibrium),* the water content value is split between mobile and immobile water contents. Second type non-equilibrium model, where time dependent water transfer can be considered, simulates natural mass transfer process unlike the first type model, which properly could not capture the velocity details of mobile-immobile flow. Little difference is observed in the contaminant spreading pattern between homogeneous and heterogeneous domain simulations, especially for the contaminant in the immobile water zone. Though sorption and ion-exchange reactions limit the contaminant transport in subsurface region, mobile-immobile flow advances the solute front. In the case of reactive transport, compared to sorption, the ion-exchange reaction is less affected by the non-equilibrium process and in case of conservative solute simulation; transport is much affected by non-equilibrium process. There are mainly two parameters i) f -

mobile water content to total water content ratio and ii) Γ - mass transfer rate constant, which affects the contaminant transport properties, and especially a high immobile water content causes a quick arrival of solute front at the downstream boundary.

TABLE OF CONTENTS

LIST OF FIGURES

LIST OF TABLES

LIST OF SYMBOLS

SYMBOL	DESCRIPTION	DIMENSION
H	Pressure head	L
h_i	Pressure head at i^{th} nodal point	L
h_a	Air entry pressure head	L
$F(h)$	Water storage capacity	L^{-1}
$K(h)$	Unsaturated hydraulic conductivity	LT^{-1}
K_s	Saturated hydraulic conductivity	LT^{-1}
k_r	Relative permeability	--
k_a	Acid catalysed rate constant	T^{-1}
k_b	Base catalysed rate constant	T^{-1}
k_n	Neutral rate constant	T^{-1}
$k_d(=dS/dC)$	Distribution coefficient	L^3M^{-1}
K_{ex}	Equilibrium coefficient	--
Q	Source/sink	$L^3T^{-1}L^{-3}$
Q	Water source/sink rate	MT^{-1}
V	Darcy flux	LT^{-1}
V_x, V_y, V_z	Components of Darcy flux	LT^{-1}
$\|V\|$	Magnitude of Darcy flux	
Z	Distance above datum	L
θ_S	Saturated water content	$L^3\ L^{-3}$
θ_r	Residual water content	$L^3\ L^{-3}$
θ_e	Effective moisture content	$L^3\ L^{-3}$
θ_m, θ_{im}	Mobile, immobile water content	L^3L^{-3}
$\varphi\ (=\theta_{fm}/\theta)$	Ratio of mobile water content to total water content	--
$S_{e(m)}$	Effective saturation of mobile water content	--
$S_{e(im)}$	Effective saturation of immobile water content	--
α, n_1, m $(m=1-1/n_1)$	Van Genuchten empirical parameters	L^{-1}, --, --
n_2	slope of the plot of log S vs. log C	--

C	Dissolved contaminant concentration	M L^{-3}
C_m	Dissolved contaminant concentration in mobile water	ML^{-3}
C_{im}	Dissolved contaminant concentration in immobile water	ML^{-3}
C_{in}	Concentration along with inflow	M/L^{-3}
C_{tot}	Total solution concentration	M/L^{-3}
S or $\bar{C}$	Sorbed phase concentration	MM^{-1}
S_{max}	Maximum concentration allowed in the medium	MM^{-1}
$\boldsymbol{D}$	Hydrodynamic dispersion coefficient tensor	L^2T^{-1}
D_m	Molecular diffusion coefficient	L^2T^{-1}
ρ_b	Bulk density	ML^{-3}
Λ	Material decay constant	T^{-1}
λ_1	First order hydrolysis rate constant for dissolved species	T^{-1}
λ_2	First order hydrolysis rate constant for sorbed species	T^{-1}
λ_b	First order biodegradation rate constant	T^{-1}
α_l, α_t	Longitudinal, transverse dispersivity	L
Γ_w	Water mass transfer rate constant	T^{-1}
Γ_c	Contaminant mass transfer rate constant	T^{-1}
β	Acid-catalyst hydrolysis rate enhancement factor for the sorbed phase with a typical value of 10	--
f	Fraction of sorption site contact with mobile water	--
$1-f$	Fraction of sorption site contact with immobile water	--
δ	Kroneckar delta tensor	--
τ	Tortuosity	--
$\hat{n}$	Outward vector normal to the boundary	--
$\hat{\theta},\hat{h},\hat{c}$	Approximate solutions of unknown variables (θ, h, c) in partial differential equations	--
$[H^+]$	Hydrogen ion concentration	Mole/L
$[OH^-]$	Hydroxyl ion concentration.	Mole/L
N_i, N_j	Shape functions	--
N^e	Shape function of an element	--
W_i	Weight function	--

R	Problem domain/Region	--
B	Region boundary	--
L_i, R_i	Load vectors	--
$(\,)_j^{n+1,m+1}$	Variable value (water content, pressure head or concentration) at current time step (n+1) and current iteration level (m+1) at the j^{th} nodal point	--
$(\,)_j^{n,m}$	Variable value (water content, pressure head or concentration) at previous time step (n) and previous iteration level (m) at the j^{th} nodal point	--
ξ, μ, ς	Local coordinates to define shape function	--
A_{ij}, a_{ij}, B_{ij}	Short form of element matrix	--
L_i, R_i	Short form of load vector	--
Δt	Time step value in numerical simulation	T
x, y, z	Used to define directions in three dimensional space	--
Δx, Δy, Δz	Spatial discretization along the x, y, z directions	L,L,L

LIST OF ABBREVIATIONS

1D, 2D, 3D	-	One dimensional, two dimensional, three dimensional
ADE	-	Advection Diffusion Equation
AMD	-	Acid Mine Drainage
ARD	-	Acid Rock Drainage
ASTM	-	American Society for Testing and Materials
BTC	-	Breakthrough Curve
CEC	-	Cation Exchange Capacity
DFNET	-	Dual porosity Flow with Non-Equilibrium Transport (Second type non-equilibrium)
FEM	-	Finite Element Method
FEMWATER	-	Finite Element Model for WATER flow
GMS	-	Groundwater Modelling System
HESFET	-	Heterogeneous medium and Single Porosity Flow, Equilibrium Transport model
HESFNET	-	Heterogeneous medium and Single Porosity Flow, Non-Equilibrium Transport model
HEDFNET	-	Heterogeneous medium and Dual Porosity Flow, Non-Equilibrium Transport model
HOSFET	-	Homogeneous medium and Single Porosity Flow, Equilibrium Transport model
HOSFNET	-	Homogeneous medium and Single Porosity Flow, Non-Equilibrium Transport model
HODFNET	-	Homogeneous medium and Dual Porosity Flow, Non-Equilibrium Transport model
IE-HESFET	-	Ion-Exchange in Heterogeneous medium with Single Porosity Flow, Equilibrium Transport model
IE-HESFNET	-	Ion-Exchange in Heterogeneous medium with Single Porosity Flow, Non-Equilibrium Transport model
IE-HEDFNET	-	Ion-Exchange in Heterogeneous medium with Dual Porosity Flow, Non-Equilibrium Transport model
IE-HOSFET	-	Ion-Exchange in Homogeneous medium with Single Porosity Flow,

		Equilibrium Transport model
IE-HOSFNET	-	Ion-Exchange in Homogeneous medium with Single Porosity Flow, Non-Equilibrium Transport model
IE-HODFNET	-	Ion-Exchange in Homogeneous medium with Dual Porosity Flow, Non-Equilibrium Transport model
LEWASTE	-	Lagrangian Eulerian WASTE transport model
MIM	-	Mobile Immobile water flow
MC	-	Concentration in mobile water content (In 2D plot)
IMC	-	Concentration in immobile water content (In 2D plot)
SWCC	-	Soil Water Characteristic Curve
SR-HOSFET	-	Sorption in Homogeneous medium with Single Porosity Flow, Equilibrium Transport model
SR-HOSFNET	-	Sorption in Homogeneous medium with Single Porosity Flow, Non-Equilibrium Transport model
SR-HODFNET	-	Sorption in Homogeneous medium with Dual Porosity Flow, Non-Equilibrium Transport model
SFNET	-	Single porosity Flow with Non-Equilibrium Transport (First type non-equilibrium)
USEPA	-	United States Environmental Protection Agency
USGS	-	United States Geological Survey

CHAPTER 1

INTRODUCTION

This chapter begins with general introduction followed by an introductory discussion on Acid Mine Drainage (AMD), contaminant distribution, physical non-equilibrium concept, and FEMWATER model. An objective of this thesis work is given and it is followed by the organization of the thesis.

1.1 General

About three-fourths of the earth surface is covered with water and it makes up to 60-95 percent of weight of any living organisms. As such, water is the most essential part of life that should be handled with utmost care. Water exists in all the three states; vapour (gaseous), liquid, and solid, in abundant form and is vulnerable to pollution in all three states. In addition, water is the most exploited and polluted among all other natural resources. Polluted water contains unwanted external ingredients, which is harmful when it is consumed and it may alter the physical, chemical, and biological characteristics of pure water. Scientists have described water standards for potable and domestic use, which are the basis for describing polluted water. Water gets polluted due to the human activities like mining, constructions, industrialization, dying, agricultural inputs, chemical and leather wastes, municipal sewage, landfills, etc. and natural processes like geochemical reactions, erosion, volcanic activities, etc.

The state and distribution of contaminants in groundwater can be analysed by field studies, laboratory observations, and mathematical modeling. Field study and geophysical methods are used to measure, collect data and observe quality of water resources in the study area. Laboratory methods including batch and column studies are used to analyse the samples collected from the field and to determine various transport and reaction coefficients and parameters. Collected and derived data are then used to predict the flow and transport trends by mathematical models. As per the American Society for Testing and Materials (ASTM D5447-04, 2010), a mathematical model is defined as “mathematical equations with assumptions expressing the physical system and deduce the system behavior with known accuracy”. Mathematical models are very powerful tools that aid in understanding the complex processes and can predict responses for different input conditions. The computational simulations provide more sophisticated results of the contaminant migration that can be applied to field problems. Apart from field scale and laboratory modelling studies, mathematical models are useful to interpret the extent of any contamination spread as well as to plan and design containment and remediation measures to the already contaminated subsurface water body. That is, the inferences from simulated results can aid in better management or containment of the pollution. In addition, the mathematical models can simulate highly complex scenarios of contamination in less cost and time. Acid Mine Drainage

(AMD) is one of the common polluting phenomena of subsurface groundwater. The actual or field conditions of acid mine drainage contaminant problems are vast and highly complex and rarely a numerical or computational model will be able to incorporate all the field conditions in its complete form, while performing the simulation. Hence, the success of numerical models on contaminant transport related to AMD involves incorporating different acceptable features and various mass transfer phenomena to simulate more or less the field situation.

Nevertheless, the acceptability of a computational model lies in its capability to handle various complexities. The governing mathematical equations that can mimic the various phenomena involved in contaminant transport and migration can be formulated using the fundamental principles in continuum mechanics (Bear 1988; Reddy 2008). The subsurface soil environment can be treated as porous continuum consisting of pores and solids. The pores may be filled with water and air and the governing partial differential equations for the movement of water (fluids) through the pores are developed using conservation of mass and momentum principles (Bear 1988). Similarly, the mass transfer of contaminant species through the pores in the subsurface media can be mimicked using partial differential equations developed from principle of conservation of mass. These partial differential equations for fluid flow and contaminant specie mass can be solved using analytical or numerical techniques. Most of the computational models on contaminant transport use the simple advection diffusion equation to simulate the contaminant movement in subsurface.

However, the presence of complexities in fluid flow as well as mass transfer due to the velocity differences and existence of dead end pores in the subsurface affect the simulated results from simple advective-dispersive transport models. Inclusion of these complexities in to transport model may potentially provide more accuracy to the simulation outputs on acid mine drainage through subsurface porous media. Consequently, this research focuses to include the physical non-equilibrium concept into the solute transport of AMD through subsurface. The governing equation for contaminant transport used in the US-EPA developed finite-element model FEMWATER is modified to accommodate for physical non-equilibrium fluid flow and contaminant transport. Thereafter, the freely available source code of FEMWATER is amended to incorporate the mass transfer of water and solute in multiple

zones of liquid as well as reactive transport of solute to simulate the AMD in the subsurface environment.

1.2 Acid Mine Drainage (AMD)

AMD or acid rock drainage (ARD) is the drainage water resulting from natural oxidation of sulphide minerals occurring in mine rocks that are exposed to air and moisture (Bell et al., 2006). Acid generation is also called as ARD in some of the literatures; ARD refers to mine related low-pH drainage water. Not all of the coal or metal mines produce acid drainage, as well as all acidic drainages are not produced by mines for example infrastructure development, agricultural practice, natural oxidation of acid sulphate soils and acid rain are other sources which produce water with acidic nature (Jacob et al. 2014).

Source and reason of AMD generation: AMD generation is a natural process, however, it is induced by mining activities and can produce a large volume of contaminated effluents. AMD arises from the oxidation reaction when sulfide minerals are exposed to the atmosphere by mining excavation processes, which leads to the release of hydrogen-ions, sulfate ions and soluble metal ions and the generation of acidity. Road cuts, quarries or other rock excavations can also expose sulphide minerals to the atmosphere, thereby prompting acid drainage. Despite that, the primary sources of AMD are usually metal mines, because economically recoverable metals occur as ore bodies of concentrated metal sulfides such as iron pyrite (FeS_2), copper chalcopyrite ($CuFeS_2$), and zinc Sphalerite (ZnS) (Salomons 1988). AMD may emerge from underground mines, as runoff from open pit mines, as effluent/leachate from waste/burden rock dumps and ore stockpiles, mill tailings (Marcus 1997). AMD is also generated when acid sulfate soils contain elevated iron sulfides, especially pyrite, that are exposed to oxygen. Sulfuric acid is generated due to the oxidation reaction and it can be carried away by rainfall or by high water table into nearby water bodies, killing aquatic organisms and vegetation (Jacob et al. 2014).

Characteristics of AMD: Acid mine drainage is characterized by high TDS, low pH, and elevated concentrations of iron, sulfate and other metals (Marcus 1997). Highly mineralized mine waters generally contain sodium and potassium in high concentrations, and mine waters that do not contain sulphate may have strontium and barium in high levels. Generally, mine

water is considered as ferruginous (contains iron in two oxidation states; ferrous and ferric ion), however, metals and pollution free mine water also drains out in some places that can be used as potable water. The low pH mine waters are commonly associated with highly ferruginous discharges. Iron in mine water, draining from coal mines, may have a more stable ferrous form, however, the ferrous form may oxidize in the presence of oxygen to form ferric ion. These ferric species form an orange precipitate termed ochre, which is seen as coating in stream beds (Bell et al. 2006). The acidic drainages are frequently enriched with Fe, Mn, Al, Cu, Zn, Cd, Pb, and As and the SO_4 anion (Jacob et al. 2014). The ability of water to leach metals from solid material primarily depends upon the pH of the solution. Lower pH affects the leaching potential by increasing the solubility of metals in carbonate, hydroxide, oxide, and silicate minerals. Concentrations of heavy metals may be high in some acid waters and may be toxic (Bell et al. 2006).

AMD and water body interaction: The primary means by which surface water is impacted from mine operations and mine wastes include: (i) discharge or overflow of wastewater, (ii) runoff due to rainfall or snow melt, (iii) drainage from the toe of waste piles, and (iv) discharge of impacted ground water to streams and springs. Metals and other constituents from mine wastes may be transported in surface water as dissolved or as suspended material (Marcus 1997).

1.3 Physical non-equilibrium

The advection-dispersion equation is one of the basic mathematical form to model the movement of contaminants in the subsurface zone. However, the use of this equation is limited to simple cases involving non-reactive and equilibrium mass transfer between the solute in the liquid state and the solute in the solid state. Some cases like non-equilibrium in mass transfer between the contaminant solute present in liquid and solid and that behave separately in different regions have to be modelled using different equations. The non-equilibrium in mass transfers may be due to physical and/or chemical influences. Occurrence of physical non-equilibrium is due to the difference in flow velocities between the water in the pores and the water that is adsorbed on the solid particles (a small layer) or due to the water that becomes stagnant at the dead end pores (Figure 1.1). The velocity of mobile pore water is high with respect to the stagnant water (where velocity is negligible). The mass transfer between these

two water regions retard the contaminant transport and the immobile water zones may act as sinks/sources of contaminants (Coats et al. 1964). Gaudet et al. (1977) and Van Genuchten and Wierenga (1977) gave experimental evidence of effects of physical non-equilibrium phenomenon on solute movement through unsaturated media. De Smedt (1981) reports the evidence of physical non-equilibrium in solute transport in unsaturated glass beads and sandy medium even when the overall flow is steady. Some laboratory experiments showed the appearance of early break through curves (BTC) in solute transport observation due to the presence of physical non-equilibrium (van Genuchten et al. 1977, Selim et al.1987, Bond et al. 1990). Non-equilibrium transport exists when the mass-transfer times are longer than system hydraulic residence times and/or the solid surface-mediated reactions are faster than the normal advective-dispersive solute mass-transfer process (Hatfield et al. 1996). By taking into account non-equilibrium concepts during the prediction of contaminant flow, the underestimation of contaminant concentration during the later stages of flow can be averted. Physical non-equilibrium processes (due to media heterogeneity, preferential flow, rate-limited diffusion, etc.) and chemical non-equilibrium processes (due to rate-limited sorption, ion exchange, and hysteretic sorption, etc.) can cause non-ideal conditions in solute transport. Therefore, the study of effects of mass transfer between mobile and immobile regions on reactive transport will give more insight in to the transport process in the field.

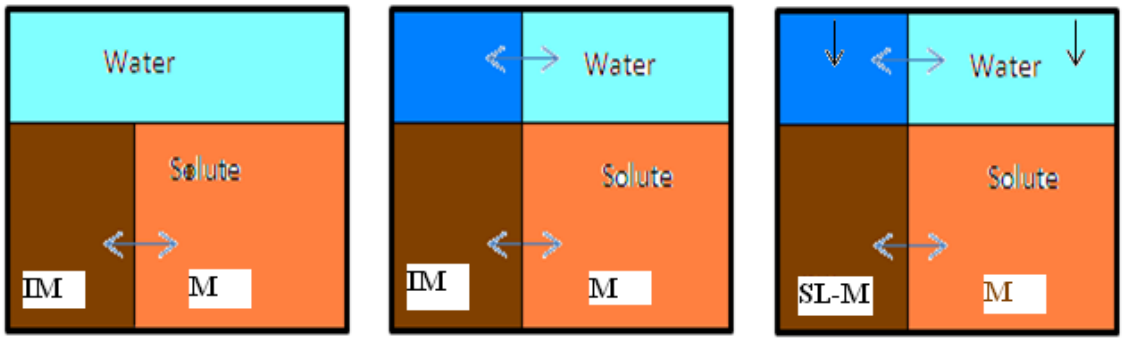

(a) (b) (c)

Fig. 1.1 Representation of different types of physical non-equilibrium (a) single porosity flow and non-equilibrium transport (first type) (b) mobile-immobile water flow and non-equilibrium transport (second type) and (c) slow moving and fast moving water flow and non-equilibrium transport. (Single sided arrow denotes flow direction; double sided arrow denotes exchange of water and solutes between two zones, IM-immobile, M-mobile, SL-M-slow moving)

Pyrite oxidation reaction adds acidity to the surface water that leads to the dissolution of heavy metals and its transport towards groundwater zone. One mole of pyrite oxidation produces two moles of positively charged hydrogen ions which increases acidity. Oxygen and ferrous ion are the main agents involved in the pyrite oxidation reaction. AMD contains ions, metals and salts as contaminants, out of which, the ferrous ion (Fe^{2+}) is soluble in the neutral pH conditions in water. In addition to oxygen, ferrous ion participates in an oxidation reaction and produces hydrogen ions that lead to the acidification of water. Therefore, the study of ferrous ion transport and its chemistry is necessary for further studies of mine water remediation and treatment. The mathematical models come in handy to study the transport nature of ferrous ion as the field studies are cumbersome, expensive and time consuming. Field conditions include aggregate soils, unsaturated zones and regions with dual porosity, dual permeability nature and fracture rock regions that may alter the transport and reactive properties. To study AMD transport in such varied site conditions, the mathematical model has to be elaborate to predict near accurate, close to ground results. The incorporation of non-equilibrium mass transfer for liquid flow as well as solute transport can address some of the heterogeneous situations of the field. That is, the ferrous ion transport with non-equilibrium study represents field conditions with more reliability.

1.4 Introduction to FEMWATER

Mathematical models are important to study the solute transport processes in the subsurface. In 1980's with the act of safe drinking water, United States Environmental Protection Agency (USEPA) has funded many projects with the aim of wellhead protection (Yeh et al. 1992). USEPA has developed many models and programs to design and implement the wellhead protection. FEMWATER is one such program and it comes under an open source code category. The FEMWATER model, developed by Yeh (1990) and upgraded by Robert Strobl for USEPA, is a 3D finite element, saturated/unsaturated, flow and transport model. FEMWATER code contains two separate modules; one for flow called 3DFEMWATER; and another for solute transport called 3DLEWASTE (3DFEMWATER, 1992). The computer code for FEMWATER is written in FORTRAN-77 language. Finite-element method is used to solve the governing partial differential equations of variably-saturated flow and solute transport. A user can use any of the two modules either separately or combined. The flow

module can simulate the unsaturated and saturated flow through subsurface. The computer code gives the pressure head, the total head and the velocity at the nodal points, and water content of an element (which is the integrated value of the nodal points of an element). The transport module 3DLEWASTE simulates leachate migration by evaluating the temporal and spatial values of concentrations of the contaminants with appropriate mass transfers due to advection, hydrodynamic dispersion, adsorption and decay.

1.4.1 3DFEMWATER – A Flow module

3DFEMWATER (**3 D**imensional **F**inite **E**lement **M**odel of **WATER** flow through saturated-unsaturated media) solves the pressure head (h) based Richards equation to represent the moisture flow in unsaturated/saturated zone. The governing equation for flow of water through a variably saturated porous medium, as derived from mass and momentum conservation principles can be written in partial differential form (Yeh et al. 1992)

$$F(h)\frac{\partial h}{\partial t} = \vec{\nabla}\cdot\left[K(h)\left(\vec{\nabla}h + \vec{\nabla}z\right)\right] + q \tag{1.1}$$

where, h is pressure head [L]; z is distance above datum [L]; q is source or sink term [T^{-1}]; $K(h)$ is unsaturated actual hydraulic conductivity [LT^{-1}]; and $F(h)$ is water storage capacity [L^{-1}]. The equation (1.1) is a 3-dimensional, non-linear (K and F are functions of the unknown variable 'h'), second order, partial differential equation also known as the strong form representation. The Galerkin Finite-Element Method is adopted to solve the above partial differential equation (1.1). The weak form or the integral form of equation (1.1) is obtained by substituting the trial function in the Galerkin Finite Element approximation and integration by parts. Solving this weak form equation is easy through numerical methods and for applying the boundary conditions is quite simple compared to the strong form, equation (1.1). The weak form is given in equation (1.2) (Yeh et al. 1992).

$$\int F(h)N_i\frac{\partial N_j h_j}{\partial t}dR + \int K(h)\left(\nabla N_i\right)\left(h_j\nabla N_j + \nabla Z\right)dR - \int N_i\cdot\hat{n}\cdot K(h)\left(h_j\nabla N_j + \nabla Z\right)dB - \int N_i q dR = 0 \tag{1.2}$$

where, N_i is weight function, N_j is shape function, and h_j is pressure head at nodal points. Non-linear nature of hydraulic conductivity and storage term varies this equation from the saturated flow equation. The following term describes the influence of water content on the magnitude of the saturated hydraulic conductivity, K_s.

$$K(h) = k_r K_s \tag{1.3}$$

where, k_r is relative permeability [-], ranging from 0 to 1, and K_s is the saturated hydraulic conductivity [LT^{-1}]. The FEMWATER code uses the Van Genuchten (1980) equations to relate hydraulic conductivity and water content, while solving the flow equation (1.1).

$$K(h) = K_s \left(\theta_e^{0.5} \left[1 - \left(1 - \theta_e^{(1/m)} \right)^m \right]^2 \right) \quad \text{for } h < h_a \tag{1.4a}$$

$$K(h) = K_s \quad \text{for } h \geq h_a \tag{1.4b}$$

$$\theta_e = \left[1 + \left(\alpha \left| h - h_a \right| \right)^{n_1} \right]^{-m} \quad \text{for } h < h_a \tag{1.5a}$$

$$\theta_e = 1 \quad \text{for } h \geq h_a \tag{1.5b}$$

$$\theta_e = \frac{\theta(h) - \theta_r}{\theta_s - \theta_r} \tag{1.6}$$

where, α is soil specific coefficient [L^{-1}]; θ_e is effective moisture content [-]; and m and n_1 are Van Genuchten parameters. Besides providing a frame of reference for transient analyses, the initial conditions are used to set the nonlinear parameters at the beginning of simulation. Initial and boundary conditions that are being used in FEMWATER along with governing and constitutive equations to solve the Richards equation are (Yeh et al. 1992)

Initial condition: $h = h_i(x, y, z, t = 0)$ (1.7)

Dirichlet Boundary: $h = h_d(x, y, z, t)$ (1.8)

Specified flux Boundary:

$$-\hat{n} \cdot k_r K_s \left(\vec{\nabla} h + \vec{\nabla} Z \right) = q_c(x, y, z, t) \tag{1.9}$$

Specified pressure head (Neumann) Boundary:

$$-\hat{n} \cdot k_r K_s \left(\vec{\nabla} h \right) = q_n(x, y, z, t) \tag{1.10}$$

Variable composite (Combined Dirichlet/specified flux) Boundary:

$$h = h_d(x, y, z, t) \tag{1.11a}$$

(or)

$$-\hat{n}\cdot k_r K_s\left(\vec{\nabla}h+\vec{\nabla}Z\right)=q_c\left(x,y,z,t\right) \tag{1.11b}$$

where, $\hat{n}$ represents the unit outward vector normal to the boundary; h_i is the initial pressure head distribution [L]; h_d is specified pressure head [L]; q_c is the specified flux rate [LT^{-1}]; q_n is the portion of the boundary flux attributable to the pressure head gradient [LT^{-1}].

1.4.2 3DLEWASTE – A Transport module

The governing equation for advective-dispersion solute transport through variably saturated porous media based on the laws of conservation of mass and flux can be written as (Yeh et al. 1992)

$$\theta\frac{\partial C}{\partial t}+\rho_b\frac{\partial S}{\partial t}=\vec{\nabla}\cdot\left(\theta\mathbf{D}\vec{\nabla}C\right)-V\vec{\nabla}C-\lambda\left(\theta C+\rho_b S\right)+QC_{in}-QC \tag{1.12}$$

where, θ is volumetric moisture content [L^3L^{-3}]; $\boldsymbol{\rho_b}$ is bulk density of the porous medium [ML^{-3}]; C is the concentration of the dissolved specie [ML^{-3}]; S is the concentration of the adsorbed phase specie [MM^{-1}]; V is the Darcy velocity [LT^{-1}]; $\boldsymbol{D}$ is the hydrodynamic dispersion coefficient [L^2T^{-1}]; λ is material decay constant [T^{-1}]; Q is the water source/sink rate [MT^{-1}]; C_{in} is the dissolved specie concentration of the source fluid [ML^{-3}]. To solve the three dimensional, second order, partial differential equation (1.12), 3DLEWASTE software uses the following initial and boundary conditions (Yeh et al.1992).

Initial condition: $C=C_i\left(x,y,z,t=0\right)$ (1.13)

Dirichlet Boundary: $C=C_d\left(x,y,z,t\right)$ (1.14)

Specified flux Boundary:

$$\hat{n}\cdot\left(\vec{V}C-\theta\boldsymbol{D}\vec{\nabla}C\right)=q^c\left(x,y,z,t\right) \tag{1.15}$$

Specified dispersive flux (Neumann) Boundary:

$$\hat{n}\cdot\left(-\theta\boldsymbol{D}\vec{\nabla}C\right)=q^n\left(x,y,z,t\right) \tag{1.16}$$

Variable composite (Combined Dirichlet/specified flux) Boundary:

$$\hat{n}\cdot\left(-\theta\boldsymbol{D}\vec{\nabla}C\right)=0 \quad \text{on boundary if} \quad \hat{n}\cdot\vec{V}>0 \tag{1.17}$$

or

$$\hat{n}\cdot\left(\vec{V}C-\theta\boldsymbol{D}\vec{\nabla}C\right)=\hat{n}\cdot\vec{V}C_v\left(x,y,z,t\right) \quad \text{on boundary if} \quad \hat{n}\cdot\vec{V}\le 0 \tag{1.18}$$

where, C_i is the initial concentration distribution [ML^{-3}]; C_d is the specified solute concentration distribution [ML^{-3}]; q^c is the specified flux rate [$MT^{-1}L^{-2}$]; q^n is the portion of the boundary flux attributable to the concentration [$MT^{-1}L^{-2}$]; $\hat{n}\cdot\vec{V}$ is the Darcy velocity normal to the boundary; C_v is the concentration of dissolved species in the water entering at the boundary [ML^{-3}].

Dispersion coefficient tensor (*D*) defines the spreading of contaminants dissolved in water that is advected through the pore space. The hydrodynamic dispersion consists of mechanical dispersion and molecular diffusion; it is defined as (Yeh et al. 1992)

$$\theta \boldsymbol{D} = \alpha_T |V| \delta + \frac{(\alpha_L - \alpha_T) VV}{|V|} + \theta D_m \tau \delta \tag{1.19}$$

where α_T is transverse dispersivity [L]; α_L is longitudinal dispersivity [L]; $|V| = \sqrt{(V_x^2+V_y^2+V_z^2)}$ is magnitude of the Darcy velocity [LT^{-1}], D_m is molecular diffusion coefficient [L^2T^{-1}], δ is Kroneckar delta tensor, τ is tortuosity coefficient [-]. Components of the tensor are given as

$$\theta D_{xx} = \alpha_T |V| + \frac{(\alpha_L - \alpha_T) V_x V_x}{|V|} + \theta D_m \tau \tag{1.20}$$

$$\theta D_{zz} = \alpha_T |V| + \frac{(\alpha_L - \alpha_T) V_z V_z}{|V|} + \theta D_m \tau \tag{1.21}$$

$$\theta D_{yy} = \alpha_T |V| + \frac{(\alpha_L - \alpha_T) V_y V_y}{|V|} + \theta D_m \tau \tag{1.22}$$

$$\theta D_{xz} = \theta D_{zx} = \frac{(\alpha_L - \alpha_T) V_x V_z}{|V|} \tag{1.23}$$

$$\theta D_{xy} = \theta D_{yx} = \frac{(\alpha_L - \alpha_T) V_x V_y}{|V|} \tag{1.24}$$

$$\theta D_{yz} = \theta D_{zy} = \frac{(\alpha_L - \alpha_T) V_y V_z}{|V|} \tag{1.25}$$

Dispersivity parameters quantify the magnitude of longitudinal and lateral spreading of the dissolved species in the porous media. Dispersion is a function of various scales and

consideration of the distance the species travels should be taken in to account for the appropriate value of dispersivity. Molecular diffusion coefficient (D_m) quantifies the spreading due to molecular diffusion, which occurs due to concentration gradient. There are three choices for relating dissolved and adsorbed phase concentration in 3DLEWASTE.

Linear isotherm:

$$\frac{dS}{dC} = k_d \tag{1.26}$$

where k_d is the distribution coefficient [$M^{-1}L^3$].

Freundlich isotherm:

$$S = kC^{n_2} \tag{1.27}$$

where n_2 is the slope of the plot of log S vs. log C;

Langmuir isotherm:

$$S = \frac{S_{\max} kC}{1 + kC} \tag{1.28}$$

where S_{max} is the maximum concentration allowed in the medium, k is the S axis intercept. The effective decay constant (λ), is a degradation constant that can be used to quantify the composite effects of hydrolysis and biodegradation (Yeh et al. 1992).

$$\lambda = \frac{\lambda_1 \theta + \lambda_2 k_d \rho_b}{\theta + k_d \rho_b} + \lambda_b \tag{1.29}$$

The dissolved species first order hydrolysis rate can be written in terms of the acid catalyzed, k_a, base catalyzed, k_b, and neutral, k_n hydrolysis rate constant.

$$\lambda_1 = k_a[H^+] + k_n + k_b[OH^-] \tag{1.30}$$

$$\lambda_2 = \beta k_a[H^+] + k_n \tag{1.31}$$

where, λ_1 is the first order hydrolysis rate constant for the dissolved species; λ_2 is the first order hydrolysis rate constant for the sorbed species; λ_b is the biodegradation rate constant; $[H^+]$ is the hydrogen ion concentration; $[OH^-]$ is the hydroxyl ion concentration.

1.5 Need for modification in FEMWATER model

In contaminant transport studies, the nature of the porous medium plays an important role, especially in modeling studies. A simple advection dispersion equation does not give satisfactory results in some laboratory transport studies (Van Genuchten et al. 1977, Gaudet 1977, deSmedt 1981). Non-equilibrium mass transfer is the additional property needed to study and understand the transport process in porous media. Regions generating the AMD such as mine waste heaps, mine waste tailings and subsurface zones under mine tailings are predominantly having the preferential or dual porosity flow. There were very few studies available on non-equilibrium study combined with AMD transport. So it is decided to study the ferrous ion transport with non-equilibrium transport, because ferrous ion plays an important role in the acidification of water. Removal of ferrous ion, positively charged, increases the water pH and ceases further oxidation processes.

These dual porosity medium can act as source or sink for contaminants, which can lead to the containment of contaminants. More experimental and field study are required to analyse the effects of non-equilibrium mass transfer on reactive contaminant transport. Conceptual and numerical modeling with assumptions makes the problem simpler and numerical simulations gives more idea of the transport nature and simulation results can be used to make physical models with specific objective. A literature review on numerical modeling of AMD and reactive transport models, is given in chapter 2, leads to the FEMWATER model with following merits: i) FEMWATER is a 3D flow and transport model, ii) which is open source public domain model, iii) manual to the model is available and iv) FEM numerical approximation is used.

Though FEMWWATER is useful to simulate contaminant transport, it is not capable of simulating the non-equilibrium effects, which is an important factor which can affect the output predictions. In order to study the reactive transport nature of AMD contaminants, it is intended to update the FEMWATER model with long term goal of providing 3D non-equilibrium reactive transport model to the public domain. As an initiation in this study FEMWATER is updated with non-equilibrium transport, dual porosity flow and ion exchange reaction to enhance the model's prediction.

1.6 Objective

The main aim of this research is to study the transport processes of dissolved species from AMD through the variably saturated subsurface zone under physical non-equilibrium conditions. The following are the important subtasks involved to achieve the main objective:

- To devise time dependent variation in the water contents of mobile and immobile zones of the unsaturated porous media in the 3DFEMWTER.
- To devise and incorporate a module on solute mass transfer between mobile and immobile zones in variably saturated porous media in the 3DLEWASTE.
- To incorporate a module on mass transfer mechanisms due to chemical reactions, in the code 3DLEWASTE.
- To analyse the effects of non-equilibrium mass transfer of liquids and solutes on transport of conservative and reactive AMD contaminants in the subsurface medium.
- To analyse the non-equilibrium effects on ferrous ion transport in homogeneous and heterogeneous medium.

1.7 Organization of the thesis

Chapter 2 presents the literature review on AMD, mobile immobile flow, physical non-equilibrium transport and reactive transport models followed by overall summary.

Chapter 3 presents the modification in the FEMWATER model. Describes the inclusion of non-equilibrium mass transport phenomena, ion exchange reaction and the concept of mobile immobile moisture to FEMWATER flow model and their validation with the literature data.

Chapter 4 presents the analysis and selection of parameters for the numerical simulation run and explains the parameters used in the simulation, also describes the results from the simulation.

Chapter 5 presents the application of and validation of the FEMWATER model, with non-equilibrium transport property, on hypothetical mine water movement situation, effects of non-equilibrium mass transfer on contaminant transport and parameter sensitivity analysis. Two

dimensional simulations are obtained for contaminant transport in homogeneous and heterogeneous medium with physical non-equilibrium, sorption and ion-exchange reactions.

Chapter 6 presents the summary and conclusions from the whole research work and model limitations. The scope for further research in is also presented in the final chapter.

CHAPTER 2

LITERATURE REVIEW

This chapter presents the literature review on Acid Mine Drainage (AMD), mobile immobile flow, physical non-equilibrium transport, reactive transport models on AMD, evolution of FEMWATER and its application to field problems followed by overall summary.

2.1 General

Though mining provides revenue to the nation and supports modern sophisticated life, it generates a huge amount of waste and its impact on environment lasts for a long period. AMD is the immediate and harmful product of mine waste and mining processes that contain Fe^{2+}, Fe^{3+}, SO_4^{2-}, H^+, etc. ions and it contaminates water severely. There are many references (Abdul-Wahab 2012, Bell 2006, Blodau 2006, Chon 1999) in the literature and in the books that give a detailed description about the pollution of surface and subsurface water bodies by heavy metals and suspended particles released from AMD, that lead to longer term environmental effects. During the period from 1940's to 1980's, researchers studied the generation process of low pH water from mine sites, mine water characteristics (acidic, neutral or alkaline water, metals present in water) and acid neutralization processes. In the beginning of 1980's numerical models were applied to assess the spread and reach of AMD polluted water and the downstream water quality. Many models were developed and made open to the public through funded projects. Some of the models were simple linear models that are utilized only to simulate uncomplicated laboratory studies. However, the complicated field conditions in real scenarios have complex mass transport processes that are rarely modeled in complete form. The physical non-equilibrium in AMD transport is less frequently modeled by the scientists that have prompted the need here for further investigations. The public domain numerical models were continuously developed, modified, and updated by individual researchers as well as by research groups. In this research work, efforts are made to update the public domain model FEMWATER with inclusion of new concepts for more sophisticated and accurate results. The focus was on the numerical modeling of reactive transport of AMD affected water through the vadose zone, and hence this chapter reviews the research works on AMD, physical non-equilibrium, numerical modeling of AMD, and the FEMWATER model.

2.2 Acid Mine Drainage

AMD is a worldwide problem that arises mainly due to the process of mining. Mine wastes (waste rocks heap), mineral process waste (tailings) and mine surroundings (soil contained pyrite minerals) react with oxygen and moisture to produce the low pH water, which is acidic in nature. Overflow of acidic natured water from mines (Ex: Coal mine, Gold mine, Copper mine, etc.) are

known as “AMD or ARD”. Acid generation potential of a mine depends on the mineral composition and is a site specific process too. Primary factors of acid generation include moisture, air (oxygen), ferrous/ferric ion, sulfide minerals and bacteria. The hydrolysis of mining soils/rocks and leachates from mine wastes are the main contributors to the AMD. Apart from mining sources, acid rain, acid sulphate soil, large scale constructions etc. also contribute to the generation of AMD. Sulphide minerals particularly Pyrite (FeS_2), Pyrohtite ($Fe_{1-x}S$, (where $0 < x < 0.2$)) etc. are exposed to atmospheric oxygen and surrounding water because of mining. Such exposure produces acid that may dissolve relatively insoluble chemical species into free ionic species, or even secondary minerals like sulphates, carbonates and hydroxides (Bernardes et al. 2011). This reaction changes the usually neutral natural water in to acidic water.

Acidic waters pose severe threat to the surface and subsurface water systems, aquatic species and microbes in soil. The pollution of surface and subsurface water due to AMD is a huge concern to the society and necessary steps have to be taken by the mining industries to prevent the drainage of such toxic pollutants into the environment. There are some methods used to cease the generation of AMD in the mine environments and some water treatment techniques to treat the contaminated water before entering the surface water bodies. But once AMD enters in to the subsurface zone, it takes a substantial time period to restore the original state of groundwater. In addition to the acid contribution, AMD causes leaching of metals such as arsenic, cadmium, copper, silver, zinc and iron from mine wastes to surface waters (USEPA, 1994) and into the groundwater (Pentreath. 1994; Jenkins et al. 2000). Many other reactions like - speciation, aqueous complexation, redox reactions, dissolution and precipitation, etc. take place during transport through the unsaturated subsurface zone.

2.2.1 Literature Review on AMD

Hoffert (1947) described the nature of acidic mine water that comes out of abandoned and active mine sites and suggested some remedial measures to control the generation of acidic water like keeping the mine sites sealed from entering of air and water, since air and water are reason for production of ferrous sulfate and sulfuric acid. *Hoffert* also discussed about the amount of acidic and alkaline water that comes out of the coal processing industries in the Pennsylvania region.

Hanna et al. (1963) classified the areas related to production of acid mine drainage in to four main categories such as chemistry, microbiology, mineralogy-petrology and geology-hydrology after critical review and suggested about setting goals for further research on abatement of acid generation in all the four categories such as determining the chemical kinetics of sulfide-sulfate system, the roles of microorganisms in acid production, mineralogic relationship of sulfides in coal and rock composition and their neutralizing potential.

Rawat et al. (1982) described about the production of mine drainage water in North eastern region of Indian peninsula. Assam, situated in the north eastern region of India, receives about 400cm rain annually, this leads to the percolation of water to underground mines and the mine water outflow is found to be highly acidic. *Rawat et al* found that the sulphur content present in the coal mine areas, and specifically pyritic sulphur as the reason for acidic mine water and iron oxidizing bacteria plays an important role in acid production and the organic sulphur is inert and does not participates in any chemical reaction.

Singh et al. (1988) studied the inhibition of bacterial activity in acid mine drainage, by conducting laboratory experiments. Results showed that organic acids, sodium benzoate and sodium lauryl sulphate, at low concentration, are effective bactericides and are able to reduce the acid formation by inhibiting the growth of Thiobacillus ferrooxidans.

Jamal et al. (1991) suggested a neutralization method from their laboratory experimental study, where mine drainage water is allowed to flow through the overburden rocks (which contain alkaline components and various mineral compounds that neutralize the acid water) to overcome the acidic nature of mine drainage water. They studied the feasibility of the above technique and found increase in the pH level of acid water. *Jamal et al* mentioned that neutralization methods like neutralization by limestone, avoidance of water filtration into acid producing minerals, submergence of acid forming minerals into stagnant water, sealing off acid producing area, etc. are lack in universal acceptance.

Webb and Sasowsky (1994) consider the process of neutralization of acid water through carbonic acid dissolution, along with the process of lime stone treatment. They found that dissociation of carbonic acid in to water and carbon di oxide process also increases the pH of acid water.

Because of de gassing of CO_2 from water increases the alkalinity of water and authors suggested that mechanical aeration of water may further induce the dissolution and dissociation reactions.

Elberling and Nicholson (1994) developed models that consider oxidation of pyrite by air in waste piles. They conclude that the oxidation rates are limited by oxygen diffusion through the wastes. Experimental results showed that the rate of oxygen consumption by pyrite is a function of time and oxygen partial pressure. The model has focused mainly on the oxygen diffusion and pyrite oxidation mechanisms to study the acid generation in mine tailings. Though simulations reflect the tailings conditions still the model needs some improvement, addition of liquid phase for transport, then only the realistic quantitative model can be achieved. Simulation results showed that the model is sensitive to the oxygen diffusion rate than the parameters like grain size and Pyrite oxidation rate.

Mcnab Jr. (1997) developed a two dimensional reactive geochemical transport model for evaluating the impact of reactive contaminants on an aquifer based on a semi-analytical solution to the advective-dispersive transport equation. Their semi-analytical model, provide good results without any oscillations which generally occurs in numerical solutions, is utilized to the test problems that include Acid Mine Drainage and hydrocarbon biodegradation. Mcnab simulated the AMD due to FeS oxidation products (Fe^{2+} and SO_4^{2-}) that are constantly given to the hypothetical domain for 20 years. The distribution of SO_4^{2-} in the domain after 20 years is simulated in the presence of oxygen. pH value, mineral saturation of Gypsum, Calcite and $Fe(OH)_3$ were also simulated. 20 years simulation results matches with the field observation trend for both acid mine drainage and hydrocarbon bio attenuation problems.

Chon et al. (1999) suggested that in order to understand the changes in the water chemistry of a stream impacted by AMD, it is necessary to determine the geochemical behaviour of Fe and Al, and the primary metal related to AMD is iron. When is iron combined with sulfate and/or sulfide, iron can cause real problems. They also found that elements in AMD were transported downstream as dissolved free ions or complexes.

Waybrant et al. (2002) designed a permeable reactive barrier to enhance sulfate reduction and metal sulfide precipitation to prevent Acid Mine Drainage and the release of dissolved metals. They conducted column experiments using simulated mine-drainage water to assess the

performance of organic carbon-based reactive mixtures under controlled groundwater flow conditions. Mine drainage water that has undergone acid neutralization within aquifers is known as simulated mine drainage. This water has near neutral pH and contains elevated concentrations of Fe(II) and SO_4. The concentrations of Zn and Ni were reduced and the pH increased slightly in the effluent water.

Nengovhela et al. (2004) studied the oxidation and precipitation of iron by chemical and biological processes and concluded that at particular conditions biological iron oxidation rate is high compared to chemical iron oxidation, they studied the effect of supporting media like plastic, coal discard and sand on the oxidation reaction and suggested that the supporting media favours the biological oxidation reaction. If the supporting media is added then the biological iron oxidation rate is increased where increment in iron oxidation rate is not found in chemical oxidation.

Blodau (2006) gave detailed review on acidity generation and consumption in acidic coal mine lakes and their watersheds due to primary and secondary geochemical, biogeochemical reactions. The review suggests that many of the involved processes, such as pyrite oxidation, carbonate weathering in the watershed, ferrous ion oxidation and iron hydroxide precipitation in lakes, may occur at similar rates.

Singh (2008) explained the processes such as chemistry of AMD (e.g. complexation of ferrous and ferric oxidation products dissolved in water imparts red and yellow characteristic colour to AMD), role of water in the production of AMD (e.g. rate of pyrite oxidation increases significantly in arid climate), microbial aspects of AMD (e.g. bacteria appears to increase the reaction rate to several times faster, by increasing the oxidation of Fe^{2+}), and bacterial inhibition process to decrease the acid water generation.

Gaikwad et al. (2010) authors explained removal of copper ion from acid mine drainage water by ion-exchange reaction and other metals also can be removed by ion–exchange process and concluded that pH is the significant factor that affects the metal removal process.

Bernardes de Souza and Mansur (2011) conducted laboratory experiments, which simulate the field conditions, to predict the reactions involved in the acid generation process in the mine sites.

Experiments include the factors that affect the acid generations such as pH level, microbiological factor and pyrite oxidation. They found that the microbiological factor plays an important role in the generation of AMD, so the models involve in the prediction of AMD should include the parameter of microbiological effect.

Sahoo et al. (2012) analysed the behaviour of rare earth elements (REE) in the mine drainage water and also analysed the influence of species (ferric, ferrous ions) on mine water characteristics. They also analysed the mobility of REE and found a typical REE-enriched pattern in the AMD contaminated stream water. Sahoo et al concluded that REE patterns can be helpful in identifying the sources of contaminants in AMD affected site.

Vyawahre et al. (2016) studied mine water characteristics of Durgapur mines, WCL Maharashtra, Coal India limited. They suggested new technologies like ion exchange, reverse osmosis and membrane technology for mine water treatment. It was also found that (i) AMD is not only a threat of acidification but also it accumulates heavy metals, which are not bio degradable, is also a threat for living organisms, (ii) AMD decreases oxygen levels in the fresh water and led to the death of various organisms and (iii) apart from chemical effects AMD also causes physical effects such as soil erosion, sediment and coal fine deposition and precipitation of ferric hydroxide.

Handayani et al. (2016) studied the downstream impact of mine drainage water from the mine area Tanjung enim, south Sumatra, Indonesia. They considered two areas named internal (up to 2 km) and external (2 to 4.5 km) to assess the mine water effect on ground and surface water. The area within two kilometer from mine contains average pH of 5.17 with exceeded level of Fe and Mn, 7.66 and 7.16 mg/l respectively. External environment region has an average pH of 6.02 and contains metals within the threshold limit of Fe and Mn, 1 and 0.5 mg/l respectively, as per the water quality standards of the waste water of the coal mining activities (Ministerial Decree No. LH RI of 2003).

Palihakkara et al. (2018) studied the mine water effects on surface water in Srilanka and suggested a method to remove heavy metals from water. Copper and Cadmium are the heavy metals present in the water in high level authors suggested that a passive treatment method, using water hyacinth, to clean the water. They referred to the literature that the absorption of metals is

taking place through the plant root system, they have not measured individual parts of the plants for metal concentration since their aim is to reduce the metal concentration from water.

Bwapwa et al. (2018) reviewed the AMD problems in South Africa and analysed the chances of using treated AMD water for domestic and agricultural purposes. The Witwatersrand gold mine, Mpumalanga and Kwazulu-Natal coal mine and O'Kiep Copper mine are the most affected sites in South Africa. They have reviewed many treatment methods for acid mine drainage like combined chemical and biological treatment, lime neutralization treatment, chemical precipitation for sulphates removal, biological sulphates removal, sulphides precipitation, membrane technologies and ion exchange; among these treatments they suggested membrane technology as the suitable one for getting drinking water from mine water, in terms of metal free and quality of water.

Summary of AMD literatures: AMD generation and transport analysis is important with the context of safeguarding the surface and groundwater systems. AMD is not only a threat of acidification but also it accumulates heavy metals, which are not bio degradable, is also a threat for living organisms, AMD decreases oxygen levels in the fresh water and led to the death of various organisms and AMD also causes physical effects such as soil erosion, sediment and coal fine deposition and precipitation of ferric hydroxide (Vyawhare et al 2016). AMD with acidic nature from abandoned/active mine sites and from coal processing industries were studied by Hoffert (1947). Production of AMD from mines and mine waste sites can be classified into mainly four areas such as chemistry, microbiology, mineralogy-petrology and geology-hydrology (Hanna et al 1963). Out of that microbiological factor (iron oxidizing bacteria) plays a vital role (Rawat et al. 1982, Bernardes de souza and Mansur 2011) in the generation of AMD. Thiobacillus ferrooxidans (oxidizing bacteria) are commonly found in the acidic conditions and accelerate the oxidation process which leads to increase in AMD generation and it can be inhibited by using of organic acids, sodium lauryl sulphate and sodium benzoate (Singh et al.1988). Geochemical behaviour of Fe and Al is necessary to assess the impact of AMD on streams and iron is the primary metal related to AMD (Chon et al. 1999). Methods to prevent the generation of AMD like prevention of water filtration into acid producing minerals, submerging the acid forming minerals under water, sealing off the acid producing area (Hoffert 1947), inhibiting the oxygen diffusion rate by sealing the surface of the tailings or mine heap, rate of

oxygen consumption by Pyrite determines the AMD generation rate (Elberling and Nicholoson 1994), were studied by numerical and experimental investigations.

Methods to neutralize the acidic water like neutralization by limestone (Hoffert 1947), flow of AMD through the overburden rocks (which contain alkaline components and various mineral compounds that can neutralize the acid water) (Jamal et al 1991), carbonic acid dissolution method (Webb and Sasowsky 1994) were studied by field and lab experiments. Risk of carrying the heavy metals through AMD is decreased, once the pH of the AMD water is increased (Blodau 2006). Study of removal of metals, sulphate and ions have also been studied; sulphate can be reduced by the organic carbon based reactive barriers (Waybrant et al. 2002), ion-exchange reaction is used to remove the copper, iron and other positively charged ions (Gaikwad et al. 2010). Along with ion-exchange reaction reverse osmosis and membrane technology also used to remove the metals from AMD (Vyawhare et al 2016). It was obvious that distance of the mine location (from water bodies) and AMD flow direction also are important factors that affecting the water bodies (Handayani et al. 2016), surface water affected by the AMD can be treated by plants for example Palihakkara et al (2018) studied the removal of copper and Cadmium ions by water hyacinth. Bwapwa et al (2018) has reviewed many treatment methods for acid mine drainage like combined chemical and biological treatment, lime neutralization treatment, chemical precipitation for sulphates removal, biological sulphates removal, sulphides precipitation, membrane technologies and ion exchange; among these they suggested membrane technology as the suitable one for getting drinking water from mine water, in terms of metal free and quality of water. AMD was studied and explained in various categories, first the AMD and its impact was studied through observation and later on it was studied through scientific approaches like measuring the water quality, analysing the reasons of AMD generation. Precautionary measurement of arresting AMD and its feasibility studies had been carried out which was followed by the mine water treatment studies based on the pH of the water. In recent days removal of particular metals is being studied by various methods.

2.2.2 Studies on the effects of mine water around the world

Active research is going on in India as well as all over the world on the following topics like mining and development in mining technologies, management of mine sites and mining wastes,

environmental effects of mining, policy making on mining, disaster prevention, etc. This section throws some light on the effects of mining and mine water around the world.

Long wall mines in Pennsylvania and its effects on aquifers were studied and results showed the deterioration of water quality in surrounding aquifers. All types of mining activities (surface mining, pit mining, underground mining and long wall mining) do affect the groundwater flow (Booth, 2002). *Mineral processing and disposal of mine wastes:* Mining and mineral processing operations can produce large amounts of waste in the form of waste rock heaps and slurry impoundments known as a tailings dam. Leachate from waste rock piles and tailings dams may cause surface and subsurface water pollution due to its acid nature. Failure of tailings dams may cause huge loss (in terms of human lives, loss of soil fertility, water pollution) and damage and also affects water quality severely, recent examples are the breakdown of iron ore tailings dams in Brazil; Bento Rodrigues dam disaster (2015) and Brumadinho (Córrego de Feijão mine) dam disaster (2019). Effluent from these dams polluted the river, submerged the nearby towns, cause huge economic loss and also killed people. *Mine dewatering:* the dewatering process is essential to stop flooding of the mine and to protect the miners and mining equipment. Dewatering water can cause water pollution and the process itself causes a depression in the water table around the mining area that affects the water flow in streams and water level around the pumping wells. In extreme cases dewatering can lead to drying up of river. *Social issues due to mining:* Time and money has to be spent on keeping a clean water supply, and preventive measures have to be taken to avoid groundwater pollution. Dewatering not only leads to a lowering of the water table level but it also leads to groundwater issues like deepening of wells and relocating wells to unaffected areas. Scarcity of aquatic species leads to demand and increase in cost. Fresh clean water scarcity may lead to a reduction in tourism and recreational activities (Younger et al. 2004).

In 1989 it was estimated that approximately 72,000 ha of land surface including lakes, rivers and reservoirs and 19,300km of streams worldwide had been affected by waters from mines (Johnson et al 2005). In the Philippines water from a waste rock dump, after a heavy rainfall event, mixed with the Mogpog river. The acidic water killed fishes and created a foul smell (Coumans et al. 2000). AMD from the Makum coal field in North-eastern India and its impact on the rivers (Burhi Dihing and Tirap) was studied and it was reported that interaction of mine water with the

river not only affects the river water but also deposits heavy metals like Cd, Fe, Cr, Mn, Ni and Zn into the river sediments (Equeenuddin et al. 2013). Rock deformation also happens due to the mine water flooding; in 1982 Fromm, analysed the effects of mine water on Russian coal bearing rocks and listed the following effects i) swelling of clayey rocks ii) deformation of broken rocks iii) sliding on rock joints iv) initiation of physico chemical processes in rocks and v) weakening of rocks. In 2018 Berezina et al, assessed the pollution created by a coal mine and its effect on Yaiva river basin, located on the Kizel coal basin territory in Russia and concluded that mine waste rock heap and tailings create more acidic water than mine itself and pollutes the river environment. In 2018 Moeng studied the awareness of the people, living around a mine field in South Africa, about health issues and produced evidence of health issues due to mining. They suggested that health issues of the people living around the mine areas should be taken in to account while planning for mining operations and the implementation of legislative actions has to be properly followed. AMD from the Dabaoshan mine, in China, contaminated the nearby groundwater as confirmed through well water analysis. Long term irrigation of contaminated stream water may lead to the contamination of well water with high concentrations of Cu and Cd that is partially responsible for high mortality rate in the study area (Chen et al. 2007).

2.3 Mass transport and non-equilibrium

Contaminants dissolved with water are called solutes and the movement of the solutes in the subsurface region is generally studied by an advection dispersion equation (ADE). However, there are some issues with the ADE in some cases, where the solute transport in porous media (or soil) behaves in a non-equilibrium manner. The non-equilibrium in solute transport may be due to time dependent mass transfer of solute from different zones of fluids as well as solids in the porous media. The presence of discrete zones of fluids having different velocities can cause time dependent solute mass transfer between the fluid zones, thereby initiating physical non-equilibrium in overall solute transport. This physical non-equilibrium affects significantly the contaminant movement. Gaudet et al. (1977) and Van Genuchten and Wierenga (1977) gave experimental evidence of effects of physical non-equilibrium phenomenon on solute movement through unsaturated media. De Smedt (1981) reported the evidence of physical non-equilibrium in unsaturated glass beads and sandy medium even when the overall flow is steady.

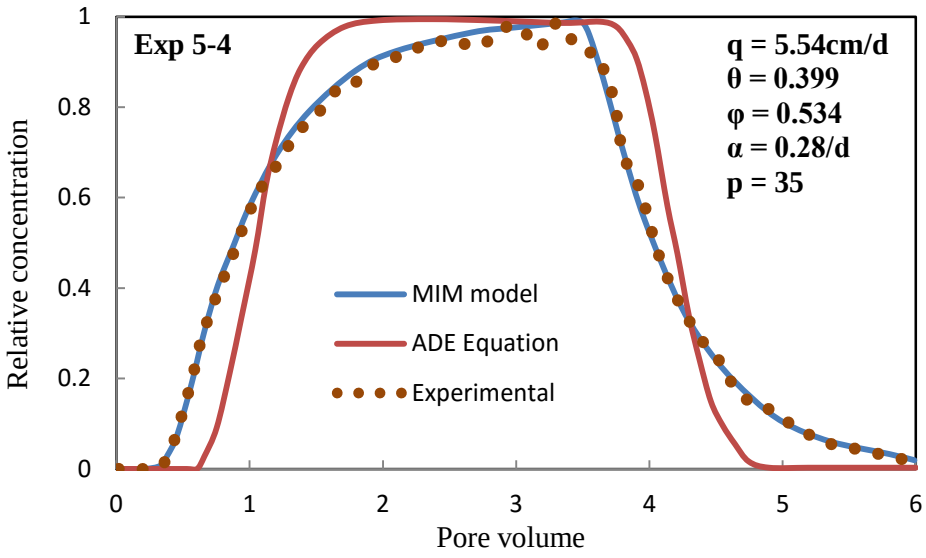

Fig. 2.1 Column experimental (dotted line), advective-dispersive equation(ADE) (brown line) and non-equilibrium transport (blue line) equation curves (recreated from van Genuchten et al.1977) (MIM-Mobile-IMmobile)

Some laboratory experiments showed the appearance of early break through curves (BTC) in solute transport observation due to physical non-equilibrium. Equilibrium equation model (or ADE) could not predict the solute front observed in the laboratory studies and the experimental solute front was more advanced than the predicted one. The distribution curve observed from the experimental data (van Genuchten et al. 1977) is in non-sigmoidal form which has tail like structure shown in Figure 2.1, these kinds of results leads to the idea of non-equilibrium transport; which exists when the mass-transfer times are longer than system hydraulic residence times and/or the solid surface-mediated reactions are faster than the normal advective-dispersive solute mass-transfer process (Hatfield et al. 1996).

2.3.1 Non-equilibrium types

Non-equilibrium mass transfer occurs due to the influence of physical or chemical processes, it is decided based on whether the porous medium or the reaction causes the mass transfer process, but to distinguish the occurrence of non-equilibrium owing to the physical or chemical process is difficult. By taking in to account of non-equilibrium concept during the prediction of contaminant flow, the underestimation of transport spreading in the downstream can be averted.

2.3.1.1 Physical non-equilibrium

The physical make-up of the soil is the reason for the presence of relatively immobile water, that is why it's called as physical non-equilibrium. A non-sigmoidal shaped effluent curve with a tail like extension (dotted line shown in Figure 2.1) can be explained by either physical or chemical non-equilibrium property in nature. Aggregated soils contain pores between the soil particles that allow free flow of liquid are termed as macropores or mobile region. Another region is the pore space present in the soil aggregate particles, which does not allow free flow of water and is termed as micropores or immobile region (Figure 2.2.a) (Rao et al. 1980). Mass transfer between mobile and immobile regions is the reason for early emergence of contaminants at downstream and also causes the tail like extension in the effluent curve. Mass transfer process diffuse contaminants into the immobile region, contaminants coming out of immobile region at later time causes the tail like extension in the effluent curve. Presence of dead end pores, pores that are separated from the main flow path or disconnected (Figure 2.2.b), in the porous medium also creates an immobile water zone that leads to the mass transfer process. In these models advective transport is assumed to occur only in the mobile water region, in immobile water region transport occurs at very slow pace (negligible) with respect to the mobile region. Diffusion is the main mode of movement that takes place between the two distinct water regions. Generally, these concepts are added to the advective dispersive model in the form of a distributed source or sink term, termed as mass transfer coefficient (Γ), whose value is determined by curve fitting (Rao et al. 1980). The potential clue for a MIM model is the early breakthrough (though a preferential flow path could also explain this aspect). The early breakthrough is due to a higher average linear flow velocity, u, when there is immobile water. For an ADE model, $u_{ADE} = V/\theta_e$ while for a MIM model $u_{MIM} = V/\theta_m$ and since $\theta_m < \theta_e$ then $u_{MIM} > u_{ADE}$ and therefore the MIM model has an earlier breakthrough curve than the ADE model for the same Darcy flux, V, through the system.

Six parameters (θ_r, θ_s, α, n_1, l, K_s) are required to model water flow with single porosity flow, while the non-equilibrium model needs an additional three parameters for immobile region description ($\theta_{r(im)}$, $\theta_{s(im)}$, Γ_w) along with above six parameters to model water flow. Gerke at al. (1988) developed a non-equilibrium flow model, which considers two water regions and are moving in slow and fast manner (Figure 1.1.c); Kartha and Srivastava (2012) developed a non-

equilibrium transport model with slow moving water region in between immobile and mobile water regions. These models needed more parameters for transport computations compared to simple non-equilibrium model with only mobile and immobile regions.

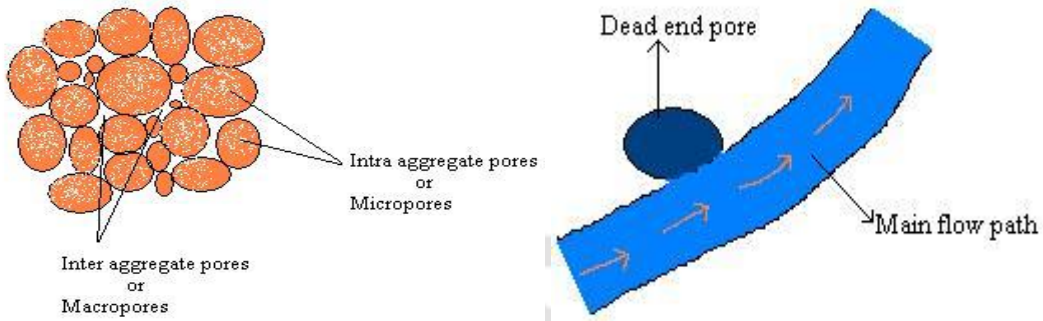

(a) (b)

Fig. 2.2 Representation of (a) aggregated soil pores and (b) dead end pores

Table.2.1. Differences of equilibrium and non-equilibrium transport variables and parameter

Variables	**Equilibrium model**	**Non-equilibrium model**
Water content	θ	θ_m, θ_{im}
Pressure head	h	h
Resident concentration	C	C_m, C_{im}
Total solute mass	$C(\theta+\rho k_d)$	$C_m(\theta_m+f\rho k_d)+ C_{im}(\theta_{im}+[1-f]\rho k_d)$
Mass transfer	---	Γ

In addition, the simple non-equilibrium model is able to provide more or less satisfactory results compared to equilibrium model. In much of the literature, the physical non-equilibrium process is assigned only to the solute mass transport. The fluid mass transfer between the mobile and immobile regions is not taken into account (Brusseau et al. 1991; Kartha and Srivastava 2008, 2012; etc.). There can be time dependent fluid mass transfer between the mobile and immobile liquid zones (Hydrus manual; Mohanasundaram et al. 2013; etc.). Some researchers numerically (Ross et al. 2000, Mohanasundaram et al. 2013) and experimentally (Simunek et al. 2001) studied mass transfer effects on water flow in soils. This research focuses on adding physical non-equilibrium water mass transfer to the Richards unsaturated flow equation as well as to the solute mass transport equation to assess the transport of AMD in downstream.

2.3.1.2 Chemical non-equilibrium

Based on the chemical reactions the tailing in effluent curves arise witnessed by accounting for different sorption mechanisms. Porous medium involving sorption reactions can behave in two ways. A portion of the sorption site involves in the instantaneous sorption reaction, called as equilibrium sorption, and the remaining site indulge in the rate limited sorption reaction called kinetic sorption. Two different types of sorption mechanism lead the effluent curve in the form of nonsigmoidal and tail like shape. And some studies combine both, physical and chemical, non-equilibrium models to analyse the transport processes (Simunek et al. 2008, Field et al. 2014). Finding out the kinetic parameters and equilibrium coefficients for sorption reactions are the difficult part of the chemical non-equilibrium models. Table 2.1 shows the equilibrium and non-equilibrium transport variable.

2.3.2 Literature Review on physical non-equilibrium

Coats and Smith (1964) explained the reasons for the asymmetry resulting in the effluent concentrations and proposed the capacitance model in place of normal diffusion model for contaminant transport. Their proposed model matched well with the asymmetric results and was used to analyse the dead end pore volumes that causes the asymmetry in effluent concentrations.

De Smedt and Wierenga (1979) assumed that the porous medium is having mobile and immobile water fractions, and gave a generalized solution for solute transport in a finite and semi-infinite column. They concluded that unsaturated conditions give rise to a bimodal pore distribution and simulate the concentration profiles by assuming, the solute transfer in a mobile water fraction with lateral diffusion towards an immobile water fraction.

Wierenga and Van Genuchten (1989) did a solute transport experiments with both long and small unsaturated sand columns and concluded that dispersivities measured in the small columns were not similar to the large columns but the same retardation factors can be applied to the long as well as small columns.

Bond and Wierenga (1991) have studied the processes of solute transport through unsaturated sand column under steady state flow and found that found that strong evidence for the presence of immobile water and its effect on contaminant distribution under steady flow conditions.

Kim (2002) developed mathematical model to describe the contaminant transport in dual porosity media in the presence of mobile colloids (bacteria) and dissolved organic matter (DOM) in riverbank filtration, where DOM and colloids affects contaminant transport and concluded that a decrease in mobile water content advances the concentration front, Most likely it is due to $u_{MIM} = V/\theta_m$ becoming larger for the same V as the mobile water content decreases.

Simunek (2003) reviewed various approaches of modelling preferential and non-equilibrium flow and transport in the vadose zone. Models vary from relatively simplistic models to more complex physically based dual-porosity, dual-permeability and multi-region type models.

Worch (2003) considered solute transport modelling under non-equilibrium conditions, because the spreading in the breakthrough curve was not possible to explain only through the process of dispersion. The non-equilibrium conditions arise due to the slow mass transfer processes, and the author introduced the mass transfer equations for film and intra particle diffusion to the transport model. To simplify the mathematical handling, he made two assumptions; the numerical solution of model is based on the Plug flow approach. The intra particle diffusion is described by a mass transfer equation with a linear driving force instead of Fick's law.

Van Genuchten and Simunek (2004) highlighted the approaches for coupling physical, chemical, and other processes on the vadose zone and address (1) the approaches for modeling flow and transport, (2) multicomponent geochemical transport, (3) colloid and colloid-facilitated transport, (4) integrated surface/subsurface modeling, and (5) process-based descriptions of preferential flow. Their studies were based on the HYDRUS codes.

Costa and Prunty (2006) experimented on solute transport in a fine sandy loam under different flow rates and explained the relationship between the dispersion coefficient and the water content that were verified only at a higher flux and under non-convective dispersive processes. The large variability of solute transport parameters made their estimation difficult. The dispersivity seems to be larger under unsaturated conditions.

Ichola and Gaidi (2006) studied the influence of the unsaturated zone on solute migration using electrical conductivity profiles and concluded that the migration mode changed during the soil saturation. The saturation process delays the solute movement even when the coefficient of permeability is higher.

Jarvis (2007) reviewed non-equilibrium water flow and solute transport in soil macro pores. Leaching of pesticide was increased due to the well-developed bipore network. The macropore flow was also strongly dependent on the surface boundary conditions. The sorption retardation in macro pores was less than in the bulk soil, partly due to the small ratio of surface area to pore volume and also due to kinetic effects during transport (sorption process depend on the pore water velocity.) He also insisted on some research areas to focus in the future – biodegradation in macro pores non-equilibrium sorption effects, sorption interactions with mobile colloids and particulate matter. Not all the solute transport models developed yielded good results when applied to the large field conditions. Therefore, author suggests that the parameter selection should be given more importance.

Kartha and Srivastava (2008) developed a non-equilibrium transport model and proposed concept of a slow moving liquid zone in between the mobile and immobile zones; and confirms the Kim (2002) result.

Leij and Bradford (2009) developed a model with combined physical and chemical non-equilibrium model (CNE); colloid transport breakthrough curves were better explained by CNE.

Mohanasundaram et al. (2013) has concluded from the non-equilibrium numerical simulation that variation in traveling depth of the soil moisture front is observed with a dual porosity model.

Baviskar and Heimovaara (2014) has conducted lab experiments on leachate from landfill waste and concluded that local heterogeneities in the landfill causes preferential flow and transport.

Hou et al. (2018) has conducted experiment on transport of Bromide and Ammonium in porous medium did consider chemical non-equilibrium (CNE) and concluded that in CNE models distribution coefficient (K_d) is more sensitive.

Summary of non-equilibrium literature: In 1964 Coats proposed a capacitance model theory for asymmetry in the BTC that suggests the presence of immobile regions inside the porous medium for which some laboratory and field experiments gave proof for the immobile region (Wierenga and Jaynes). Non-equilibrium transport study can be applicable to remediation purposes in the field scale (Pang et al. 1999). Mass transfer between mobile and immobile regions is the reason for tailing and asymmetry in the BTC, as this process retards the concentration movement.

Increase in immobile water content increases the asymmetry and advances the concentration front (Kim 2002 and Kartha and Srivastava 2008). Further transport models studied combined effect of chemical and physical non-equilibrium on contaminant transport (Leij, et al. 2009, Hou et al. 2018). A few early studies were attempted to simulate mobile/immobile water effects on the mine drainage contaminants (Bibby, 1981 and Selim et al. 1987), production of acid mine drainage in waste rock dump and mill tailings piles (Narasimhan et al. 1986, Gerke et al.1998, Xu et al. 2000), column experiments on treatment of mine drainage by a reactive barrier (Waybrant et al. 2002), effect of a reactive barrier on mine water transport in an aquifer (Ludwig et al. 2002), variably saturated flow in the spoil heap (Bussiere et al. 2003), column barrier study to reduce the acid production (Amos et al. 2004), slow and fast moving of metals in a heap leaching process (Kartha and Srivastava 2012), transport of mine drainage water through an aquifer (Jeong et al. 2016, Bain et al. 2000, Zhu et al. 2001). These are some of the notable works that have led to the combined study of AMD and non-equilibrium mass transfer.

2.4 Numerical models

Modeling is an important tool that can be used to understand hydrological or geochemical processes by interpreting the experimental results as well as by making predictions. Though experiments are required to validate modeling it is not always possible to conduct experiments to observe long term results. In such cases, models can be used to predict various processes. The advection dispersion equation is frequently used to explain the mathematics of transport processes. Many of the reactive transport models were developed as extensions to the existing flow and transport models for example FEMWATER, 3DHYDROGEOCHEM, etc. Initially these were developed as a simple one dimensional finite element model to simulate flow and transport, later they were added with reactions and developed as commercial software to analyze three dimensional field problems. Since this research work focuses on non-equilibrium reactive transport of AMD, the focus was on public domain reactive transport model and the literature reviews were confined to numerical modeling of AMD transport and geochemical models that are given in the following section and in Tables 2.2 and 2.3.

2.4.1 Literature review on application of numerical models to AMD problem

Narasimhan et al. (1986) has developed and applied the DYNAMIX model to validate against

the transport data of contaminated low pH water from uranium mill tailings to the shallow aquifer at Riverton, Wyoming. DYNAMIX is a two dimensional model, which couples chemical speciation model (PHREEQE) and transport model (TRUMP).

Walter et al. (1994) has investigated the two dimensional reactive transport of dissolved toxic metals from mine tailings using the multicomponent reactive transport model MINTRAN. They analysed the effect of continuous and finite source input on metal transport in a hypothetical domain that resembled a site in the northern Ontario. MINTRAN comprised of two modules, finite element transport module (PLUME2D) and a geochemistry module (MINTEQA2). A two-step sequential solution algorithm was employed for the coupling of the transport and reactive processes. Their model also dealt with ion exchange and dissolution/precipitation chemistry. The authors concluded that finite source input had control on the contaminant spreading by the formation of geochemically stable precipitation zone. Mine tailings are subject to the risk of releasing metals due to oxidation reaction, this is mainly due to the supply of oxygen through the top surface of the tailings. Flooding the top surface of tailings with water ceases the oxygen diffusion in to the tailings, this leads to the cessation of reaction and also release of metals; where pH of the water will be high (5 to 7) and the metal concentration also will be less. Under this scenario a stable precipitation zone will be formed in the subsurface region and the contaminant distribution is controlled due to the precipitation. In the case of continuous source input, pH of the water will be low (3-5) and it carries dissolved metals; If the pH is less the formation of stable precipitation zone won't occur and this leads to the enhanced spreading of contaminant.

Wunderly et al. (1995) has analysed oxygen diffusion and kinetically controlled pyrite oxidation in mine wastes and the subsequent transport of the oxidation product to the subsurface using the model MINTOX, which is the combination of a reactive transport model (**MIN**TRAN) and oxidation model (PYR**OX**). Their model predicted the acid generation quantity and its chemical nature. also, their model assessed the acid producing nature and its mitigation methods. Based on the data from Nordic mine tailings impoundment, Elliot lake, Ontario, the one dimensional simulations were run.

Mayer et al. (1999) has developed a multicomponent reactive transport model MIN3P, which is applied to study the oxidation and transport processes of mine water at the Nickel Rim mine site, Sudbury, Ontario. They also applied their model to study the treatment processes of mine water.

Xu et al. (2000) has employed TOUGHREACT and TOUGH2-CHEM to analyze the pyrite oxidation in saturated and unsaturated media. One dimensional flow in porous medium and two dimensional flow in fractured medium simulations were run with TOUGHREACT model. TOUGH2-CHEM uses fully coupled approach, where flow, transport and reaction equations are solved simultaneously. TOUGHREACT model uses the sequential iteration approach to couple flow, transport and reactions. Chemical transport and reactions are iteratively solved till the occurrence of convergence and the author has concluded that sequential iteration approach is numerically efficient for the problems with limited time steps and problems with high transient changes. Xu et al verified their model with five test conditions (saturated medium and equilibrium pyrite oxidation, aqueous advection and equilibrium pyrite oxidation, aqueous advection and kinetic pyrite oxidation, Aqueous Advection, Gaseous Transport, and Kinetic Pyrite Oxidation) and found the results are matching with experiments. This particular model can be applied to the problems based on the reactions involved.

Gao et al. (2001) has developed a two dimensional model named REACTRAN2D, which is the result of coupling of transport model (SUTRA) and geochemical model (MINTEQA2), to analyse the influence of heat distribution on transport of acid mine water in the aquifers. Sequential iteration approach were used to solve the simulation of coupled flow, reactive multiple component transport, and heat transport.

Vereeckeen et al (2002) based on the one dimensional experimental results reactive parameters like distribution coefficient and ion-exchange were obtained by authors. These parameters were used to model the two dimensional field results with the objective to make the transport model more accurate by incorporating the reaction in to it. TRACE model is used to solve Richards equation, transport of contaminants is solved by PARTRACE code and PHREEQC is incorporated in to the PARTRACE code for chemical interactions, coupling is done by sequential non-iterative approach. Authors got satisfactory results and suggested that discrepancies observed can be addressed by three dimensional model with Monte Carlo simulation results. Results of the two dimensional model qualitatively agreed with the measured break through curves, that was mentioned as satisfactory results. Details in the breakthrough curves show slight discrepancies, like underestimation of maximum concentration, in the 2D model. Authors explained that the field results were measured throughout the sampling area and

the 2D model approach is by averaging over the vertical dimension of the aquifer and this leads to the discrepancies. And they suggested that the use of 3D models in combination with chemical heterogeneous parameters may give better results.

Molson et al. (2005) studied the pyrite oxidation process and subsequent AMD transport in the unsaturated mine waste piles by applying HYDRUS model for flow and the POLYMIN model for transport. The models were also applied to study the proccesses to stop AMD generation by arresting the infiltration of oxygen and moisture in to the unsaturated piles.

Ardejani et al. (2007) has analyzed the generation of AMD and pyrite oxidation in the backfill of opencast mines, which is exposed to atmosphere, with numerical model. This three dimensional finite volume numerical model was developed by modifying the CFD package PHOENICS.

Abdelghani et al. (2009) has studied transport nature of the mine waste contaminants within the fractured rock. This unsaturated modeling study was performed with a three dimensional flow and transport model HYDROGEOSPHERE.

Molson et al. (2012) developed a numerical model (POLYMIN/DFN) to investigate the transport behavior of AMD in discretely fractured porous media. Model was developed from the existing POLYMIN model by adding an extra feature to deal with discretely fractured network (DFN). This model uses a two-step sequential coupling method to solve reactive transport.

Noosai et al. (2014) applied the geochemical model, PHREEQC, to investigate the treatment system for AMD. PHREEQC is designed to perform geochemical calculations, speciation and saturation-index, batch reaction and one dimensional transport process.

2.4.2 AMD and numerical models

Many numerical models and experiments were developed to study transport process of mine drainage water through an aquifer (Jeong et al. 2016, Bain et al. 2000, Zhu et al. 2001), production of acid mine drainage in a waste rock dump and mill tailings piles (Narasimhan et al. 1986, Gerke et al.1998, Xu et al. 2000), variably saturated flow in the spoil heap (Bussiere et al. 2003), slow and fast moving of metals in heap leaching process (Kartha and Srivastava 2012), column experiments on treatment of mine drainage by reactive barrier (Waybrant et al.

2002), effect of reactive barrier on mine water transport in aquifer (Ludwig et al. 2002) and column barrier study to reduce the acid production (Amos et al. 2004). Very few studies were attempted to simulate mobile/immobile water effects on the transport of mine drainage contaminants (Bibby, 1981 and Selim et al. 1987). Based on a review of the literature, this study attempts to analyse the immobile water effects on the transport of AMD contaminants from waste rock heap/mine tailings site to the underneath aquifer. The modified numerical model considers various physical processes (variably saturated flow, medium heterogeneity, physical non-equilibrium of the medium) and sorption reactions to simulate the AMD transport through the subsurface soil. The scope of the non-equilibrium transport study is to make the model prediction more accurate and to give insight to the process of treatment of mine water. In addition, the model may be useful in the designing of reactive barriers.

Table 2.2 Public domain reactive transport models available in USGS site

Models	**General capabilities**
2DFATMIC	1D/2D variably saturated flow, transport of microbes and chemicals with simple chemical reactions (decay kinetics, linear/non-linear adsorption).
3DFATMIC	1D/2D/3D variably saturated flow, transport of microbes and chemicals with simple chemical reactions (decay kinetics, linear/non-linear adsorption).
CHEMFLO	1D variably saturated flow and solute transport.
CHAIN_2D	2D water flow, heat and multi-solute transport in variably saturated porous media.
FEHM	1D/2D/3D multiphase, multicomponent, non-isothermal, reactive flow through variably saturated porous medium and fractured media
HydroBioGeoChem123	1D/2D/3D solute transport, heat transport, mixed, heterogeneous, chemical kinetics and equilibrium and coupled reactive transport in variably saturated porous media.
PESTAN	1D analytical simulation of organic solute transport in the unsaturated zone
RITZ	1D analytical simulation of unsaturated zone flow and transport of oily wastes.
SUTRA	Variably saturated, variable-density ground-water flow with solute and energy transport.
UNSATCHEM	1D simulation of variably saturated water flow, heat transport, CO_2 production and transport, multicomponent transport with major ion equilibrium

	and kinetic chemistry.
UNSATCHEM-2D	2D simulation of variably saturated water flow, heat transport, CO_2 production and transport, multicomponent transport with major ion equilibrium and kinetic chemistry.
VLEACH	1D simulation of advection, sorption, diffusion, and three-phase equilibration in vadose zone.
HYDRUS1D	1D simulation of water flow, heat and multiple solutes transport in variably saturated media with non-equilibrium mass transfer.
PHREEQC	Chemical reaction and 1D reactive transport
VS2DI	1D/2D heat or solute transport in variably saturated porous media
HP1	1D simulation of flow water, heat and multiple solutes reactive transport in variably saturated media.
SWMS_2D	1D/2D water flow and solute transport in vadose zone.
SWMS_3D	1D/2D/3D water flow and solute transport in variably saturated porous media.
RETRASO	1D/2D multiphase flow, heat and reactive transport in variably saturated porous media.
SHAW	1D simulation of water flow, heat and solute transport in variably saturated media.

Table 2.3 Commercial reactive transport models

Models	**General capabilities**
3DFEMFAT	3D flow and solute transport in variably saturated porous media including salt water intrusions.
AIRFLOW-SVE	Simulation of vapor flow and multi-component vapor transport in unsaturated, heterogeneous and anisotropic soil.
CTRAN/W	1D/2D water flow and solute transport in variably saturated porous media.
FEFLOW	2D/3D simulation of water flow, heat and solute transport in variably saturated media.
FRAC3DVS	1D/2D/3D simulation of water flow and solute transport in variably saturated porous fractured media.
HYDROGEOCHEM	1D coupled simulation of water flow, chemical reactions and reactive solute transport in variably saturated porous media zone.
HYDROGEOCHEM2	2D coupled simulation of water flow, chemical reactions and reactive solute transport in variably saturated porous media zone.

HYDRUS2D/3D	2D/3D simulation of flow water, heat and multiple solutes in variably saturated media.
KYSPILL	1D/2D/3D simulation of water flow and solute transport in variably saturated porous media.
MIGRATE	1D/2D water flow and solute transport in variably saturated porous media.
MODFLOW-SURFACT	1D/2D/3D MODFLOW based simulation of water flow and solute transport in variably saturated porous media.
MOFAT	1D/2D multiphase flow and transport of up to five non-inert chemical species.
POLLUTE	1D simulation of water flow and solute transport in variably saturated porous media zone.
TOUGHREACT	1D /2D/3D simulation of chemical reaction and multiphase fluids, heat and reactive transport in variably saturated porous and fractured media.

2.4.3 Evolution of FEMWATER

Initially in 1976 Reeves and Duguid had developed a model FEMWASTE for transport simulation, in which finite element method was used to solve the advective dispersive equation. In 1983 and 1985 Yeh and Huff developed FEWA model for water flow simulation and FEMA model for transport simulation, respectively. Then in 1990's both the models were combined together to create coupled flow and transport model named 3DFEMWATER/3DLEWASTE. Then model was named as HYDROGEOCHEM and continuously being updated to simulate density dependent flow, reactive transport, geochemical reactions and thermal energy transport. 3DFEMWATER/3DLEWASTE was integrated with graphical user interface and also added to the Groundwater Modeling System (GMS) package. Though model has been developed for these many years still the source code of FEMWATER3D is available for public users through United States Environmental Protection Agency (USEPA).

2.4.4 Application of FEMWATER to the field study

Lafleur and Raven (1990) simulated flow and transport to assess the data obtained from Canadian uranium mine tailings site by applying FEMWATER/FEMWASTE. They suggested that model needs adequate data with multispecies and three dimensional model to satisfy the field results. *Lin et al. (1995)* developed Groundwater Modeling System (GMS) and combined the models 3DFEMWATER and 3DLEWASTE then incorporated as FEMWATER module in to GMS. This FEMWATER model handles all the functions of those two models and additionally

has the option of density driven flow. GMS-FEMWATER was applied to study the herbicide transport in to the water bodies and it was demonstrated to be an effective tool for evaluating the fate of non-point source pollution. Probability and uncertainty were introduced to the density dependent flow and transport model FEMWATER. It was modified by means of Latin Hypercube Sampling (LHS) and comes with an Argus ONE GUI and named as FEMWATER-LHS. Model was validated with two benchmark problems (Hardyanto and Merkel 2007). *Kim et al. (2012)* used GMS-FEMWATER to analyze the seawater intrusion in to the aquifer. Based on the limited field data of water table level, sea level and inflow conditions simulation was run. When setting up or developing the deep groundwater it is important to do the preliminary examination due to the pollution or intrusion of seawater into the aquifer. And this preliminary examination will be useful for the simulation of groundwater pollution distribution.

2.5 Summary

This chapter presents an introduction to Acid Mine Drainage (AMD) followed by the literature review on AMD generation, prevention and neutralizing methods. Transport behaviour of contaminants in aggregated soil is explained by the non-equilibrium mass transfer theory and the following section presents types of non-equilibrium and its merits and limitations along with literature review. Subsequent sections gave information on numerical models, developed and applied to study AMD transport, and the details about FEMWATER model with few literatures studies are also presented. Study of AMD transport needs interdisciplinary knowledge and it is important to understand the reactive transport of AMD to predict its impact on groundwater and for the treatment purpose (in situ treatment). Existing numerical models and experiments are mainly focusing on predicting and mitigating the AMD generation in mine sites, and studying reactive transport of AMD in to aquifers and streams without considering the non-equilibrium effects. So this study attempts to analyse the immobile water effects on the transport of AMD contaminated water from waste rock heap/mine tailings site to the downstream. The scope of the non-equilibrium reactive transport study is to make the model prediction more accurate and to give insight to the process of treatment of mine water. In addition, the study may be useful in the designing of reactive barriers. Tailings observed in the break through curves are due to the release of contaminants from immobile region (to mobile region by diffusion process). This nature, holding the mass and releasing it later, of the dual porosity or dual permeability flow can

be used in the reactive barriers to capture the contaminants. If the captured contaminants in the immobile regions are subject to reactions like oxidation and precipitation it may be more effective in the remediation process.

CHAPTER 3

MODIFICATION AND UPDATION OF FEMWATER MODEL AND ITS VALIDATION

This chapter describes the modifications done in FEMWATER model and its validation. Physical processes like mobile immobile flow, physical non-equilibrium in contaminant mass and chemical reaction (ion-exchange) were added into the USEPA developed FEMWATER model for the simulation of AMD reactive transport scenarios.

3.1 Introduction

Transport of Acid Mine Drainage (AMD) and its reactive nature in the subsurface medium has to be studied intensively. Experimental observations and analysis from field and laboratory studies can give us insights on parameters in field conditions. Using the parameters, mathematical models are very much handy in cases like management and predictive studies as well as for large scale field studies. Numerical transport models are much helpful to interpret and study the nature of reactive transport in the subsurface. Commercially developed software were purpose oriented and contain complex ground properties for better results and those are not made open to public use or for further updating by the general public. Besides, the public domain software may not cater to model all the transport phenomena for porous media. There are very few freely available software packages that can be used to model the AMD in the subsurface environment. These two reasons were the motivation for updating the open source code, FEMWATER, for AMD related contaminant transport study. Since this work is focused on the non-equilibrium mass transfer effects, emphasis was given to the mass transfer of both the liquid and solute between the mobile and immobile regions. FEMWATER contains two modules, 3DFEMWATER and 3DLEWASTE. The transport module, 3DLEWASTE was modified to handle the non-equilibrium solute mass transport and the flow module 3DFEMWATER was modified to accommodate liquid mass transfer between the mobile and immobile regions. Due to the liquid mass transfer between mobile and immobile regions, the seepage velocities of liquid flow in porous media is affected and the corresponding change made in 3DFEMWATER is a significant contribution of this research. FEMWATER is a sequentially coupled model, where flow simulation has to be done first to obtain the pressure heads and liquid flow velocities and thereafter, these values are used in contaminant transport module. The code also allows independent simulations of flow and transport, provided the respective data are available. This chapter presents the modifications done to FEMWATER model and its validation with the literature data.

3.1.1 Finite Element Method (FEM)

In finite element method, the considered problem domain is subdivided in to a set of smaller regions (or) finite elements. Instead of providing continuous solutions as in the exact solutions, FEM concept is to determine solutions at predefined locations. Idea of FEM is to transform the

partial differential equations in to a set of algebraic equations for each node/element. Finite element method procedures are given as follows,

(i) Discretization of the computational domain into a number of elements.

(ii) Selecting element type and their interpolation functions.

(iii) Deriving the finite element equations.

(iv) Assembling the element equations to form a system of equations.

(v) Applying boundary conditions and solving the equations for nodal solutions.

3.1.2 Element type and shape function

The problem domain is divided into line elements in case of 1D problem; space is divided into triangular, rectangular and quadrilateral elements in case of 2D problem. In 3D problem, domain space is divided into tetrahedral, regular and irregular hexahedral elements. The small elements have its own physical properties, in each element flow and transport is described in terms of head and concentration, respectively, in the nodal points. The function employed to represent the nature of the solution inside each element are called shape function/interpolating function/basis function. Regular hexahedral element is used in FEMWATER, since it is a three dimensional model. A linear Shape function of 8-noded hexahedral 3D element with 6 faces and 12 sides is,

$$N_i = (1/8)\left[(1+\xi\xi_i)(1+\mu\mu_i)(1+\varsigma\varsigma_i)\right] \tag{3.1}$$

where, ξ, μ, ς are local coordinates; i is the number of nodes in an element.

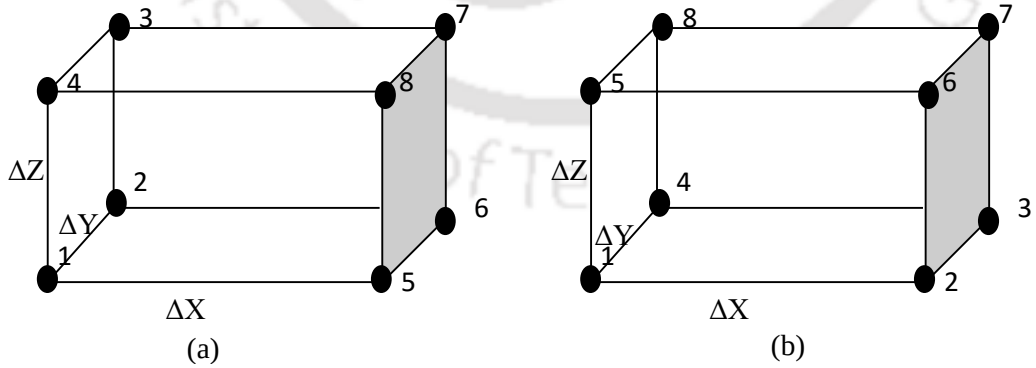

Fig.3.1. Regular hexahedral element

Two types of nodal numbering of an element are followed in FEMWATER, shown in Figure 3.1. In this research, the method shown in Fig 3.1(b) is followed. Nodal numbering technique

in 2D and 3D are based on the least number of nodes in the horizontal or in the vertical direction. That is, if there are 10 nodes in vertical direction and 15 nodes in horizontal direction then the numbering sequence should be in vertical direction to reduce the bandwidth of matrix.

3.2 Pressure head based Richards equation

The pressure head based Richards equation (3.2) in FEMWATER, is solved to get the flow velocity and water content value. Equation (3.2) is known as Richards equation for variably saturated flow, governs fluid flow, also known as single porosity model, can be applicable to the heterogeneous medium as well. However, mass balance errors that may occur during simulations can be overcome by the method of mass lumping.

$$F(h)\frac{\partial h}{\partial t} = \vec{\nabla}\cdot\left[K(h)\left(\vec{\nabla}h + \vec{\nabla}z\right)\right] + q \tag{3.2}$$

where, h is pressure head [L]; z is distance above datum [L]; q is source or sink term [T^{-1}]; K(h) is unsaturated actual hydraulic conductivity [LT^{-1}]; and $F(h)$ is water storage capacity [L^{-1}].

3.2.1 Mixed form Richards equation

Rather than equating pressure head with respect to time and space, the mixed form equation equates the variation of volumetric water content with respect to time and pressure head variation with respect to space.

$$\frac{\partial \theta}{\partial t} = \vec{\nabla}\cdot\left[K(h)\left(\vec{\nabla}h + \vec{\nabla}z\right)\right] + q \tag{3.3}$$

where, θ is volumetric water content [M^3M^{-3}].

3.2.2 Numerical modelling using Galerkin Finite Element Method

In order to solve equation 3.3, using the finite element method, the domain has to be discretized into a number of subdomains, called elements. The variables of moisture content (θ) and pressure head (h) are approximated by an interpolating polynomial of the form; these approximations are made over the elements and nodes

$$\theta(\mathrm{x,y,z},t) \approx \hat{\theta}(\mathrm{x,y,z},t) = \sum_{j=1}^{n}\theta_j(t)M_j(h,\mathrm{N}_j) \tag{3.4}$$

$$h(x,y,z,t) \approx \hat{h}(x,y,z,t) = \sum_{j=1}^{n} h_j(t) N_j(x,y,z) \tag{3.5}$$

where N_j, M_j are basis/shape function of an element; j denotes the number of nodes in an element; $h_j(t)$ and $\theta_j(t)$ are the nodal values of pressure head and water content at time t, respectively. Substituting the approximations given in equations 3.4 and 3.5 into the equation 3.3 and applying the Galerkin criterion, a set of weighted residual minimization equations are generated

$$\int W_i \left[\frac{\partial \hat{\theta}}{\partial t} - \vec{\nabla} \cdot \left[K(h)\left(\vec{\nabla}\hat{h} + \vec{\nabla} z\right)\right] - q \right] dR = 0 \tag{3.6}$$

where, W_i is the weighting functions and R is the region/domain being simulated. For the Galerkin method, the weighting functions are the same as the shape functions, $W_i = N_i$ and if there is linear variation of variables inside an element then M_j equals N_j. Substituting the trial function into the equation 3.6 gives:

$$\int N_i \left[\frac{\partial(\theta_j N_j)}{\partial t} - \vec{\nabla} \cdot \left[K(h)\left(h_j \vec{\nabla} N_j + \vec{\nabla} z\right)\right] - q \right] dR = 0 \tag{3.7}$$

where, i, j = 1,2,3,…n, 'n' is the number of nodes. Integration by parts is used to get rid of all the second order derivatives and gives a set of equations of the form

$$\int N_i N_j dR \frac{d\theta_j}{dt} + \int \nabla N_i K(h) \nabla N_j dR\, h_j - \int N_i n \cdot K(h)\left(h_j \nabla N_j + \nabla z\right) dB + \int K(h)\left(\nabla N_i\right)\left(\nabla z\right) dR - \int N_i q dR = 0 \tag{3.8}$$

where, B is the region boundary. The integrals given in equation 3.8, which are taken over the entire region being modeled, are replaced by the summation of integrals taken over the individual elements. This approximation generates a set of 'n' nodal equations of the form:

$$a_{ij} \frac{d\theta_j}{dt} + B_{ij} h_j = L_i \tag{3.9}$$

where

$$a_{ij} = \sum_{e=1}^{m} \int_{R_e} N_i^e N_j^e dR \tag{3.10}$$

$$B_{ij} = \sum_{e=1}^{m} \int_{R_e} \nabla N_i^e K(h) \nabla N_j^e dR \tag{3.11}$$

$$L_i = \sum_{e=1}^{m}\left[-\int_{R_e} K(h)\nabla N_i^e \nabla z dR + \int_{B_e} n \cdot N_i^e K(h)\left(h_j \nabla N_j + \nabla z\right) dB + \int_{R_e} N_i^e q dR \right] \quad (3.12)$$

where *m* is the number of elements, R_e is the elemental region and N^e is the elemental shape function.

3.2.3 Numerical approximation and solution technique in 3DFEMWATER

Richards equation is approximated using Galerkin FEM and the time differential term is approximated using finite difference method. The nonlinearity of the system, relation between water content versus pressure head and conductivity in unsaturated medium, is treated using Picard iteration and the generated set of linearized equations is solved using a block iterative method. To solve the series of linearized ordinary differential equation 3.9 the time differential is replaced by finite difference formulations. For each time step the solution method involves an outer and inner iterative scheme, where the outer iterations control convergence of the nonlinear terms in the equation and the inner iterative scheme controls the block iterative method solving the linearized set of equations shown in Figure 3.2. For transient simulations, a reduction of the time step size can also help in increasing the stability of the solution scheme.

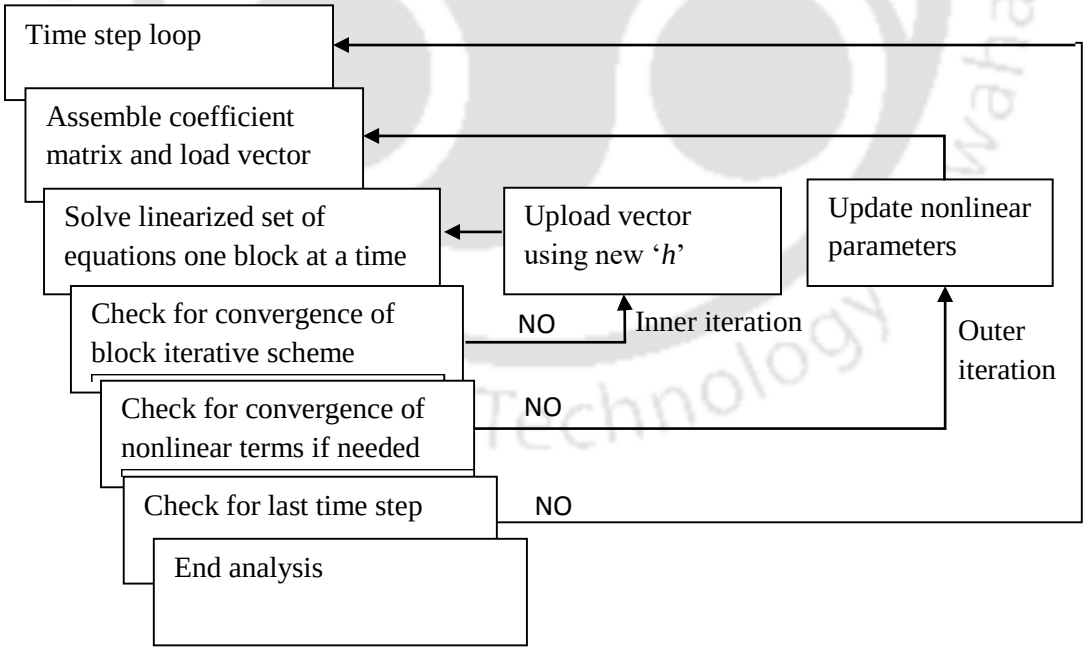

Fig.3.2. Solution scheme for unsaturated flow analysis (Yeh et al. 1992)

A fully implicit scheme with a Picard iterative technique was used for solving the equation 3.9, resulting in

$$a_{ij}\left(\frac{\theta_j^{\,n+1,m+1}-\theta_j^{\,n}}{\Delta t}\right)+B_{ij}^{\,n+1,m}h_j^{\,n+1,m+1}=L_i^{\,n+1,m} \tag{3.13}$$

where *n+1* and *n* represents current and previous time step, respectively, *m+1* represents the current iteration level, *m* the previous iteration level, Δt is the length of the current time step. After Celia et al. (1990), $\theta_j^{n+1,\,m+1}$ is expanded using a first order truncated Taylor series in terms of the pressure head.

$$\theta_j^{\,n+1,m+1}\approx\theta_j^{\,n+1,m}+\left.\frac{d\theta}{dh}\right|^{n+1,m}\left(h_j^{\,n+1,m+1}-h_j^{\,n+1,m}\right) \tag{3.14}$$

where $d\theta/dh$ is water capacity of soil [L^{-1}], hereafter will be mentioned by F(h). Substituting 3.14 to $\theta_{ij}^{n+1,\,m+1}$ in $\frac{\partial\theta}{\partial t}$ gives

$$\frac{\partial\theta}{\partial t}\approx\frac{\theta_j^{\,n+1,m+1}-\theta_j^{\,n}}{\Delta t}=\frac{\theta_j^{\,n+1,m}-\theta_j^{\,n}}{\Delta t}+F\left(h\right)^{n+1,m}\left(\frac{h_j^{\,n+1,m+1}-h_j^{\,n+1,m}}{\Delta t}\right) \tag{3.15}$$

The first term on the right hand side is an explicit estimate for the time derivative of water content, based on the m^{th} Picard level estimates of pressure head. The second term is an estimate of the error in the pressure head at node *j* between two successive Picard iterations; this term diminishes as the Picard iteration process converges. Substituting 3.15 in to 3.13 results in:

$$a_{ij}\left(\frac{\theta_j^{\,n+1,m}-\theta_j^{\,n}}{\Delta t}\right)+a_{ij}F\left(h\right)^{n+1,m}\left(\frac{h_j^{\,n+1,m+1}-h_j^{\,n+1,m}}{\Delta t}\right)+B_{ij}^{\,n+1,m}h_j^{\,n+1,m+1}=L_i^{\,n+1,m} \tag{3.16}$$

$$\left(\frac{a_{ij}F\left(h\right)^{n+1,m}}{\Delta t}+B_{ij}^{\,n+1,m}\right)\left(h_j^{\,n+1,m+1}\right)=L_i^{\,n+1,m}+\left(\frac{a_{ij}F\left(h\right)^{n+1,m}}{\Delta t}\right)h_j^{\,n+1,m}-a_{ij}\left(\frac{\theta_j^{\,n+1,m}-\theta_j^{\,n}}{\Delta t}\right) \tag{3.17}$$

For each time step the solution method involves an outer and inner iterative scheme, where the outer iterations control convergence of the nonlinear terms in the equation and the inner iterative scheme controls the block iterative method solving the linearized set of equations. For transient simulations, reduction of the time step can also help increase the stability of the solution scheme.

3.3 Dual porosity/mobile-immobile flow

Dual porosity flow in the unsaturated zone is a completely different conceptualization than single porosity model. In dual porosity model the assumption is that fraction of water flows faster through preferential paths and the remaining fraction of water holds on to the soil matrix and moves relatively very slow. As a result, water flow in dual porosity medium at given depth at particular time may differ from the water flow simulated by the single domain/porosity model.

3.3.1 Governing equation

The volumetric water content is divided into two regions. There is a mobile region and immobile region, which is sticking to the soil particles and flow velocity is negligible while compared to the mobile region flow velocity, thus θ is now split as follows

$$\theta = \theta_m + \theta_{im} \tag{3.18}$$

Based on the assumption of separation of regions, the flow equation gets modified and having the mobile and immobile components (Van Genuchten et al. 1977) and assumption of residual water content (θ_r) term zero, effective saturation of mobile and immobile region is defined based on the assumptions from Van Genuchten formula which describes the relationship between soil moisture and pressure head in the unsaturated zone.

$$\frac{\partial \theta_m}{\partial t} + \frac{\partial \theta_{im}}{\partial t} = \vec{\nabla} \cdot \left[K\left(h\right)\left(\vec{\nabla} h + \vec{\nabla} z\right)\right] + q \tag{3.19}$$

$$\frac{\partial \theta_{im}}{\partial t} = \Gamma_w \left(S_{e(m)} - S_{e(im)} \right) \tag{3.20}$$

$$K\left(h\right) = k_r K_s = \left(\theta_e \left[1 - \left(1 - \theta_e^{(1/\mathrm{m})} \right)^m \right]^2 \right) * K_s \tag{3.21}$$

$$\theta_e = \frac{\theta\left(h\right) - \theta_r}{\theta_s - \theta_r} \tag{3.21a}$$

$$\theta_m\left(h\right) = \begin{cases} \dfrac{\left(\theta_s * \varphi\right)}{\left[1 + \left(\alpha \left| h - h_a \right| \right)^{n_1} \right]^m} & ; \text{ for } h < h_a \\ \left(\theta_s * \varphi\right) & ; \text{ for } h \geq h_a \end{cases} \tag{3.22}$$

$$S_{e(m)} = \frac{\theta_m(h)}{\theta_s * \varphi} \tag{3.23}$$

$$S_{e(im)} = \frac{\theta_{im}}{\theta_s * (1-\varphi)} \tag{3.24}$$

where θ_m is mobile water content, θ_{im} is immobile water content, Γ_w is the first order mass transfer coefficient (T^{-1}), φ is ratio of mobile water content with total water content (-), α is soil specific coefficient, $S_{e(m)}$ and $S_{e(im)}$ are effective saturation of mobile and immobile water region, respectively. Substitution of the trial function for variables into the equation 3.19 and applying the Galerkin criterion generates a set of weighted residual minimization equation of the form

$$\int N_j \left[\frac{\partial \hat{\theta}_m}{\partial t} + \frac{\partial \hat{\theta}_{im}}{\partial t} - \nabla \cdot \left[K(h)\left(\nabla \hat{h} + \nabla z\right)\right] - q \right] dR = 0 \tag{3.25}$$

Second order terms can be removed by applying the integration by parts

$$\int N_i N_j dR \left(\frac{\partial \theta_{mj}}{\partial t} + \frac{\partial \theta_{imj}}{\partial t} \right) + \int \nabla N_i K(h) \nabla N_j dR\ h_j - \int N_i \hat{n} \cdot K(h)\left(h_j \nabla N_j + \nabla z\right) dB + \int K(h) \nabla N_i (\nabla z) dR - \int N_i q dR = 0 \tag{3.26}$$

After approximation a set of *n* nodal equations of the form was generated

$$a_{ij}\left(\frac{d\theta_{mj}}{dt} + \frac{d\theta_{imj}}{dt} \right) + B_{ij} h_j = L_i \tag{3.27}$$

$$\frac{d\theta_{imj}}{dt} \approx \frac{\theta_{imj}^{\,n+1,m+1} - \theta_{imj}^{\,n}}{\Delta t} \tag{3.28}$$

As discussed in the section 3.2.3, $\theta_{mj}^{\,n+1,\,m+1}$ is expanded as

$$\theta_{mj}^{\,n+1,m+1} \approx \theta_{mj}^{\,n+1,m} + \left.\frac{d\theta_m}{dh}\right|^{n+1,m} * \left(h_j^{\,n+1,m+1} - h_j^{\,n+1,m} \right) \tag{3.29}$$

An explicit finite difference formulation for change in immobile water content is given as

$$\theta_{imj}^{n+1,m+1} = \theta_{imj}^{n} + \Delta t\left[\Gamma_w * \left(S_{em}^{n+1,m} - S_{eim}^{n+1,m}\right)\right] \tag{3.30}$$

$$a_{ij}\left(\frac{\theta_{mj}^{n+1,m} - \theta_{mj}^{n}}{\Delta t}\right) + a_{ij}F\left(h^{n+1,m}\right)\left(\frac{h_{mj}^{n+1,m+1} - h_{mj}^{n+1,m}}{\Delta t}\right) + a_{ij}\left(\frac{\theta_{imj}^{n+1,m} - \theta_{imj}^{n}}{\Delta t}\right) + B_{ij}^{n+1,m}h_j^{n+1,m+1} = L_i^{n+1,m} \tag{3.31}$$

where

$$a_{ij} = \sum_{e=1}^{m}\int_{R_e} N_i^e N_j^e dR \tag{3.32}$$

$$B_{ij} = \sum_{e=1}^{m}\int_{R_e} \nabla N_i^e K\left(h\right)\nabla N_j^e dR \tag{3.33}$$

$$L_i = \sum_{e=1}^{m}\left[-\int_{R_e} K\left(h\right)\nabla N_i^e \nabla z dR + \int_{B_e} n\cdot N_i^e K\left(h\right)\left(h_j\nabla N_j + \nabla z\right)dB + \int_{R_e} N_i^e q dR\right] \tag{3.34}$$

After rearranging the known and unknown terms respectively on the right and left hand sides the following final nodal equation for dual porosity flow is obtained as

$$\left(\left(\frac{a_{ij}}{\Delta t} * \mathrm{F}\left(h^{n+1,m}\right)\right) + B_{ij}^{n+1,m}\right)\left(h_j^{n+1,m+1}\right) = L_i^{n+1,m} + \left(\frac{a_{ij}}{\Delta t} * \mathrm{F}\left(h^{n+1,m}\right)\right)h_j^{n+1,m} - \frac{a_{ij}}{\Delta t}\left[\left(\theta_{mj}^{n+1,m} - \theta_{mj}^{n}\right) + \left(\theta_{imj}^{n+1,m} - \theta_{imj}^{n}\right)\right] \tag{3.35}$$

An explicit formulation is sensitive to the time step size and a Δt restriction has to be imposed, to avoid this an implicit formulation is used to define the change in immobile water content, as follows,

$$\theta_{imj}^{n+1,m+1} = \theta_{imj}^{n} + \Delta t\left[\Gamma_w * \left(S_{emj}^{n+1,m+1} - S_{eimj}^{n+1,m+1}\right)\right] \tag{3.36}$$

$$S_{emj}^{n+1,m+1} = \frac{\theta_{mj}\left(h_j^{n+1,m+1}\right)}{\theta_{sm}};\quad S_{eimj}^{n+1,m+1} = \frac{\theta_{imj}^{n+1,m+1}}{\theta_{sim}} \tag{3.37}$$

Substituting the effective saturation of mobile and immobile region values into the above equation and rearranging gives the following equation,

$$\theta_{imj}^{\,n+1,m+1}=\left(\frac{\theta_{sim}}{\theta_{sim}+\left(\Gamma_w*\Delta t\right)}\right)\left[\theta_{imj}^{\,n}+\left(\frac{\Gamma_w*\Delta t}{\theta_{sm}}\right)\left(\theta_{mj}^{\,n+1,m+1}\right)\right] \tag{3.38}$$

$$a_{ij}\left(\frac{\theta_{mj}^{\,n+1,m+1}-\theta_{mj}^{\,n}}{\Delta t}+\frac{\theta_{imj}^{\,n+1,m+1}-\theta_{imj}^{\,n}}{\Delta t}\right)+B_{ij}^{n+1,m}\left(h_j^{n+1,m+1}\right)=L_i^{\,n+1,m} \tag{3.39}$$

Substitution of the present time step and present iterate value of immobile water content in to the above equation 3.39 yields

$$\frac{a_{ij}}{\Delta t}\left[\left(\left(\frac{\theta_{sim}}{\theta_{sim}+\left(\Gamma_w*\Delta t\right)}\left(\frac{\Gamma_w*\Delta t}{\theta_{sim}}\right)\right)+1\right)\left(\theta_{mj}^{n+1,m+1}\right)-\theta_{mj}^{n}+\left(\frac{\theta_{sim}}{\theta_{sim}+\left(\Gamma_w*\Delta t\right)}-1\right)\theta_{imj}^{n}\right] \tag{3.40}$$

$$+B_{ij}^{n+1,m}\left(h_j^{n+1,m+1}\right)=L_i^{\,n+1,m}$$

$$\frac{a_{ij}}{\Delta t}\left[\left(D1*\theta_{mj}^{n+1,m+1}\right)-\theta_{mj}^{n}+\left(D2*\theta_{imj}^{n}\right)\right] \tag{3.41}$$

$$+B_{ij}^{n+1,m}\left(h_j^{n+1,m+1}\right)=L_i^{\,n+1,m}$$

$$D1=1+\left(\frac{\theta_{sim}}{\theta_{sim}+\left(\Gamma_w*\Delta t\right)}\left(\frac{\Gamma_w*\Delta t}{\theta_{sim}}\right)\right);\qquad D2=\left(\frac{\theta_{sim}}{\theta_{sim}+\left(\Gamma_w*\Delta t\right)}\right)-1 \tag{3.41a}$$

Based on equation 3.14 equation 3.41 can be written as

$$\frac{a_{ij}}{\Delta t}\left[\left(\left(D1*\theta_{mj}^{n+1,m}\right)-\theta_{mj}^{n}\right)+\left(\left[D1*\left(F\left(h_j^{n+1,m}\right)\left(h_j^{n+1,m+1}-h_j^{n+1,m}\right)\right)\right]\right)+\left(D2*\theta_{imj}^{n}\right)\right] \tag{3.42}$$

$$+B_{ij}^{n+1,m}\left(h_j^{n+1,m+1}\right)=L_i^{\,n+1,m}$$

$$\left[\left(\frac{a_{ij}}{\Delta t}*F\left(h_j^{n+1,m}\right)*D1\right)+B_{ij}^{n+1,m}\right]h_j^{n+1,m+1}=L_i^{\,n+1,m}+\left(\frac{a_{ij}}{\Delta t}*F\left(h_j^{n+1,m}\right)*D1\right)h_j^{n+1,m} \tag{3.43}$$

$$-\frac{a_{ij}}{\Delta t}\left[\left(\left(D1*\theta_{mj}^{n+1,m}\right)-\theta_{mj}^{n}\right)+\left(D2*\theta_{imj}^{n}\right)\right]$$

3.3.2 Validation of mobile-immobile water flow problem

The modified FEMWATER flow model was verified for a one dimensional mobile/immobile infiltration problem using the results from a review study (Simunek et al. 2003). Van Genuchten relationship functions of soil mobile and immobile moisture content are given in Table 3.1. The problem geometry is depicted in the Figure 3.3, which describes a soil column of 60 cm height filled with loamy soil. The pressure head of -150 cm was set as initial condition and the soil hydraulic and numerical parameters are given in Table 3.2. At the top, column is provided with 1 cm ponding depth, bottom of the column is provided with fixed head condition of -150 cm. Validation is shown in the Figure 3.4.

Table.3.1. Van Genuchten relationship and functions of soil mobile and immobile moisture content

Mobile region	**Immobile region**
$\theta_{sm} = \theta_s * \varphi \;;\; \varphi = 0 \; to \; 1 \left(\varphi = \frac{\theta_{fm}}{\theta} \right)$	$\theta_{sim} = \theta_s * (1 - \varphi)$
$T_{initial}$ $\theta_m(h) = \frac{\theta_{sm}}{\left[1 + \left(\alpha \lvert h_{in} - h_a \rvert\right)^{n_1}\right]^m}$ for $h_{in} < h_a$ $\theta_m(h) = \theta_{sm}$ for $h_{in} > h_a$	$T_{initial}$ $\theta_{im}(h) = \frac{\theta_{sim}}{\left[1 + \left(\alpha \lvert h_{in} - h_a \rvert\right)^{n_1}\right]^m}$ for $h_{in} < h_a$ $\theta_{im}(h) = \theta_{sim}$ for $h_{in} > h_a$
$S_e = \left[1 + \left(\alpha \lvert h - h_a \rvert\right)^{n_1}\right]^{-m}$ for $h < h_a$ $S_e = 1$ for $h > h_a$	NA
T > $T_{initial}$ $\theta_m(h) = \frac{\theta_{sm}}{\left[1 + \left(\alpha \lvert h - h_a \rvert\right)^{n_1}\right]^m}$ for $h < h_a$ $\theta_m(h) = \theta_{sm}$ for $h > h_a$	T > $T_{initial}$ $\theta_{imj}^{n+1,m+1} = \left(\frac{\theta_{sim}}{\theta_{sim} + (\Gamma_w * \Delta t)} \right) \left(\theta_{imj}^{n} + \left[\left(\frac{\Gamma_w * \Delta t}{\theta_{sm}} \right) \left(\theta_{mj}^{n+1,m+1} \right) \right] \right)$ $j = 1,2,3,....,n; n - number$ of nodes
$S_{emj}^{n+1,m+1} = \frac{\theta_{mj}\left(h_j^{n+1,m+1}\right)}{\theta_{sm}}$ $j = 1,2,3,....,n; n - number$ of nodes	$S_{eimj}^{n+1,m+1} = \frac{\theta_{imj}^{n+1,m+1}}{\theta_{sim}}$ $j = 1,2,3,....,n; n - number$ of nodes

$K(h) = K_s * \left(\theta_e^{0.5} \left[1 - \left(1 - \theta_e^{(1/m)} \right)^m \right]^2 \right)$ for $h < h_a$ $K(h) = K_s$ for $h > h_a$	NA

Table.3.2. Parameters for mobile-immobile water flow validation problem (Simunek et al. 2003)

Parameters	**Values**
Residual water content, θ_r	0.0
Saturated mobile water content, θ_{sm}	0.20
Saturated immobile water content, θ_{sim}	0.15
Saturated water content, θ_s	0.35
Van Genuchten α and n	0.041 cm^{-1} and 1.964
Saturated hydraulic conductivity, K_s	0.000722 cms^{-1}
Initial pressure head, h_{in}	-150 cm
Mass transfer constant, Γ_w	0.00001 s^{-1}
Simulation time, T_{sim} and Δt	2 h and 0.01388 h
Spatial discretization, Δz	0.1 cm
Length,	60 cm
Dirichlet boundary at Top and bottom	1 cm and -150 cm

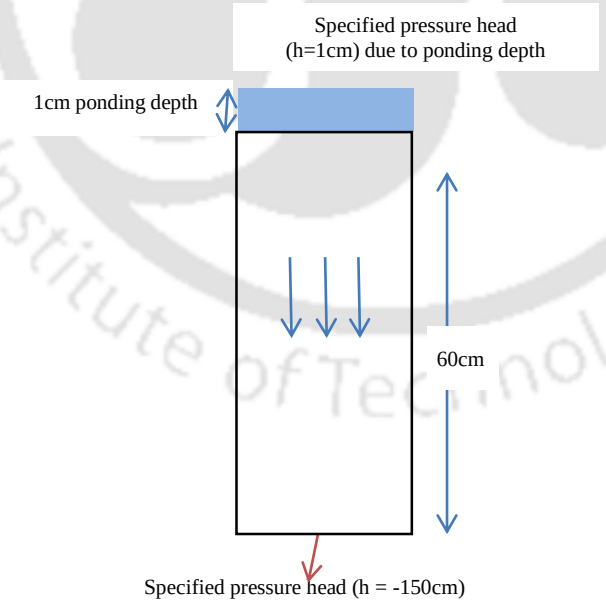

Fig.3.3. Representation of one dimensional soil column (Simunek et al. 2003) for modified FEMWATER flow validation

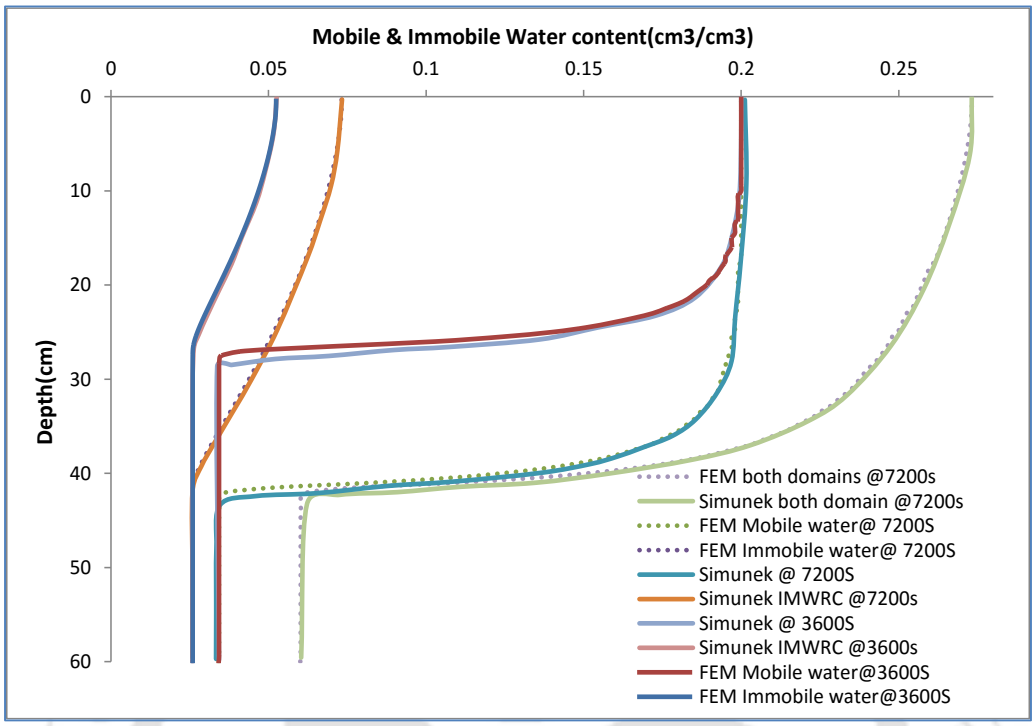

Fig.3.4. Validation of FEMWATER mobile-immobile water flow with Simunek et al. (2003)

3.4 Transport with non-equilibrium mass transfer

In the solute transport equation, fractions of mobile and immobile water contaminant (C_m, C_{im}) and mass transfer rate coefficient to model the physical non-equilibrium contaminant transport was included. θ_m and θ_{im} are the notations used for mobile and immobile water content, respectively, which was the notation used by Van Genuchten et al. (1976)

$$\left(\theta_m+\rho_b \mathrm{fk}_d\right)\frac{\partial C_m}{\partial t}+\left[\theta_{im}+\left(1-f\right)\rho_b k_d\right]\frac{\partial C_{im}}{\partial t}-C_m\frac{\partial \theta_{im}}{\partial t}=\vec{\nabla}\cdot\left(\theta_m D\vec{\nabla}C_m\right)-V\cdot\vec{\nabla}C_m-\lambda\left(\theta_m C_m+\rho_b S\right)+QC_{in}-QC_m \tag{3.44}$$

$$\left[\theta_{im}+\left(1-f\right)\rho_b k_d\right]\frac{\partial C_{im}}{\partial t}=\Gamma_c\left(C_m-C_{im}\right)-QC_{im} \tag{3.45}$$

In order to solve equation 3.44 and 3.45 using the finite element method it begins with the discretization of the domain into a number of subdomains called elements. The variables C_m and C_{im} are approximated by an interpolating polynomial of the form:

$$C_m\left(\mathrm{x,y,z},t\right)\approx\hat{C}_m\left(\mathrm{x,y,z},t\right)=\sum_{j=1}^{n}C_{mj}\left(t\right)N_j\left(\mathrm{x,y,z}\right) \tag{3.46}$$

$$C_{im}(\mathrm{x,y,z},t) \approx \hat{C}_{im}(\mathrm{x,y,z},t) = \sum_{j=1}^{n} C_{imj}(t) N_j(\mathrm{x,y,z}) \tag{3.47}$$

where N_j, M_j are basis/shape function of an element; j denotes the number of nodes in an element; $C_m(t)$ and $C_{im}(t)$ are the nodal values of mobile concentration and immobile concentration at time t, respectively. Weighted residual minimization equation is generated by substituting trial function for dependent variable and applying Galerkin formulation.

$$\int \mathrm{N}_i \left(\left(\theta_m + \rho_b \mathrm{fk}_d\right) \frac{\partial \hat{C}_m}{\partial t} + \left(\theta_{im} + \left[1-f\right]\rho_b \mathrm{k}_d\right) \frac{\partial \hat{C}_{im}}{\partial t} - \vec{\nabla} \cdot \left(\theta_m D \nabla \hat{C}_m\right) + V \cdot \vec{\nabla} \hat{C}_m + \lambda\left(\theta_m \hat{C}_m + \rho_b S\right) - QC_{in} + Q\hat{C}_m - \frac{\partial \theta_{im}}{\partial t} \hat{C}_m \right) dR = 0 \tag{3.48}$$

$$\int N_i \left(\left[\theta_{im} + \left(1-f\right)\rho_b \mathrm{k}_d\right] \frac{\partial \hat{C}_{im}}{\partial t} - \Gamma_c \left(\hat{C}_m - \hat{C}_{im}\right) - Q\hat{C}_{im} \right) dR = 0 \tag{3.49}$$

where, $\mathbf{N_i}$ is the shape function that is same as weighting function in Galerkin method and **R** denotes the region of interest. Integration by parts can be applied to the second order terms to make sure that the continuity of dependent variable is maintained along the element surfaces and substituting the trail function into the equation gives

$$\begin{aligned} &\int \mathrm{N}_i \mathrm{N}_j \left(\theta_{mj} + \rho_b \mathrm{fk}_d\right) dR \left(\frac{\partial C_{mj}}{\partial t} \right) + \int \mathrm{N}_i \mathrm{N}_j \left[\theta_{imj} + \left(1-f\right)\rho_b \mathrm{k}_d\right] dR \left(\frac{\partial C_{imj}}{\partial t} \right) + \int \nabla \mathrm{N}_i \theta_{mj} D_m \nabla \mathrm{N}_j dR \left(C_{mj}\right) - \\ &\int n\theta_{mj} D_m \nabla \mathrm{N}_j dB \left(C_{mj}\right) + \int \mathrm{N}_i V_m \nabla \mathrm{N}_j dR \left(C_{mj}\right) + \int \mathrm{N}_i \mathrm{N}_j \left[\lambda\left(\theta_{mj} + \rho_b S\right) + Q\right] dR \left(C_{mj}\right) - \int \mathrm{N}_i Q dR C_{in} - \frac{\partial \theta_{im}}{\partial t} \int N_i N_j C_{mj} dR = 0 \end{aligned} \tag{3.50}$$

$$\int N_i N_j \left[\theta_{imj} + \left(1-f\right)\rho_b \mathrm{k}_d\right] dR \left(\frac{\partial C_{imj}}{\partial t} \right) - \int N_i N_j \Gamma_c dR \left(C_{mj} - C_{imj}\right) + \int N_i N_j Q C_{imj} dR = 0 \tag{3.51}$$

where, B is the region boundary. The integrals given in the above equations are taken over the entire modeling domain, can be replaced by the summation of integrals taken over the individual elements. This approximation generates a set of n nodal equations of the form:

$$A_{ij} \frac{dC_{mj}}{dt} + B_{ij} \frac{dC_{imj}}{dt} + \left(D_{ij} + E_{ij} - \frac{\partial \theta_{im}}{\partial t} \right) C_{mj} = R_i \tag{3.52}$$

where i, j =1, 2, 3, ... n (nodes) ,

$$A_{ij} = \sum_{k=1}^{m} \int_{R_e} N_i^e N_j^e \left(\theta_{mj} + \rho_b \mathrm{fk}_d\right) dR \tag{3.52a}$$

$$B_{ij} = \sum_{k=1}^{m} \int_{R_e} N_i^e N_j^e \left(\theta_{imj} + \left(1-f\right)\rho_b \mathrm{k}_d\right) dR \tag{3.52b}$$

$$D_{ij} = \sum_{k=1}^{m} \int_{R_e} \left[\nabla N_i^e \;\; \theta_{mj} D \;\; \nabla N_j^e \right] + N_i^e V_m \nabla N_j^e \; dR \tag{3.52c}$$

$$E_{ij} = \sum_{k=1}^{m} \int_{R_e} N_i^e \left[\lambda \;\; \theta_{mj} + \rho_b \, \mathrm{k}_d \;\; + \mathrm{Q} \right] N_j^e dR \tag{3.52d}$$

$$R_i = \sum_{k=1}^{m} \left[\int_{R_e} Q N_i^e dR \;\; C_{in} \;\; + \int_{B_e} n \cdot \theta_{mj} D_m \nabla N_j^e dB \;\; C_{mj} \right] \tag{3.52e}$$

3.4.1 Numerical approximation and solution technique in 3DLEWASTE

3DLEWASTE model was developed to simulate solute transport in porous media. Equation (1.12) is approximated by a Galerkin finite element technique. Approximation of backward differencing in time is applied for time derivative term. The solution method involves an inner iterative scheme which controls the block iterative method of solving the linear equations at each time step. When non-linear isotherms are used solution method involves an outer iterative scheme, where iterations help in the convergence of the non-linear terms. For each non-linear iteration, linearized set of equations is solved using the concentration values, stored and updated, of previous non-linear iteration. To solve the series of linearized ordinary differential equations (3.52), an implicit finite difference formulation is used to replace the time differential, resulting in

$$A_{ij}^{n+1} \left(\frac{C_{mj}^{n+1} - C_{mj}^{n}}{\Delta t} \right) + B_{ij}^{n+1} \left(\frac{C_{imj}^{n+1} - C_{imj}^{n}}{\Delta t} \right) + \left(D_{ij}^{n+1} + E_{ij}^{n+1} - \left(\frac{\theta_{im}^{n+1} - \theta_{im}^{n}}{\Delta t} \right) \right) C_{mj}^{n+1} = R_i^{n+1} \tag{3.53}$$

where, *m* represents the number of elements; N^e is the element shape function; and *B* denotes the boundary region; n+1 and n represents the current and previous time steps, respectively.

$$\frac{A_{ij}^{n+1}}{\Delta t} \left(C_{mj}^{n+1} \right) + \frac{B_{ij}^{n+1}}{\Delta t} \left(C_{imj}^{n+1} \right) + \left(D_{ij}^{n+1} + E_{ij}^{n+1} - \left(\frac{\theta_{im}^{n+1} - \theta_{im}^{n}}{\Delta t} \right) \right) C_{mj}^{n+1} = R_i^{n+1} + \frac{A_{ij}^{n+1}}{\Delta t} \left(C_{mj}^{n} \right) + \frac{B_{ij}^{n+1}}{\Delta t} \left(C_{imj}^{n} \right) \tag{3.54}$$

The above equation contains two unknown variables; the mobile concentration (C_m) and the immobile concentration (C_{im}). To find immobile concentration, the mobile concentration is also needed, so immobile concentration equation can be solved by the finite difference method for nodal values as given below

$$\left(\frac{\theta_{imj}+\left[1-f\right]\rho_b \mathrm{k}_d}{\Delta t}\right)\left(C_{imj}^{n+1}\right)-\left(\frac{\theta_{imj}+\left[1-f\right]\rho_b \mathrm{k}_d}{\Delta t}\right)\left(C_{imj}^{n}\right)=\Gamma_c\left(C_{mj}^{n+1}-C_{imj}^{n+1}\right)-Q\left(C_{imj}^{n+1}\right) \quad (3.55)$$

$$\left(\frac{\theta_{imj}+\left[1-f\right]\rho_b \mathrm{k}_d}{\Delta t}+\Gamma_c+Q\right)\left(C_{imj}^{n+1}\right)=\Gamma_c\left(C_{mj}^{n+1}\right)+\left(\frac{\theta_{imj}+\left[1-f\right]\rho_b \mathrm{k}_d}{\Delta t}\right)\left(C_{imj}^{n}\right) \quad (3.56)$$

$$C_{imj}^{n+1}=\left(\left(\frac{\theta_{imj}+\left[1-f\right]\rho_b \mathrm{k}_d}{\Delta t}+\Gamma+Q\right)^{-1}\right)\left(\Gamma\left(C_{mj}^{n+1}\right)+\left[\left(\frac{\theta_{imj}+\left[1-f\right]\rho_b \mathrm{k}_d}{\Delta t}\right)\left(C_{imj}^{n}\right)\right]\right) \quad (3.57)$$

$$IM=\frac{\theta_{imj}+\left(\left[1-f\right]\rho_b \mathrm{k}_d\right)}{\Delta t}$$

$$C_{imj}^{n+1}=\left(\frac{\Gamma_c}{\left(IM+\Gamma_c+Q\right)}\right)\left(C_{mj}^{n+1}\right)+\left(\frac{IM}{\left(IM+\Gamma_c+Q\right)}\right)\left(C_{imj}^{n}\right) \quad (3.58)$$

Now substitute the above immobile concentration formulation in to main equation (3.54) and equate known and unknown values

$$\frac{A_{ij}^{n+1}}{\Delta t}\left(C_{mj}^{n+1}\right)+\frac{B_{ij}^{n+1}}{\Delta t}\left(\left(\frac{\Gamma_c}{\left(IM+\Gamma_c+Q\right)}\right)\left(C_{mj}^{n+1}\right)+\left(\frac{IM}{\left(IM+\Gamma_c+Q\right)}\right)\left(C_{imj}^{n}\right)\right)+$$

$$\left(D_{ij}^{n+1}+E_{ij}^{n+1}-\left(\frac{\theta_{im}^{n+1}-\theta_{im}^{n}}{\Delta t}\right)\right)C_{mj}^{n+1}=R_i^{n+1}+\frac{A_{ij}^{n+1}}{\Delta t}\left(C_{mj}^{n}\right)+\frac{B_{ij}^{n+1}}{\Delta t}\left(C_{imj}^{n}\right) \quad (3.59)$$

$$\left(\frac{A_{ij}^{n+1}}{\Delta t}+\frac{B_{ij}^{n+1}}{\Delta t}\left(\frac{\Gamma_c}{IM+\Gamma_c+Q}\right)+D_{ij}^{n+1}+E_{ij}^{n+1}-\left(\frac{\theta_{im}^{n+1}-\theta_{im}^{n}}{\Delta t}\right)\right)C_{mj}^{n+1}=$$

$$R_i^{n+1}+\frac{A_{ij}^{n+1}}{\Delta t}\left(C_{mj}^{n}\right)+\left[\frac{B_{ij}^{n+1}}{\Delta t}-\frac{B_{ij}^{n+1}}{\Delta t}\left(\frac{IM}{IM+\Gamma_c+Q}\right)\right]\left(C_{imj}^{n}\right) \quad (3.60)$$

FEMWATER software, which is coded using FORTRAN 77, is subsequently modified using the formulations described in equations 3.60.

3.4.2 Validation of non-equilibrium transport problem

The modified FEMWATER transport model was verified for a one dimensional dual porosity transport model using the results from an experimental study by van Genuchten et al. (1976). The problem geometry is depicted in the Figure 3.5, where the soil column is of 30 cm height which is filled with Glendale clay loam. A zero concentration is set as the initial condition and the transport and numerical parameters are given in Table 3.3, top portion of the soil column is leached with tritium. Validation are shown in Figures 3.6 and 3.7.

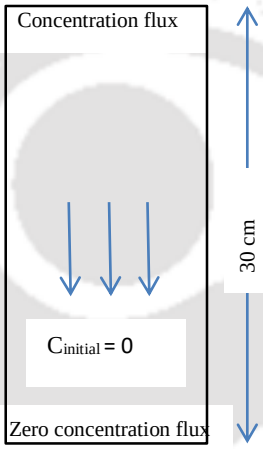

Fig.3.5 One dimensional soil column for modified FEMWATER transport validation for constant mobile – immobile water content

Table.3.3. Parameters for the validation of FEMWATER non-equilibrium transport problem (van Genuchten et al. 1976)

Parameters	**Values**
Darcy flux, q	5.54cmd^{-1}
Water content, θ	0.399
Mobile water content, θ_m	0.21307
Van Genuchten α and n	0.041 cm^{-1} and 1.964
Diffusion coefficient, D_m	22 cmd^{-1}
Mass transfer constant, Γ_c	0.28 d^{-1}
Simulation time, T_{sim} and Δt	13 days and 0.01
Length	30cm
Space discretization, Δz	0.1cm
Source concentration	1g/cm^3
Concentration pulse time (t)	6.822d
Soil type	Glendale clay loam soil

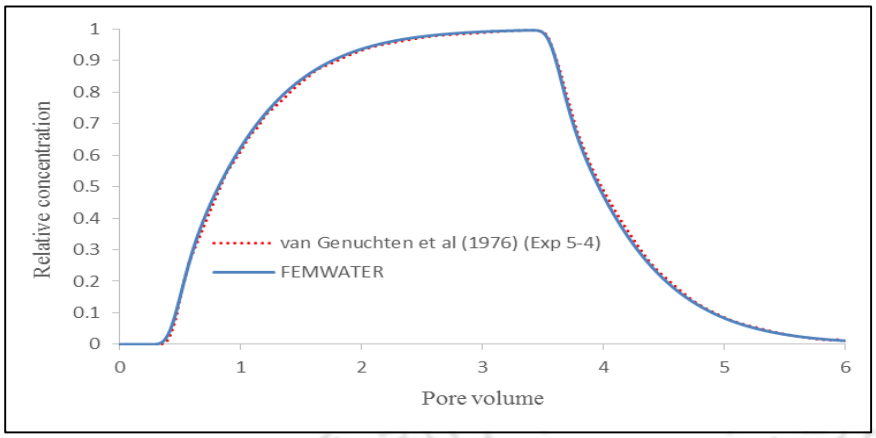

Fig.3.6 Validation of FEMWATER non-equilibrium concentration transport with Van Genuchten et al. (1976)

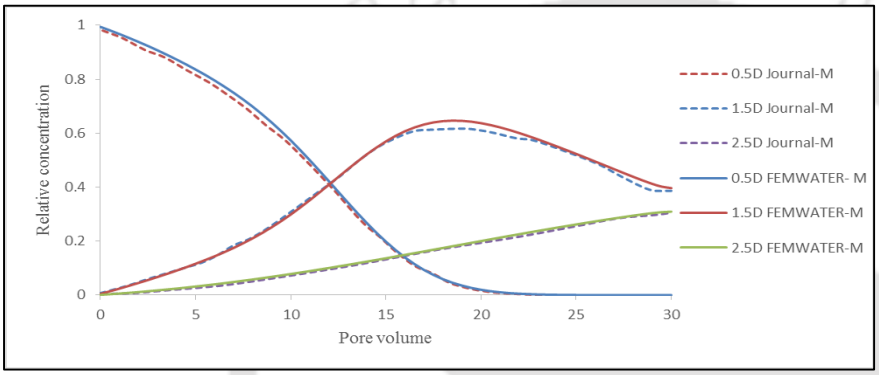

(a)

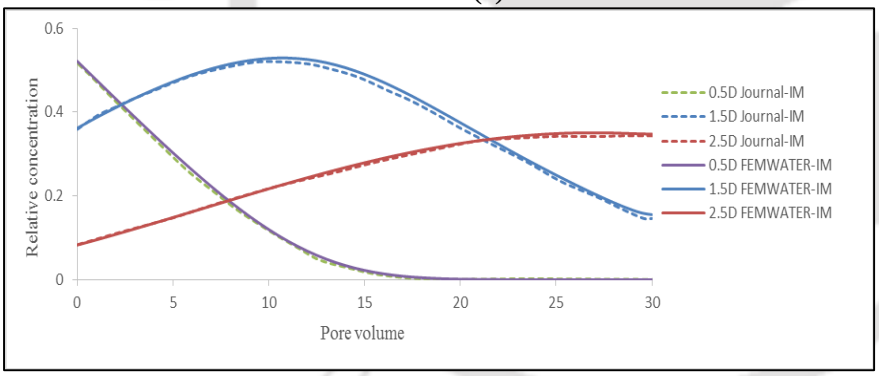

(b)

Fig.3.7 Validation of FEMWATER simulation with Van Genuchten et al., (1976) for concentration inside the column with pulse duration of 1 day for (a) mobile and (b) immobile concentration. (JOURNAL-M and JOURNAL-IM refers concentration in mobile and immobile water, respectively, from Van Genuchten et al., (1976))

3.5 Ion Exchange

Ion exchange is a special type of adsorption characterized by a replacement of an adsorbed ion with an exchangeable ion from solution (Stumm and Morgan, 1996). The unwanted ion in the solution can be replaced by other ions, which will not be considered as contaminant to the environment, in that way the solution is purified. Precipitation, oxidation and reduction, ion exchange and adsorption are some of the important reactions taking place during the transport of AMD in subsurface. Exchange reactions can be considered as one of the mechanisms governing

the fate of metals in soil (Valocchi, 1984). During the modeling process, ion exchange and adsorption cannot be modeled at the same time. Four classes of ion exchange processes (monovalent-monovalent, monovalent-divalent, divalent-divalent and divalent-monovalent) follow mass-action equilibrium for the relation (Grove et al, 1984)

$$uc_1^v + v\bar{c}_2 \rightleftharpoons u\bar{c}_1 + nc_2^u \tag{3.61}$$

where *v* and *u* are the valence of ion 1 and ion 2, respectively. The thermodynamic equilibrium coefficient for above ion exchange reaction is

$$k_{ex} = \frac{\left[\bar{c}_1\right]^u \left[c_2\right]^v}{\left[c_1\right]^u \left[\bar{c}_2\right]^u} \tag{3.62}$$

If the total solution concentration (c_1+c_2) and ion exchange capacity (or) total sorbed concentrations ($\bar{c}_1 + \bar{c}_2$) is constant, and only two ions are involved, then

$$\begin{aligned} vc_1 + uc_2 &= c_0 \\ v\bar{c}_1 + u\bar{c}_2 &= \bar{c}_0 \end{aligned} \tag{3.63}$$

Values of c_1 and c_2 are derived and substituted in the above equation to eliminate ion 2 from the equation, and the slope of the ion exchange isotherm can be computed as below, for the monovalent- monovalent (v=u=1) ion exchange reaction.

$$\bar{c} = \frac{k_{ex}\bar{c}_0 C}{\mathrm{C}\left(\mathrm{k}_{ex} - 1\right) + \mathrm{c}_0} \tag{3.64}$$

$$\frac{d\bar{c}}{dC} = \frac{k_{ex}\bar{c}_0 c_0}{\left[\mathrm{C}\left(\mathrm{k}_{ex} - 1\right) + \mathrm{c}_0\right]^2} \tag{3.65}$$

If the assumption of constant total concentration ($C=c_1+c_2$) is made, then there is a similarity that exists between divalent-monovalent and monovalent-monovalent ion exchange. Hence, heterovalent and homovalent exchanges are analogous to each other (Dou and Jin, 1996). These ion exchange isotherms can be incorporated in to the contaminant transport equation.

3.5.1 Inclusion of ion exchange reaction into FEMWATER Model

The governing equation for advective-dispersion solute transport through porous media based on the laws of conservation of mass and flux can be written as, given in equation 1.12;

$$\theta\frac{\partial C}{\partial t}+\rho_b\frac{\partial \bar{C}}{\partial t}=\vec{\nabla}\cdot\left(\theta D\vec{\nabla}C\right)-V\cdot\vec{\nabla}C-\lambda\left(\theta C+\rho_b\bar{C}\right)+QC_{in}-QC \tag{3.66}$$

The adsorbed concentration needs to be expressed in terms of dissolved concentration, to solve the above equation. The isotherms, as determined in laboratory partitioning experiments, can be plotted in log-log form to derive:

$$\log\ \bar{c}=n\log C+\log K$$
$$or \tag{3.67}$$
$$\bar{c}=KC^n$$

Where 'n' is the slope of the plot of log $\bar{c}$ Vs log C and K is the X axis intercept. When the isotherm has a slope n=1, the isotherm is linear ($\bar{c}=K_dC$). Non-linear isotherm depends on the dissolved concentration.

$$\frac{d\bar{c}}{dC}=nK_{ex}C^{n-1} \tag{3.68}$$

Ion exchange modelling was based on the Local Equilibrium Assumption (LEA); therefore, an ion exchange reaction is faster than the rate of physical transport processes (advection, dispersion and diffusion) at a particular time step is the assumption (Rubin and James, 1973). In a reaction system, at equilibrium, there is no availability of chemical energy to alter the distribution of mass among the reactants and products. Then equation with nonlinear ion-exchange (sorbed concentration, $\bar{c}$, depends on total dissolved concentration, C) reaction can be described as,

$$\left(\theta+\rho_b\frac{d\bar{c}}{dC}\right)\frac{\partial C}{\partial t}=\vec{\nabla}\cdot\left(\theta\boldsymbol{D}\vec{\nabla}C\right)-\mathbf{V}\cdot\vec{\nabla}C-\lambda\left(\theta C+\rho_b\bar{c}\right)+QC_{in}-QC \tag{3.69}$$

Retardation related to nonlinear ion exchange is

$$R_f\left(C\right)=\theta+\rho_b\left(\frac{d\bar{c}}{dC}\right) \tag{3.70}$$

Final equation with physical non-equilibrium as well as nonlinear ion exchange is described as,

$$\left(\theta_{\mathrm{m}}+\rho_b f\frac{d\bar{c}}{dC}\right)\frac{\partial C_{\mathrm{m}}}{\partial t}+\left[\theta_{\mathrm{im}}+\rho_b\left(1-f\right)\frac{d\bar{c}}{dC}\right]\frac{\partial C_{\mathrm{im}}}{\partial t}-\frac{\partial\theta_{im}}{\partial t}C_m=\vec{\nabla}\cdot\left(\theta_{\mathrm{m}}D_{\mathrm{m}}\vec{\nabla}C_m\right)-V\cdot\vec{\nabla}C_m+QC_{in}-QC_m \tag{3.71}$$

$$\left[\theta_{\mathrm{im}}+\rho_b\left(1-f\right)\frac{d\bar{c}}{dC}\right]\frac{\partial C_{\mathrm{im}}}{\partial t}=\Gamma_c\left(C_m-C_{im}\right)-QC_{im} \tag{3.72}$$

After the application of FEM on the above equations it gives a system of algebraic equations. The accuracy and stability of the problem depends upon the numerical parameters like spatial element size, shape of elements, number of nodes in each elements, etc.

$$\int N_i \left[\left(\theta_{\mathrm{m}} + \rho_b f \frac{d\bar{c}}{dC} \right) \frac{\partial C_{\mathrm{m}}}{\partial t} + \left[\theta_{\mathrm{im}} + \rho_b \left(1-f\right) \frac{d\bar{c}}{dC} \right] \frac{\partial C_{\mathrm{im}}}{\partial t} - \frac{\partial \theta_{im}}{\partial t} C_m - \vec{\nabla} \cdot \left(\theta_{\mathrm{m}} D_{\mathrm{m}} \vec{\nabla} C_m \right) + V \cdot \vec{\nabla} C_m - Q C_{in} + Q C_m \right] dR = 0 \tag{3.73}$$

$$\int N_i \left[\left[\theta_{\mathrm{im}} + \rho_b \left(1-f\right) \frac{d\bar{c}}{dC} \right] \frac{\partial C_{\mathrm{im}}}{\partial t} - \Gamma_c \left(C_m - C_{im} \right) - Q C_{im} \right] dR = 0 \tag{3.74}$$

Where, $\mathbf{N_i}$ is the weighting function same as shape function in Galerkin method and **R** denotes the region of interest. Integration by parts can be applied to the second order terms to make sure that the continuity of dependent variable is maintained along the element surfaces and a set of 'n' nodal equations of the following form can be generated

$$A_{ij} \frac{dC_{mj}}{dt} + B_{ij} \frac{dC_{imj}}{dt} + \left(D_{ij} + E_{ij} - \frac{\partial \theta_{im}}{\partial t} \right) C_{mj} = R_i \tag{3.75}$$

Where i=1, 2, 3... n (nodes); j= 1, 2, 3,... n (nodes) and,

$$A_{ij} = \sum_{k=1}^{m} \int_{R_e} N_i^e N_j^e \left(\theta_{mj} + \rho_b \, \mathrm{f} \, \frac{d\bar{c}}{dC} \right) dR \tag{3.75a}$$

$$B_{ij} = \sum_{k=1}^{m} \int_{R_e} N_i^e N_j^e \left(\theta_{imj} + \left(1 - \mathrm{f} \;\; \rho_b \frac{d\bar{c}}{dC} \right) \right) dR \tag{3.75b}$$

$$D_{ij} = \sum_{k=1}^{m} \int_{R_e} \left[\nabla N_i^e \;\; \theta_{mj} D \;\; \nabla N_j^e \right] + N_i^e V_m \nabla N_j^e \;\; dR \tag{3.75c}$$

$$E_{ij} = \sum_{k=1}^{m} \int_{R_e} N_i^e \left[\lambda \;\; \theta_{mj} + \rho_b \, \mathrm{k}_d \;\; + \mathrm{Q} \right] N_j^e dR \tag{3.75d}$$

$$R_i = \sum_{k=1}^{m} \left[\int_{R_e} Q N_i^e dR \;\; C_{in} \;\; + \int_{R_e} n \cdot \theta_{mj} D_m \nabla N_j^e dB \;\; C_{mj} \right] \tag{3.75e}$$

where 'm' is number of elements, N^e is element shape function, B denotes the boundary region and R_i represents the load vector. The time derivative is approximated by backward finite-difference and the subsequent algebraic form is represented as:

$$\left(\frac{A_{ij}^{n+1}}{\Delta t} + \frac{B_{ij}^{n+1}}{\Delta t} \left(\frac{\Gamma_c}{IM + \Gamma_c + Q} \right) + D_{ij}^{n+1} + E_{ij}^{n+1} - \left(\frac{\theta_{im}^{n+1} - \theta_{im}^{n}}{\Delta t} \right) \right) C_{mj}^{n+1} =$$

$$R_i^{n+1} + \frac{A_{ij}^{n+1}}{\Delta t} \left(C_{mj}^{n} \right) + \left[\frac{B_{ij}^{n+1}}{\Delta t} - \frac{B_{ij}^{n+1}}{\Delta t} \left(\frac{IM}{IM + \Gamma_c + Q} \right) \right] \left(C_{imj}^{n} \right) \tag{3.76}$$

where, n+1 and n represents current time step and previous time step, respectively.

3.5.2 Validation of ion-exchange problem

The FEMWATER model is validated with the Grove et al. (1984) model for a simple one-dimensional monovalent-monovalent ion exchange problem. The column length is 16 cm and the concentrations were measured at 8 cm. A pulse input concentration was given and the experiment was run for three different input concentration values and the model matches well with the literature data, which is shown in the Figure.3.9.

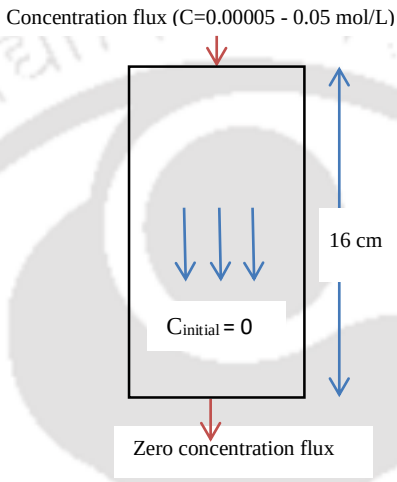

Fig.3.8 One dimensional soil column setup for validation of modified FEMWATER with ion exchange reaction

Table.3.4. Parameters for the validation of FEMWATER ion-exchange problem (Groove et al. 1984)

Parameters	**Values**
Moisture content (θ)	0.37
Darcy flux	0.037 cm/sec
Diffusion coefficient (D)	0.01 cm^2s^{-1}
Bulk density (ρ_b)	1.587 g/cm^3
Input concentration (C_{in})	0.00005 to 0.05 moles/liter,
Total sorption capacity/cation exchange capacity (Q)	0.003 meq/g
Total solution concentration (C_{tot})	0.10 eq/liter
Equilibrium ion exchange coefficient (K_{ex})	10
Simulation time	480 s
Input concentration pulse period	160 s
Concentration measurement at	8^{th} cm

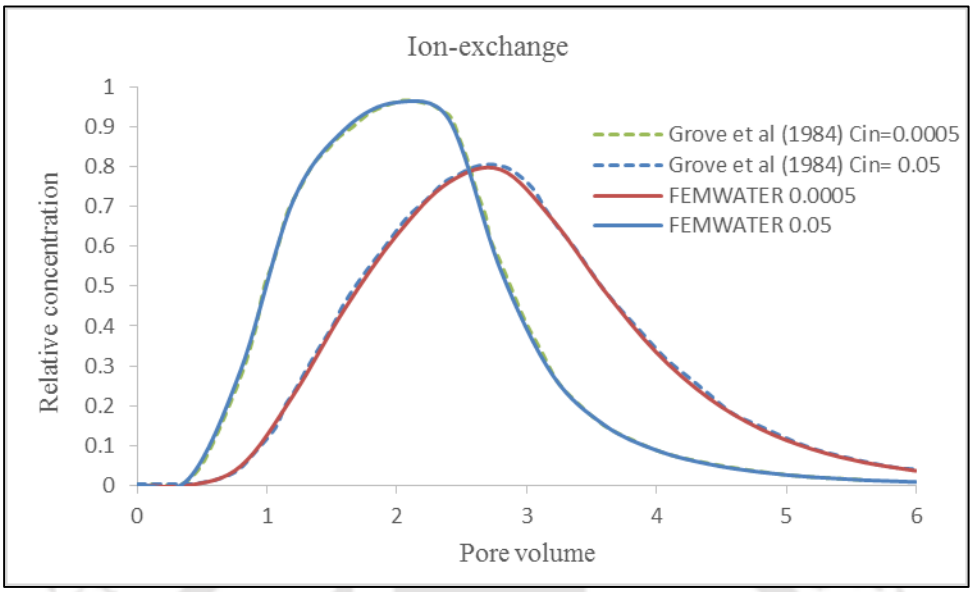

Fig. 3.9. Validation of FEMWATER model with Grove et al. (1984) for ion exchange reaction

3.6 Multispecies transport:

FEMWATER is further modified to simulate multispecies transport, but without any interaction between the species. For each component initial, boundary conditions and inflow concentration should be given in the input and the transport equation takes the following form

$$\theta\frac{\partial C_j}{\partial t}+\rho_b\frac{\partial S_j}{\partial t}=\vec{\nabla}\cdot\left(\theta D\vec{\nabla}C_j\right)-\vec{V}\cdot\vec{\nabla}C_j-\left(\lambda\theta C_j+\rho_b S_j\right)+QC_{in_j}-QC_j \qquad (3.77)$$

where j=1, 2, 3,….., N_c (number of species), C_j is the concentration of the j^{th} dissolved species [ML^{-3}]; S_j is the concentration of the j^{th} adsorbed phase species [MM^{-1}];

For the sake of the numerical solution to the fully coupled (transport and reaction) equations some assumptions have to be made; (i) Chemical reactions are sufficiently fast, relative to hydrological processes, for the local equilibrium condition to be established throughout the transport domain. (ii) In a multi-component system all individual components have an identical transport behaviour. When chemical reactions take place during the transport, the easiest way to introduce them into the advection-dispersion equation is by way of accumulation rates (R_j) for all components. A chemically reactive multi-component transport equation can be written for each component ‘j’ as follows (Gao1998 & 2001)

$$\theta\frac{\partial C_j}{\partial t}=\vec{\nabla}\cdot\left(\theta D\vec{\nabla}C_j\right)-\vec{V}\cdot\vec{\nabla}C_j+QC_{in_j}+R_j;\quad \text{j=1,2,....,N}_c \tag{3.78}$$

where R_j represents the accumulation rate of component 'j' due to different chemical reactions.

$$R_j=R_j^a+R_j^s+R_j^p+R_j^{ex}+R_j^{rd}+R_j^{ab} \tag{3.79}$$

R_j^a is the rate of accumulation of the j[th] substance due to the aqueous complexation,

R_j^s is the rate of accumulation of the j[th] substance due to adsorption-desorption,

R_j^p is the rate of accumulation of the j[th] substance due to precipitation-dissolution,

R_j^{ex} is the rate of accumulation of the j[th] substance due to ion exchange reaction,

R_j^{rd} is the rate of accumulation of the j[th] substance due to redox reaction,

R_j^{ab} is the rate of accumulation of the j[th] substance due to acid base reaction,

Since the rate of the accumulation of the j[th] substance due to an ion-exchange reaction, redox reaction and acid-base reaction can be described mathematically in terms of accumulation of component 'j' due to aqueous complexation, adsorption/desorption and precipitation/dissolution reactions respectively (Yeh and Tripathi 1998; Gao 1998) then rate of accumulation equation can be simplified as (Gao et al. 2001)

$$R_j=R_j^a+R_j^s+R_j^p \tag{3.80}$$

The rate of accumulation of the j[th] substance due to the aqueous complexation is

$$R_j^a=-\frac{\partial}{\partial t}\left[\sum_{i=1}^{N_x}a_{ij}^x X_i\right] \tag{3.81}$$

$$X_i=\frac{K_i^x}{\gamma_i^x}\prod_{j=1}^{N_c}\left(\gamma_j C_j\right)^{a_{ij}^X} \tag{3.82}$$

where, $\mathbf{a_{ij}^x}$ is the stoichiometric coefficient for the total aqueous concentration of component j in complex X_i, $\mathbf{N_x}$ is the number complex for component j, $\mathbf{K_i^x}$ is the equilibrium constant of the i[th] complexed species, $\boldsymbol{\gamma_i^x}$ is the activity coefficient of complex i, $\boldsymbol{\gamma_j}$ is the activity coefficient of the component j.

The rate of accumulation of the j[th] substance due to adsorption-desorption is

$$R_j^s = -\frac{\partial}{\partial t}\left[\sum_{i=1}^{N_s} a_{ij}^s S_i^x\right] \tag{3.83}$$

$$S_i^x = \frac{K_i^s}{\gamma_i^s}\left(\prod_{j=1}^{N_c}\left(\gamma_j^c C_j\right)^{a_{ij}^c}\right)\left(\prod_{j=1}^{N_s}\left(\gamma_j^s S_j\right)^{a_{ij}^s}\right) \tag{3.84}$$

where, $\mathbf{a_{ij}^s}$ is the stoichiometric coefficient for the total adsorbed concentration of component j in adsorbed site S_i^x, $\mathbf{N_s}$ is the number of sorbed complexes for component j, $\mathbf{K_i^x}$ is the equilibrium constant of the i[th] complexed species, $\boldsymbol{\gamma_i^s}$ is the activity coefficient of i[th] sorbed species, $\boldsymbol{\gamma_j^c}$ is the activity coefficient of the component j[th] adsorbate component, $\boldsymbol{\gamma_j^s}$ is the activity coefficient of the component j[th] adsorbent.

The rate of accumulation of the j[th] substance due to precipitation-dissolution is

$$R_j^p = -\frac{\partial}{\partial t}\left[\sum_{i=1}^{N_p} a_{ij}^p P_i^x\right] \tag{3.85}$$

$$K_i^p \geq \prod_{j=1}^{N_c}\left(\gamma_j^p C_j\right)^{a_{ij}^p} \quad i = 1,\ldots,N_p \tag{3.86}$$

$\boldsymbol{a_{ij}^p}$ is the stoichiometric coefficient for the total precipitated concentration of component j in precipitate P_i^x, $\boldsymbol{N_p}$ is the number of precipitates for component j, $\boldsymbol{K_i^p}$ is the solubility product equilibrium constant for the precipitate. The ***inequality indicates*** that a precipitate is formed only when the solution is supersaturated with respect to the components of that precipitate. The reactive transport equation can be expressed in terms of concentration C_j by replacing the R_j with appropriate expressions. Taking into account that the aqueous complexes are mobile, while adsorbent and precipitate species are not and assuming a constant porosity, the final form of multi-component reactive transport equation is given by:

$$\theta\frac{\partial}{\partial t}\left(C_j + \sum_{i=1}^{N_x} a_{ij}^x X_i + \sum_{i=1}^{N_s} a_{ij}^s S_i^x + \sum_{i=1}^{N_p} a_{ij}^p P_i^x\right) = \vec{\nabla}\cdot\left(\theta D\vec{\nabla}\left[C_j + \sum_{i=1}^{N_x} a_{ij}^x X_i\right]\right) - \vec{V}\cdot\vec{\nabla}\left(C_j + \sum_{i=1}^{N_x} a_{ij}^x X_i\right) + QC_{in_j} \tag{3.87}$$

On defining the total concentration of component *j*, as C_j^{tot}, the advective dispersive operator L will be as follows

$$C_j^{tot} = C_j + \sum_{i=1}^{N_x} a_{ij}^x X_i + \sum_{i=1}^{N_s} a_{ij}^s S^x{}_i + \sum_{i=1}^{N_p} a_{ij}^p P^x{}_i \tag{3.88}$$

$$L\left(C_j + \sum_{i=1}^{N_x} a_{ij}^x X_i\right) = \vec{\nabla}\cdot\left(\theta D\vec{\nabla}\left[C_j + \sum_{i=1}^{N_x} a_{ij}^x X_i\right]\right) - \vec{V}\cdot\vec{\nabla}\left(C_j + \sum_{i=1}^{N_x} a_{ij}^x X_i\right) \tag{3.89}$$

Then, the general form of multi-component reactive transport equation can be written along with the 3DLEWASTE as

$$\theta\frac{\partial C_j^{tot}}{\partial t} = L\left(C_j + \sum_{i=1}^{N_x} a_{ij}^x X_i\right) - \left(\lambda\theta C_j + \rho_b S_j\right) + QC_{in_j} - QC_j \tag{3.90}$$

Then the multi-component reactive transport equation with physical non-equilibrium phenomena becomes

$$\theta_m\frac{\partial C_{jm}^{tot}}{\partial t} + \theta_{im}\frac{\partial}{\partial t}\left(C_{jim} + \sum_{i=1}^{N_x} a_{ij}^x X_{i,im}\right) - \left(C_{jim} + \sum_{i=1}^{N_x} a_{ij}^x X_{i,im}\right)\frac{\partial\theta_{im}}{\partial t} = \nabla\cdot\left(\theta_m D\nabla\left(C_{jm} + \sum_{i=1}^{N_x} a_{ij}^x X_i\right)\right) - V\cdot\nabla\left(C_{jm} + \sum_{i=1}^{N_x} a_{ij}^x X_i\right)$$
$$-\lambda\left(\theta_m C_{jm} + \rho_b S\right) + QC_{in} - QC_{jm}$$

(3.91)
$$\theta_{im}\frac{\partial}{\partial t}\left(C_{jim} + \sum_{i=1}^{N_x} a_{ij}^x X_{i,im}\right) = \Gamma\left[\left(C_{jm} + \sum_{i=1}^{N_x} a_{ij}^x X_{i,m}\right) - \left(C_{jim} + \sum_{i=1}^{N_x} a_{ij}^x X_{i,im}\right)\right] - Q\left(C_{jm} + \sum_{i=1}^{N_x} a_{ij}^x X_{i,m}\right) \tag{3.92}$$

$$C_{jm}^{tot} = C_{jm} + \sum_{i=1}^{N_x} a_{ij}^x X_{i,m} + \sum_{i=1}^{N_s} a_{ij}^s S^x{}_i + \sum_{i=1}^{N_p} a_{ij}^p P^x{}_i \tag{3.93}$$

$$X_{i,m} = \frac{K_i^x}{\gamma_i^x}\prod_{j=1}^{N_c}\left(\gamma_j C_{jm}\right)^{a_{ij}^x} \tag{3.94}$$

Solution to coupled transport equations:

1) Primary Dependent Variable (PDV) has to be defined; here total concentration is chosen as the PDV.
2) A sequential iteration approach is the most efficient way to solve coupled transport and reactive equations. Sequential iteration can be visualized as a two-step process.
3) In the first physical step, the set of coupled equations are solved at time‘t’ to give concentration space profiles at time t+Δt.
4) The second, chemical step, consists of solving chemical equilibrium equations to obtain the concentrations of all species at time t+Δt.

5) On completion of the second step, the new concentration of species are used as initial conditions in the physical step to solve the solute transport equations for time $t+2\Delta t$.

The chemical reaction equation system has to be included in the FEMWATER model and the MINTEQ program is selected for the chemical reactions. For now only the physical transport of multi species has been added, thus this study has not included any multi species reactive transport simulations.

3.7 Summary

In this chapter, development and validation of the FEMWATER model that is going to be applied for AMD transport simulation (in Chapter-5) through variably saturated porous media were discussed. A single porosity flow model was updated with a dual porosity flow model; now FEMWATER can handle additional two models, i) mixed form Richards equation for flow ii) dual porosity/mobile-immobile flow, along with already existing pressure head based Richards equation. Based on the methods proposed by Celia et al. (1990) a modified Picard iteration method is implemented into the FEMWATER code to handle the mixed form of Richards equation. An ion exchange reaction was added to the model; and model was updated for multicomponent transport; but without any interactions between the solutes. With these modifications the modified FEMWATER model is applied to the AMD transport scenarios, which will be described in the subsequent two chapters.

CHAPTER 4

PARAMETER ANALYSIS AND SELECTION

This chapter presents the parameter analysis and selection for the numerical simulation run and explains the flow, transport and numerical parameters used in the simulation. It also describes the results from the base case simulation and based on the results parameters are selected.

4.1 General

Modification of FEMWATER model and its validation was presented in the chapter 3, following which the application of the modified model to the subsurface AMD transport must be discussed in this thesis. The extensive application of the model to the AMD cases will be elaborated in chapter 5. Validation is the process of comparing the model results with the problems chosen from literature to ensure the suitability of the model for prediction studies. Before applying the model for analysis, effects of numerical parameters on model outcomes have to be verified for the stability of the results. Sensitivity analysis, which is the evaluation of the influence of model inputs on model outputs are performed to ascertain the usability of the numerical model. In any numerical model input/parameters selection are very crucial for making the model more trustable and therefore, this chapter gives an insight to the parameter analysis and its selection. The main advantage of any numerical model is that different parameter values can be assigned to each element/cell or domain. In the case of heterogeneous porous medium, the numerical model can define multiple layers by assigning different parametric values (Kumar, 2012). This chapter presents brief view of flow, transport and numerical parameters used in the simulation and also describes the results from the simulation of parameters analysis.

4.2 Flow parameters

Complete input file, for simulation run, consists of parameters that define the medium and its character for fluid flow. Input parameters like hydraulic conductivity, porosity, soil water capacity and pressure head versus water content relationship are crucial in deciding the flow pattern and velocity distribution, which can be used in the transport model to analyse the contaminant transport.

4.2.1 Residual (θ_r) and saturated (θ_s) moisture content, [-]

Soil moisture is numerically measured by volumetric moisture content, θ, and is defined as

$$\theta = \frac{V_w}{V_T} \tag{4.1}$$

where, V_w is volume of soil filled with water and V_T is total volume of the soil medium.

Saturated water content (θ_S) is equal to the porosity of the medium for non-deformable porous medium, since all the pore space of the soil medium is saturated with water. If the pore space is

filled partially with air and water it is categorised as unsaturated medium. The moisture content that cannot be removed from soil, because it sticks to the soil grains, by gravity drainage is known as residual moisture content (θ_r).

4.2.2 Saturated hydraulic conductivity (K_s), [L/T]

Hydraulic conductivity is a function of the solid medium as well as of the flowing fluid. It is the proportionality coefficient that appears in Darcy's law. Conductivity expresses the ease with which the fluid flow through the porous medium and its value depends on the moisture content when the medium is partially saturated with liquid phase. In an anisotropic medium conductivity varies with direction at any point in space and is expressed as a symmetric second rank tensor for three dimensional flow.

$$K_{ij} = \begin{bmatrix} K_{xx} & K_{xy} & K_{xz} \\ K_{yx} & K_{yy} & K_{yz} \\ K_{zx} & K_{zy} & K_{zz} \end{bmatrix} \tag{4.2}$$

where, K_{ij} is the hydraulic conductivity tensor, x, y and z are the three dimensional coordinate axes. Out of nine terms from the hydraulic conductivity tensor, six distinct terms are sufficient to describe the hydraulic conductivity as the tensor is symmetrical (i.e. K_{xx}, K_{yy}, K_{zz}, $K_{xy}=K_{yx}$, $K_{xz}=K_{zx}$, $K_{yz}=K_{zy}$). If the coordinate axes coincide with the principal directions of anisotropy then the number of distinct terms in the hydraulic conductivity tensor reduces to three (K_{xx}, K_{yy}, K_{zz}). For isotropic media, the hydraulic conductivity is independent of the direction (i.e. K_{xx} = K_{yy} = K_{zz}). Generally vertical hydraulic conductivity is smaller than the horizontal hydraulic conductivity for most of the soils.

4.2.3 Permeability (k), [L^2]

Permeability, is a property of the porous medium and is a measure of the resistance to fluid flow through the medium. Resistance is less when permeability is greater. The hydraulic conductivity inputs in FEMWATER can be provided either by furnishing hydraulic conductivity values directly to the domain or by providing the intrinsic permeability values. The hydraulic conductivity is related with the intrinsic permeabilities as:

$$K_{ij} = \frac{k_{ij}\rho g}{\mu} \tag{4.3}$$

where, k_{ij} is the intrinsic permeability tensor, ρ is density, g is acceleration of gravity and μ is dynamic viscosity. It should be noted here that the fluid is treated as isotropic and homogeneous and therefore, the dynamic viscosity of the fluid is taken as a single coefficient rather than the fourth ranked viscosity coefficient tensor used while solving Navier-Stokes equations for fluid flow (Kundu et al. 2012; Reddy 2008; etc.).

4.2.4 Relative permeability (or Hydraulic conductivity) (k_r) [-]

The permeability of liquid phase in the unsaturated medium is a function of the degree of liquid saturation in the pores; the permeability is more for higher degrees of water saturation (Mualem, 1976). In unsaturated subsurface porous media consisting of air and water in pores, the permeability of air and permeability of water are different. However, presuming that, the transport phenomena in water phase is of more concern in the AMD problems, the permeability of water is therefore related with the degree of saturation. Relative permeability of water phase is defined as the ratio between the actual intrinsic permeability and saturated intrinsic permeability and it ranges between the value zero (0.0) and one (1.0).

$$k_r = \frac{k(\theta)}{k_s} \tag{4.4}$$

where, k_s is saturated intrinsic permeability, k(θ) is the actual intrinsic permeability, and k_r is the relative permeability.

4.2.5 Pressure head (h), [L]

Pressure head, measured in gage units, is the pressure per unit weight of water in the subsurface media. The water table is defined as the location at which pressure is equal to the atmospheric and hence the gage pressure on water table is zero. In the unsaturated zone, above the water table, the pressure is less than the atmospheric pressure and therefore the unsaturated zone pressure head is negative. The unsaturated zone pressure head is a function of moisture content. The magnitude of the unsaturated pressure head (i.e. after removing the negative sign) can also be termed as suction head. The suction head is high for low water content and near to zero for

saturation condition. In the saturated zone, from the water table to downwards, the water pressure increases with respect to atmosphere pressure and it is denoted by positive sign.

4.2.6 Moisture content capacity (F(θ)), [L^{-1}]

Relationship between water content and pressure head, θ(h), in soil is termed as soil moisture characteristic curve (SWCC), because the curve is unique characteristic for each soil. Inverse of the slope of this curve is called "water capacity or moisture content capacity" and is defined as:

$$F(\theta) = \frac{d\theta}{dh} \tag{4.5}$$

4.3 Solute Transport parameters

Though results of transport models primarily are dependent on output of flow model, parameters like distribution coefficient, bulk density, dispersivity, diffusion coefficient and sorption parameters can make much impact on the contaminant spreading pattern.

4.3.1 Distribution coefficient (K_d), [L^3/M]

The distribution coefficient provides the constitutive relationship between the dissolved species concentration, C (M/L^3) and adsorbed species concentration, S (M/M),

$$S = KC^n \tag{4.6}$$

where, coefficients K and n depend on many factors, which includes the solute species and the nature of the medium. If the isotherm is linear, n=1, K is known as the distribution coefficient, (dS/dC=) K_d.

4.3.2 Bulk density (ρ_b), [M/ L^3]

Bulk density is defined as the mass of a unit volume of dry soil. The retardation of solutes is directly influenced by the parametric variations in bulk density.

Bulk density (g/cm^3) = Dry soil weight (g) / Soil volume (cm^3)

4.3.3 Longitudinal (λ_L) and transverse dispersivity (λ_T), [L]

Hydrodynamic dispersion is an irreversible mixing process by which contaminant spreading occurs in subsurface. It results from the effects of molecular diffusion and mechanical dispersion. Dispersion is caused by the variation in pore water velocities in soil. Though

mechanical dispersion is a second order tensor it can be expressed in terms of the average groundwater velocity with two constants: longitudinal and transverse dispersivity. Longitudinal dispersivity is defined as the characteristic mixing length in the groundwater flow direction and transverse dispersivity is defined as the mixing length in the direction perpendicular to liquid flow. Longitudinal dispersivity values are commonly thought to be higher than transverse dispersivity.

4.3.4 Molecular diffusion coefficient (D_m), [L^2/T]

Molecular diffusion is less significant compared to mechanical dispersion in the process of dispersion of solutes in most of the subsurface systems. When the groundwater velocities are considerably low, molecular diffusion can become significant. Fick's law, describes the flux of a solute in a fluid due to molecular diffusion, states that the flux is proportional to the concentration gradient. Coefficient of proportionality is called as molecular diffusion coefficient (D_m).

4.3.5 Tortuosity (τ), [-]

Molecular diffusion coefficient for a solute in porous medium is less than the diffusion coefficient in water. This reduced amount of diffusion is expressed by tortuosity, which is a second rank tensor and reduced to a scalar for isotropic conditions. The FEMWATER manual cites that the tortuosity varies in from 0.1 for clays to 0.7 for sands and the tortuosity is always less than one. Usual values of tortuosity are between 0.01 and 0.5.

4.4 Dual porosity parameters

In addition to the parameters, which are used to simulate the flow in single porosity medium, the following parameters are added to simulate the dual porosity/mobile-immobile flow and non-equilibrium transport.

4.4.1 Mobile (θ_m) and immobile water (θ_{im}) content, [-]

The portion of water content that allows the motion of water through the pores due to pressure difference is known as mobile water. The portion of water that sticks on to the soil particles or trapped in dead end pores or unconnected pore spaces and moves with negligible velocity, is known as immobile water.

4.4.2 Transfer coefficient (Γ), [T^{-1}]

In the case of water flow, due to the difference between effective water contents of mobile and immobile water zones, water mass transfer happens between these regions. This water mass transfer is dependent on transfer coefficient, Γ. In the case of contaminant transport, transfer of contaminant mass occurs between mobile and immobile region due to the concentration difference. This mass transfer process is assumed as a first order process and is again dependent on the transfer coefficient.

4.4.3 Fraction of site available for sorption (f), [-]

The fraction of the pore space region in soil having contact with mobile water is the available region (f) for sorption of contaminants from mobile water. And the remaining fraction (1-f) having contact with immobile water is the available region for sorption of contaminants from immobile water.

4.5 Ion-exchange parameters

Ion-exchange is one of the prominent reactions that affect the contaminant transport severely due to the exchange of ions between soil water and the solid. Ion-exchange is also used as a treatment process, which removes the unwanted ions from water. It is considered as equilibrium reaction, which means the chemical (reaction) process happens quicker than the physical (transport by advection and dispersion) process.

4.5.1 Cation exchange capacity (Q_{ct}), [meq/g]

Cation exchange is a reversible chemical reaction in soil and cation exchange capacity (CEC) is described as the sum of the exchangeable cations that a soil can absorb or the soils capacity to hold cations. There is a limit to the number of cations that a mineral can accommodate, which is elucidated in cation exchange capacity. CEC is defined as the moles of adsorbed cation charge that can be displaced by an index ion per unit mass of solid. It is expressed as milliequivalents per hundred (100) grams of soil.

4.5.2 Total solution concentration (C_{tot}), [eq/L^3]

Defines the total concentration of the solution, including the sorbed and replaced solutes available in the solution.

4.5.3 Equilibrium ion exchange coefficient (K_{ex}), [-]

If two ions participate in the ion-exchange reaction, the mass action equilibrium is as follows:

$$uc_1^v + v\bar{c}_2 \rightleftharpoons v\bar{c}_1 + nc_2^u \tag{4.7}$$

where v and u are the valence of ion 1 and ion 2, respectively.

$$k_{ex} = \frac{\left[\bar{c}_1\right]^u \left[c_2\right]^v}{\left[c_1\right]^u \left[\bar{c}_2\right]^u} \tag{4.8}$$

Generally, there is not an equal distribution of ions between the solid and dissolved phases at equilibrium; instead, certain ions are preferentially exchanged. This is called selectivity, and is defined in terms of the selectivity coefficient or equilibrium ion exchange coefficient.

4.6 Problem description and parameter analysis

4.6.1 Description of two dimensional domain

Two dimensional transient flow is simulated in this problem and the Figure 4.1 shows the cross sectional view of the hypothetical domain. The region of interest is bounded on the right side by river, and the infiltrated water, from the surface, flow towards river. The medium is assumed to have saturated horizontal and vertical hydraulic conductivity of 0.624 m/d, a porosity of 0.35 and a residual moisture content of 0.02. The unsaturated characteristic hydraulic properties are given by the van Genuchten analytical functions, equation 1.4 and 1.5; given in chapter one, with alpha equal to 4.1 m^{-1} and beta (β) or n equal to 1.964, defined as soil specific exponents derived by cure fitting method. The vertical left, front, back surface and horizontal bottom of the region are impermeable boundaries. The sloping region on the top right is a variable flow boundary with either zero ponding depth or a net rainfall rate of 0.00139 m/day. The horizontal region on the top is a Cauchy flow boundary with an infiltration rate of 0.0139 m/day. The vertical line and the bottom on the right side are assumed as known head conditions (Dirichlet boundary conditions). Water table is at 12.5 m at the left side and 5 m at right side and initial condition is assumed as hydrostatic pressure head (height of water table – height of nodal points from bottom) at each nodes. The region of interest is discretized with 38×1×53 = 2014 elements with the elements size varies in x direction between 2.5 and 0.6 m and the variation in z direction ranges from 1.3 to 0.1

m, element size is varying due to the nature of sloping boundary, this results in 2106 nodal points. Simulation is done for 365 days with constant time step size of $\Delta t = 1$ day.

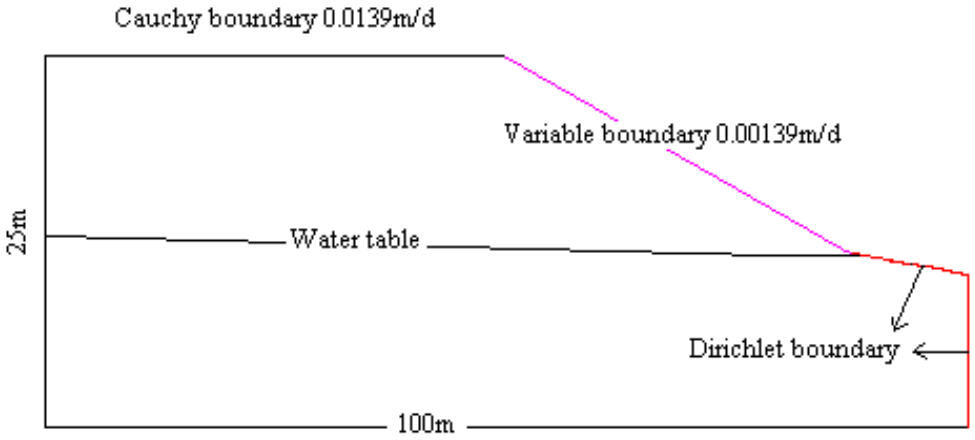

Fig.4.1 Two dimensional vertical cross section of the hypothetical domain

4.6.2 Parameter effects

Soil parameters, flow parameters, transport and numerical parameters are important in any solute transport model, which predicts the contaminant distribution in a domain. The effects on the output results of the numerical model is dependent on the input values/parameters. Sensitivity analysis, mentioned in section 4.1, is performed to find out the parameter influence on the output. During the sensitivity analysis, the computer model is run for a particular user defined parameter, which is varied from its theoretically possible maximum to minimum values, while keeping all of the remaining input parameters as unchanged. In this way, numerous model runs are performed to identify the parameter, which influences the accuracy of the output results. Sensitivity analysis also aid in interpreting the nature and influence of each parameter on the model outputs.

4.6.2.1 Effect of Van Genuchten parameter, α

Van Genuchten (1980), who used the statistical pore size distribution model of Mualem (1976) to obtain predictive equation for the unsaturated hydraulic conductivity (K(h)) function in terms of soil water retention parameters:

$$K(h) = K_s\left(\theta_e^{0.5}\left[1-\left(1-\theta_e^{(1/m)}\right)^m\right]^2\right) \quad ; h<h_a$$
$$= K_s \quad ; h>h_a \tag{4.9}$$

$$\theta_e = \left[1+\left(\alpha|h-h_a|\right)^{n_1}\right]^{-m} \quad ; h<h_a \tag{4.10}$$
$$= \theta_s \quad ; h>h_a$$

$$\theta_e = \frac{\theta(h)-\theta_r}{\theta_s-\theta_r} \tag{4.11}$$

where, α is a parameter related to the model pore size (L^{-1}), n_1 is the function of the pore size distribution (-).

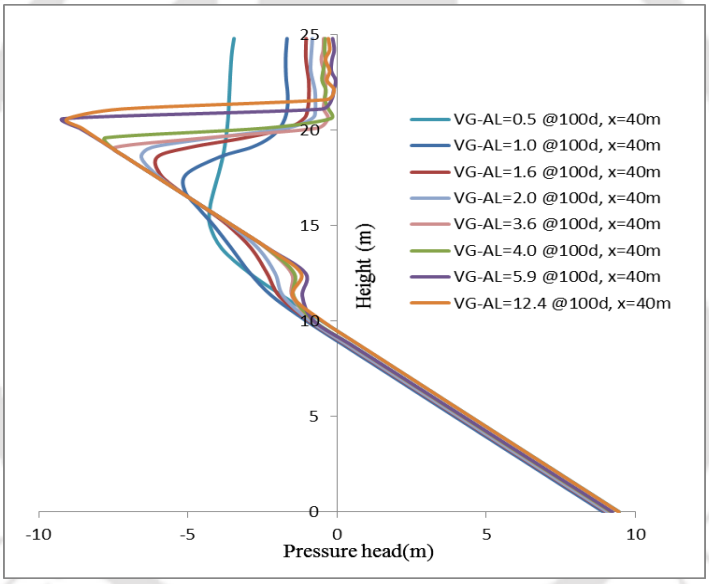

Fig.4.2 Effect of Van Genuchten parameter, α, on pressure head profile (VG-AL refers Van Genuchten – alpha values, in meters)

Both parameters α and n_1 have significant influence on moisture movement through unsaturated zones; these are empirical parameters needed to solve the Van Genuchten analytical equations which are used to model unsaturated flow. As the value of α increase, the wetting front in unsaturated zone moves at a slower rate due to the decrease in hydraulic conductivity. Eight simulations were run, except alpha (α) other flow parameters (θ_s, θ_r, n_1 and m) are same for all the simulations. Within the range of alpha values from 0.5 to 2, variations in the pressure head profile is significant and between the values 2 and 4 there is slight variation and from six

onwards only small variation in pressure profile is observed which is shown in Figure 4.2. Loamy soil properties are assigned to the medium which are given in the section 4.6.1. Where higher value of alpha (12.4) is assigned to loamy sand and the lowest alpha value (0.5) is assigned to silty clay.

4.6.2.2 Dual porosity / mobile-immobile flow parameters

Non-equilibrium transport and dual porosity flow has got importance due to the accelerated movement of contaminants through unsaturated zone to the groundwater. Preferential movement/rapid migration leads to error in the model outcome and causes imperfection in predictions, this problem occurs when the uniform flow model is employed. Important characteristic of dual porosity flow is that during wetting, part of the liquid front propagates quickly to significant depths by bypassing a portion of the pore space (Simunek et al. 2003). Dual porosity model assumes that the porous medium consists of two interacting regions, macropore (inter-aggregate region) and micropores (intra-aggregate region). In this model it is assumed water in the micropores is stagnant with respect to water in macropore, which is assumed to be largely moving. Water and solute mass transfer occurs between these two pore regions that influences the water and solute transport in the domain. The following sections present the parameter sensitivity of the mobile/immobile water zones and its mass transfer coefficients. The parameter values are given as transfer rate coefficient (Γ_w) is 0.005 per day, mobile water fraction (φ) is 0.6, and immobile water fraction ($1-\varphi$) is 0.4 (Simunek et al. 2003).

4.6.2.3 Effect of ratio of mobile water to total water content

Amount of mobile water content present in the medium may affect the water flow as well as mass transport. When mobile water increases, eventually the immobile water decreases and it exhibits or resembles the moisture flow properties of single domain flow. Observation of moisture content in the unsaturated zone at a point (z=19 m and x=40 m) above the water table is shown (Figure 4.3). When the mobile water decreases results show the characteristics of dual porosity flow and the water travel bit faster (Figure 4.3a). When the value of mobile water fraction is very less (say = 0.4), then the observation point reached maximum saturation by around 118th day, however, the maximum saturation at the same observation point for higher mobile water fraction (say = 0.8) reached only around 148th day (Figure 4.3b).

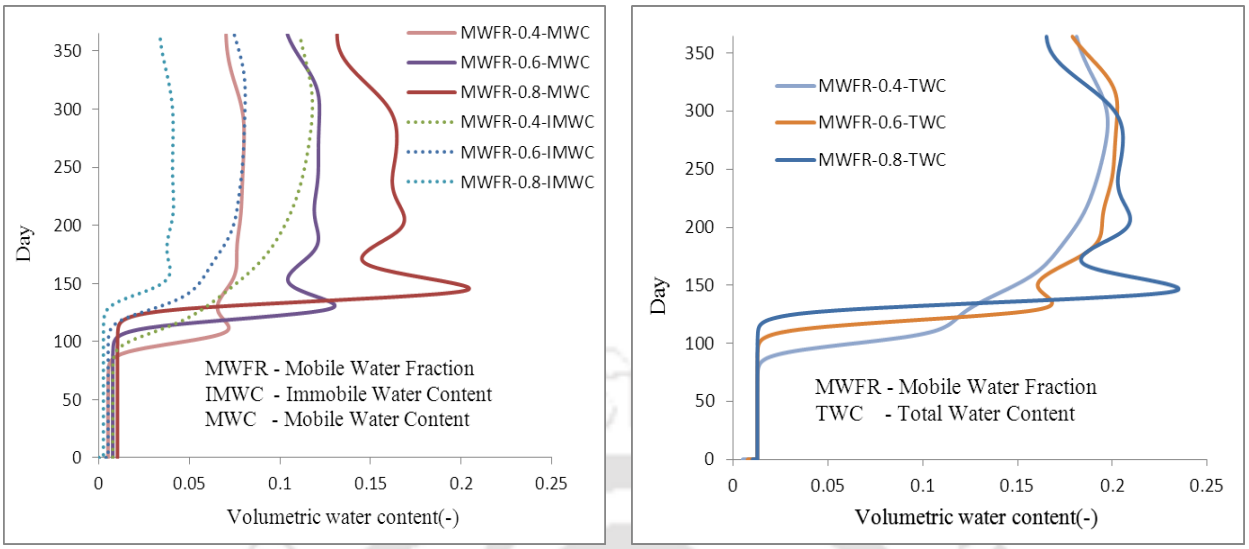

(a) (b)

Fig.4.3 (a) Mobile and immobile water content (b) Total water content at z=19m and x=40m for different mobile water fraction (MWFR)

4.6.2.4 Effect of mass transfer rate

Mass transfer term is represented as a first order linear term; it indicates the transfer of water from the mobile zone to immobile zone. Mass transfer rate is directly proportional to the difference in effective fluid saturation between mobile and immobile zones. Value of transfer rate increases with the flow velocity, high mass transfer rate results in single porosity flow or

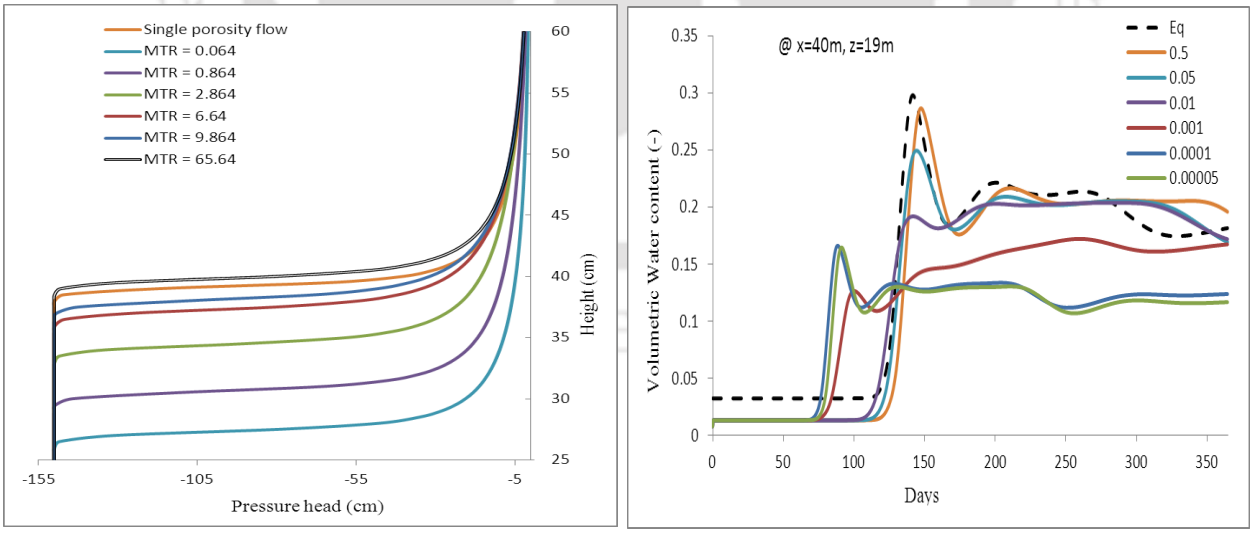

(a) (b)

Fig.4.4 (a) Effect of water transfer rate (d^{-1}) on pressure head profile in the one dimensional unsaturated flow (MTR=Mass Transfer Rate) (b) Effect of moisture transfer rate (d^{-1}) on moisture profile for two dimensional variably saturated flow at particular point (x=40m, z=19m)

slow flow and this is validated with one dimensional (Simunek et al, 2003) and two dimensional hypothetical domain flow. Figure 4.4(a) is the result from the infiltration problem described in the section 3.2.2 of chapter-3. The result of the two dimensional hypothetical domain is shown in the Figure 4.4(b). When the water transfer rate to immobile region is high, mobile region will have less water fraction; it will exhibit the trend of single porosity flow and process will be vice versa when the mass transfer rate to immobile region is higher.

4.6.2.5 Effect of spatial discretization

In Finite Element Method, the problem of oscillations and slow convergence rate have been noticed by a number of researchers in many consolidation, heat diffusion, and seepage flow problems. The calculated value's accuracy is based on the solutions' convergence and the oscillations in the results are due to spatial element size and time step sizes (Thomas and Zou 1997 as referred in Karthikeyan et al. 2001)

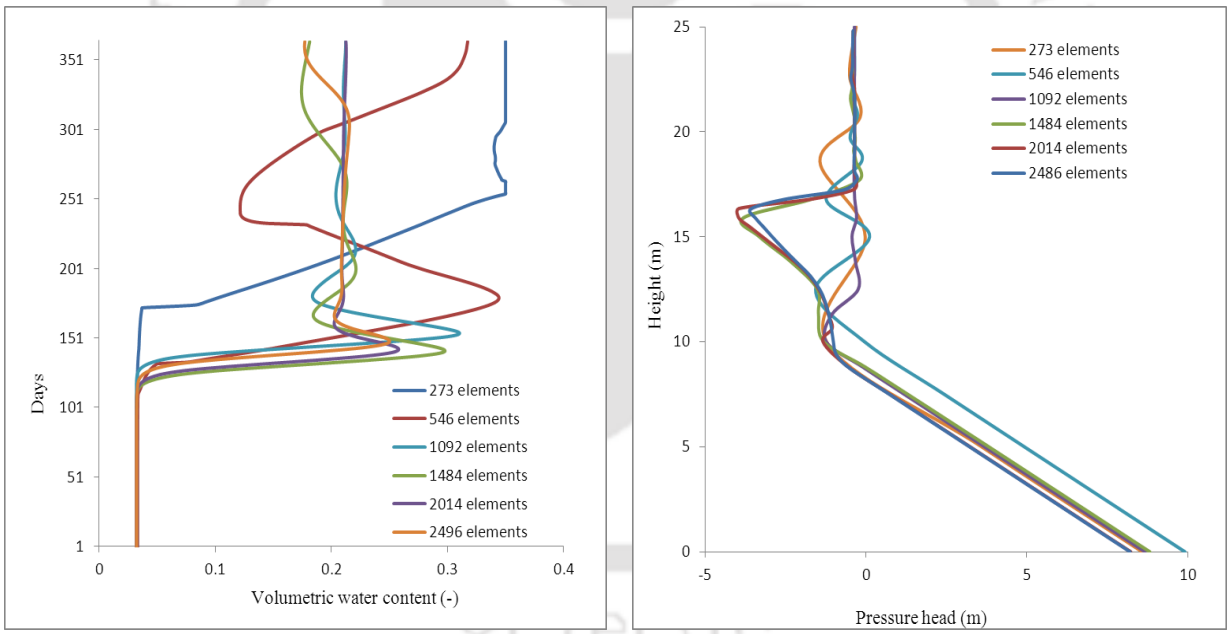

(a) (b)

Fig.4.5 Spatial discretization effect on (a) moisture content profile at particular point (z=19m and x=40m) in the domain (b) pressure head profile at vertical segment (x=40m) at 180th day

To avoid the oscillation and numerical dispersion, the discretization should be small near the regions of large variations of the variable Due to the process of infiltration and vertical flow, unsaturated region is discretized with small element size, than the saturated zone. It is evident from the above Figures 4.5(a) and (b); discretization I and II are sparse in the unsaturated zone

and their results are with oscillations, discretization III is sparse in column wise so its result is kind of transition between oscillation and non-oscillation. Discretization IV, V, VI comparatively did not cause much variation in the flow and pressure head profile as shown in Figure 4.5. The tabulated results of different simulations with distinct discretizations are given in the Table 4.1.

Table.4.1 Two dimensional domain discretization details

Discretization	Δz Range (m)	Δx Range (m)	Rows (R)	Columns (C)	Elements ((R-1)*(C-1))	Nodes (R*C)
I	5.0-2.3	5.1-0.6	08	40	273	320
II	2.5-1.2	5.1-0.6	15	40	546	600
III	1.3-0.5	5.1-0.6	29	40	1092	1160
IV	1.3-0.5	2.5-0.6	29	54	1484	1566
V	1.3-0.1	2.5-0.6	39	54	2014	2106
VI	1.3-0.1	2.3-0.6	40	65	2496	2600

4.6.2.6 Effect of time discretization

Apart from spatial discretization (Δx/Δz), length of the current time step (Δt) is also the reason which causes oscillation in the numerical result (Karthikeyan et al. 2001). Time differential in the Richards equation is replaced by a finite difference formulation.

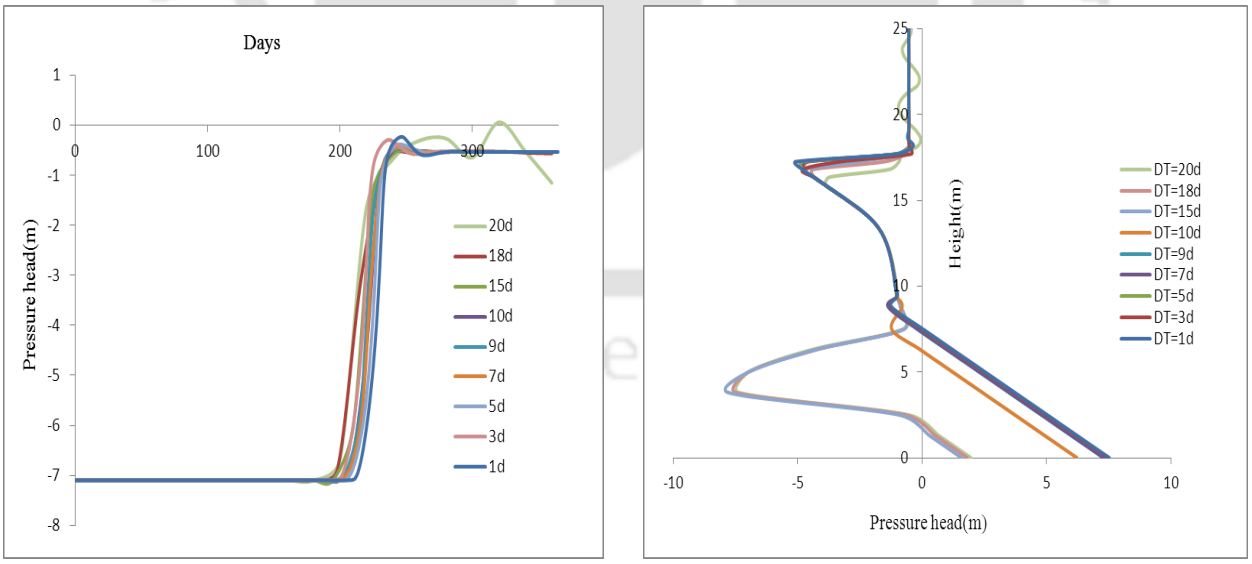

(a) (b)

Fig.4.6 Time discretization effect on (a) pressure head profile at particular point (z=19m and x=25m) in the domain (b) pressure head profile at vertical segment (x=25m) at 280th day

Figure 4.6(a) shows the variation of pressure head at a point in the domain with change in time step size. Between the time step size of one and ten days there is no oscillation observed in the pressure head, however, for bigger time step size the oscillations are prominent (Table 4.2). Time step restriction must be imposed through implicit formulation, which is the limitation of this model.

Table.4.2 Time discretization details

Δx(m)	Δz(m)	Δt(d)	q(m/d)	θ_s	C_x	C_z	$C_r = C_x + C_z$
2.3	1.3	3	0.00346	0.35	0.01289	0.0228	0.03571
2.3	1.3	5	0.00346	0.35	0.02149	0.038	0.05951
2.3	1.3	7	0.00346	0.35	0.03009	0.0532	0.08332
2.3	1.3	9	0.00346	0.35	0.03868	0.0684	0.10712
2.3	1.3	10	0.00346	0.35	0.04298	0.076	0.11903
2.3	1.3	15	0.00346	0.35	0.06447	0.1141	0.17854
2.3	1.3	20	0.00346	0.35	0.08596	0.1521	0.23805

In Figure 4.6(a), change in pressure head (at the point) starts at 210th day for time step size of one day, change in pressure profile starts at 207th day for the time step size of three days and this is reducing by one day for every one increment in time step size. For the time step size of twenty day, severe oscillations are observed. Hence, the current model would not give numerically a stable result beyond the time size of eighteen days for the given simulation inputs. However, the vertical segment analysis in Figure 4.6(b) shows that beyond the time step size of nine days variation in the results are observed for the pressure profiles. Consequently, it is decided to keep the time step size between one and nine days and dense spatial discretization, with 2496 elements, for the rest of the simulation to avoid the numerical oscillation problems.

Table.4.3 Parameters for simulation of two dimensional flow and transport process

Parameters	Values	Source
Saturated water content, (θ_s)	0.35 and 0.39	Loamy soil and Sandy clay loam
Residual water content, (θ_r)	0.02 and 0.1	Loamy soil and Sandy clay loam
Saturated Hydraulic conductivity, ($K_{xx} = K_{zz}$)	0.624 and 0.314 m/d	Loamy soil and Sandy clay loam
Van Genuchten parameters, (α, n, m(=1-(1/n)))	4.1 m^{-1}, 1.964, 0.49084 and 5.9 m^{-1},1.48,0.324	Loamy soil and Sandy clay loam
Mobile water fraction, ($\varphi = \theta_{fm}/\theta$)	0.6	Simunek et al. (2003) and parameter analysis
Immobile water fraction, (1- φ)	0.4	-do-
Transfer rate coefficient of water, (Γ_w)	0.0001 d^{-1}	Parameter analysis
Dispersivities, (α_L, α_T)	$\alpha_L = 0.1*di$, $\alpha_T = \alpha_L/3$ (di–distance from the source to the downstream)	FEMWATER manual
Diffusion coefficient, (D)	1.37E-5 m^2/d	Molson et al. (2005)
Bulk density, (ρ_b)	1500 kg/m^3	FEMWATER manual
Adsorption coefficient, (K_d)	1.2E-4	Walter et al.1994
Transfer rate coefficient of contaminant, (Γ_c)	0.0001 d^{-1}	Assuming same as water transfer rate
Fraction of site available for mobile contaminant equilibrium sorption, (f)	0.6	Assuming same as mobile water fraction. (Selim et al. 1987)
Fraction of site available for Immobile contamination equilibrium sorption, (1-f)	0.4	Assuming same as immobile water fraction (Selim et al. 1981)
Cation exchange capacity, (Q_{ct})	0.0001 eq/g	Grove et al. 1984
Total solution concentration, (C_{tot})	0.1 eq/l	-do-
Equilibrium ferrous ion exchange coefficient, (K_{ex})	0.5	-do-
Equilibrium Magnesium ion exchange coefficient, (K_{ex})	0.2	-do-
Space discretization, (Δx and Δz)	1.3-0.5 m and 2.5-0.6 m	Parameter analysis
Time discretization, (Δt)	1 d	Parameter analysis

4.7 Summary

Based on the above analysis and from the literature, the following flow and transport parameters, given in table 4.3 are fixed for further simulation of conservative and reactive contaminant transport in two dimensional hypothetical domain. Out of all parameters some are taken from the FEMWATER manual, some from literatures, and some parameters are assumed for the simulation based on the parameter analysis done here.

CHAPTER 5

RESULTS AND DISCUSSIONS

This chapter presents the application of the modified FEMWATER model, with non-equilibrium transport property, on a hypothetical acid mine water movement situation. The effects of non-equilibrium mass transfer on contaminant transport and parameter sensitivity analysis are also reported in this chapter. Two dimensional simulations are obtained for contaminant transport in homogeneous and heterogeneous medium with physical non-equilibrium, sorption, and ion-exchange reactions.

5.1 General

Modified FEMWATER model is applied to a two-dimensional hypothetical domain to simulate and study the reactive transport of AMD through the subsurface porous media having mobile and immobile water zones. The immobile liquid zones are observed in some unsaturated soil regions, even without the presence of aggregated soil particles. These immobile zones may act as source or sink for the transport of contaminants. Therefore, the transport characteristics in unsaturated zone are important for the overall prediction of AMD contaminant movement. There are only very few studies available for reactive transport of AMD with physical non-equilibrium and reactions. For example, the effects of static water content on chloride transport from mines, in the chalk aquifer was simulated and verified with the field data (Bibby, 1981). Improvements in the predictions of Ca and Mg breakthrough curves by combining ion-exchange and non-equilibrium model were reported in Selim et al. (1981).

Pyrite oxidation and ferrous ion: Pyrite oxidation process in mine sites, mine tailings, waste rock heaps, etc., adds acidity to the surface water that leads to the dissolution of heavy metals and its transport towards groundwater zone. One mole of pyrite oxidation produces two moles of hydrogen ion and these positively charged hydrogen ions are the reason for the acidic nature of mine water. Oxygen and ferrous ion are the main agents which involve in pyrite oxidation reaction. Near the land surface, oxygen diffuses more in to the soil and this process fuels the oxidation reaction and releases hydrogen ion. In the deeper part of unsaturated region, or in the zones where oxygen is not available, ferrous ion induces oxidation reaction. Ferrous ion is soluble in water under normal pH conditions; however, the decrease in ferrous ion concentration in AMD water ceases further oxidation process. Therefore, the knowledge of ferrous ion transport as well as transport of other metals under the conditions of mobile-immobile/dual porosity and reactive environment will be useful for natural treatment processes (Pang et al. 1987) of AMD water both in situ and in industrial scale. The objective of this research work is to assess the reactive transport properties of AMD contaminants, especially ferrous ion, under physical non-equilibrium transport condition.

With this objective FEMWATER model is modified to simulate water and solute mass transfer between the mobile and immobile regions. After modification, FEMWATER can simulate water flow by three models, i) head-based Richards equation (default available in previous version), ii)

mixed form Richards equation (included in this modified version) and iii) dual porosity/mobile-immobile model (included in this modified version). It can simulate contaminant movement by two models i) equilibrium transport by conventional advection-diffusion equation (default available in previous version) and ii) non-equilibrium model, which is included in to this modified FEMWATER. Reactive transport of ferrous ion in the subsurface zone under homogeneous and heterogeneous, equilibrium and non-equilibrium conditions are simulated and discussed in this chapter. Apart from the study of ferrous ion, application of these concepts can be extended to other contaminants too. However, in this research it is limited to ferrous ion transport. It is assumed that no interaction of contaminants with other chemical species.

5.2 Two dimensional transport of AMD using modified FEMWATER

Mine waste sites and mine sites can contaminate surface and subsurface water bodies by releasing heavy metals and salt due to the chemical processes of sulphide minerals. These contaminants migrate through the unsaturated zone and reach the saturated groundwater aquifer. Further, these contaminants travel along with the flow direction of the groundwater. Based on these mining situations, the simulations in this research are designed to assess the AMD migration phenomenon through variably saturated porous subsurface. Acid Mine Drainage contains metals, heavy metals, salts and ions in dissolved form, depends on the solution pH. Ferrous ion, available in dissolved form under pH conditions of above 5, is the main reason for acidified water due to its oxidizing nature. In this study, focus is on the transport nature of ferrous ion with non-equilibrium conditions and reaction. Most of the non-equilibrium transport models obtain the water content value from flow simulation using Darcian conditions and thereafter, split this water content into mobile and immobile regions, for the simulation of contaminant transport. In those kinds of simulations, the distributed values of mobile and immobile water contents do not influence the hydraulic head used in flow simulations. That is the Darcian mechanism evaluate only the total water content by solving the head based and/or water content based flow equations. However, in practical situations, it is intuitive to perceive that the immobile water zones can affect the flow pressure and in this research new method is adopted to incorporate the influence of immobile liquids on fluid flow. Therefore, this research work involves mass transfers of water as well as contaminants between the mobile and immobile regions in the subsurface zone to enhance the accuracy of the model prediction.

5.3 Field condition and problem domain selection

Two-dimensional hypothetical domain is selected on the basis of representation of a real field situation (Figure 5.1) that considers the release and migration of contaminants from a land surface to the subsurface region. The problem domain consists of mine tailings, unsaturated zone below the mine tailings, river, and saturated zone bounded by an impermeable rock. Contaminated water from tailings enter in to the vadose zone and may emerge as spring or may flow in to the stream or river, which affects the water quality and are harmful to aquatic species. The scenario analysis will focus on the transport nature of contaminants in the porous medium.

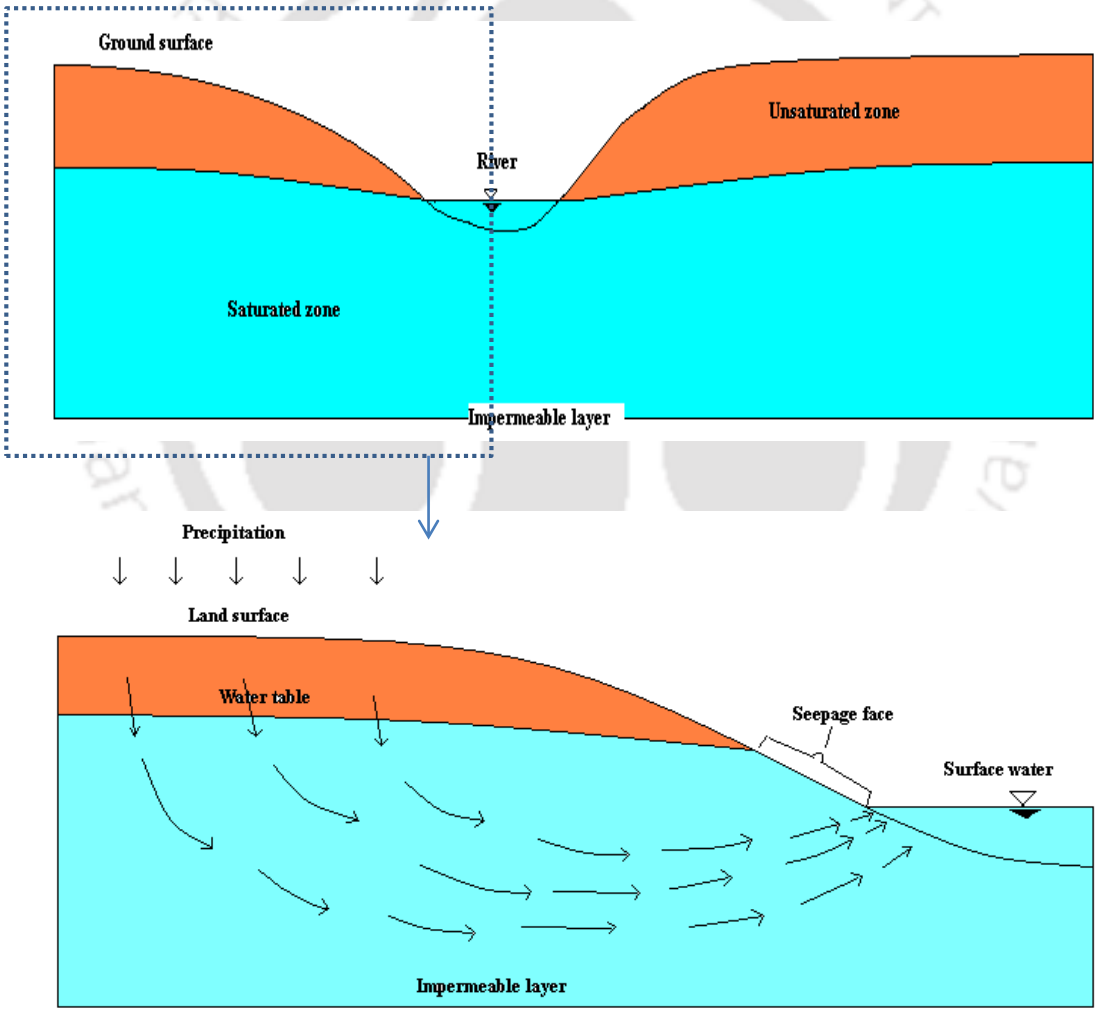

Fig.5.1 Conceptual cross sectional view of field condition

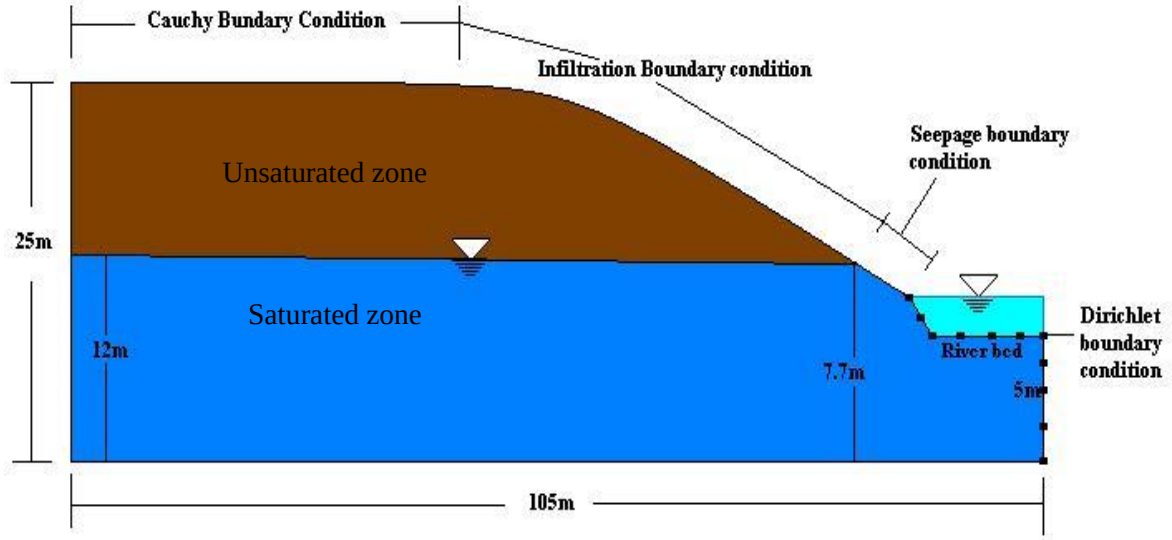

(a)

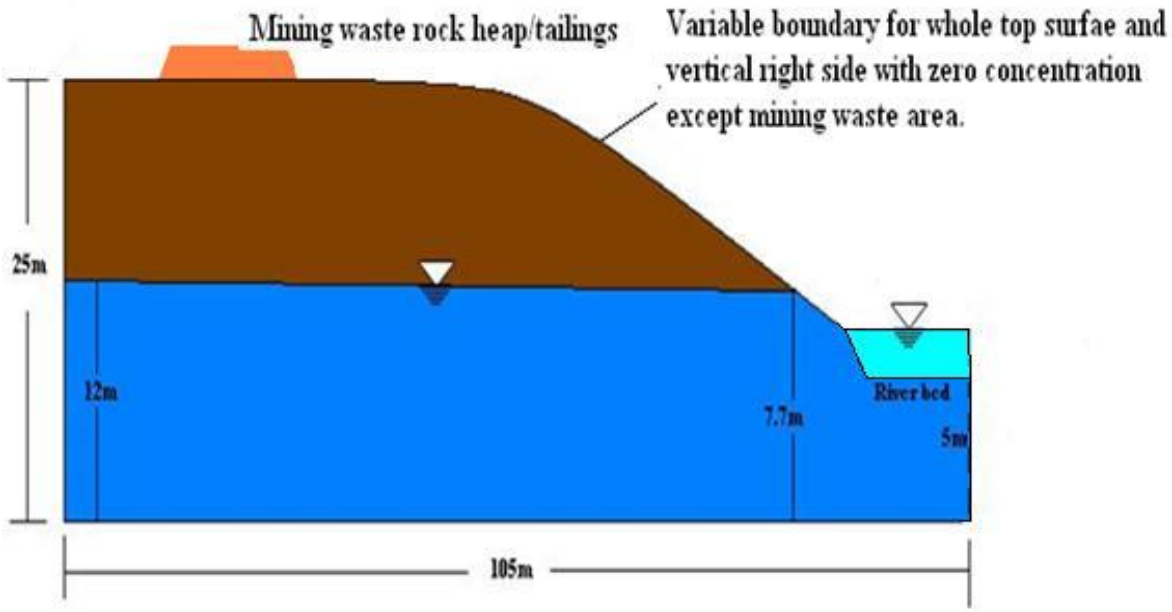

(b)

Fig.5.2 Two dimensional vertical cross section of the hypothetical domain with boundary conditions (a) of flow simulation and (b) of transport simulation

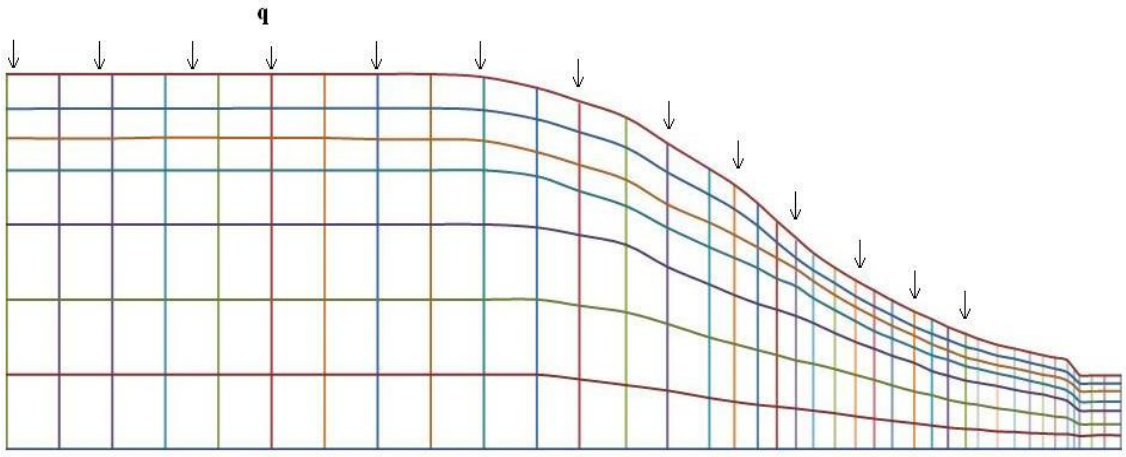

Fig.5.3 Mathematical approximation of the hypothetical domain

5.3.1 Boundary conditions

Solutions to the flow and transport equations are generated by solving the governing equations, given in chapter 1 (equations 1.1 and 1.12), in conjunction with a set of boundary conditions defined at the physical sides of the modeled system and source/sink terms. Boundary conditions available in FEMWATER model for flow and transport model are explained below and its equation form is given in the section 1.4.1 and 1.4.2 of chapter 1.

5.3.1.1 Flow boundary conditions

Fixed head (Dirichlet) boundary is defined by assigning pressure head values to the boundary nodes.

Infiltration or evapotranspiration can be represented in the boundary portion by ***specified-flux (Cauchy) boundary*** condition. Simulation is done by assigning water flux rate to specified flux type boundary nodes. The flux boundary condition is applied when infiltration rates into the subsurface media is known. The flux is assigned a negative value when it enters the region and a positive value when it leaves the region.

Rainfall-seepage (variable) boundary condition is used to simulate evaporation, seepage due to precipitation and seepage exit faces. The name variable not represents the time variance, but they correspond to either a Dirichlet or a flux boundary condition depending on rainfall, evaporation and groundwater level. It represents a combined Dirichlet/specified flux boundary conditions to simulate boundaries with known pressure head or flux rates.

5.3.1.2 Transport boundary conditions

Dirichlet or prescribed concentration boundary is defined by assigning dissolved species concentration at boundary nodes.

Specified flux (Cauchy) boundary represents the boundary where infiltration can be quantified. It represents 1) infiltration of leachate migration from a landfill, mine tailings or surface impoundments, 2) application of pesticides, fertilizers to field and 3) the dilution of existing contaminants by rainfall or irrigation. It is simulated by assigning mass flux rates along specified element sides.

Specified dispersive flux (Neumann) boundary represents the portion of the boundary, especially exit boundary, subject to dispersive flux condition. If dispersive flux is assigned zero it physically simulates advection of mass out of the system.

Variable boundary condition represents the combined specified flux and dispersive flux based on the process infiltration or water loss at boundary nodes. Same as flux boundary condition it represents 1) infiltration of leachate migration from a landfill, mine tailings or surface impoundments, 2) application of pesticides, fertilizers to field and 3) the dilution of existing contaminants by rainfall or irrigation. When the boundary being modeled may be an exit or infiltration boundary then the variable condition is proper choice. In FEMWATER there is an option that if the boundary condition is not assigned it is automatically assigned as zero gradient flow or zero gradient concentration.

5.4 Domain description

The problem domain considered is a two dimensional saturated-unsaturated domain, Figure 5.2. Hydraulic head difference between left and right side is taken as 4.8 m. The domain's slope is running towards the river, so as the groundwater flow. The vertical left surface, front surface, back surface and horizontal bottom of the region have zero gradients for water flow and contaminant transport. The sloping region on the top right is a variable flow boundary with either zero ponding depth or a net rainfall rate of 0.00346 m/day. The horizontal region on the top is a Cauchy flow boundary with an infiltration rate of 0.00346 m/day, one year (June, 2016 to May, 2017) rainfall value of Guwahati city. The vertical line and horizontal line (river bed) on the

right side are assigned with known head conditions (Dirichlet boundary conditions) for flow model and for transport it is assigned variable boundary condition with zero concentration. The region of interest is discretized with 2014 (38×1×53) elements with the elements size varies in x-direction between 2.5 and 0.6 m and the variation in z-direction ranges from 1.3 to 0.1 m, element size is varying due to the nature of sloping boundary, this results in 2106 nodal points. Simulation is done for 5 years with constant time step size of 1 day. Concentration source is placed on the top surface of the domain (10 m to 30 m) and remaining portion of the domain is free of concentration. After entering the saturated aquifer zone contaminant travels along with the direction of bulk fluid movement. The contaminant concentration in the domain varies due to the transport processes like advection, dispersion, and diffusion, etc.

5.4.1 Assumptions

For carrying out the simulations the following assumptions are incorporated,

- Throughout the simulation period inflow is provided
- Single specie transport
- Temperature is constant at 25^0C
- Neutral pH condition throughout the simulation time
- Initial pressure head is assumed to be in hydrostatic condition
- Initially domain is free of contaminants
- Entering of contaminants into the domain is restricted to particular portion of the top surface
- Reactions are taking place in mobile water region only

5.4.2 Simulation in homogeneous medium

This section presents the simulation results of contaminant transport in homogeneous medium. Simulations are carried out to understand the concentration distribution process of AMD with in the subsurface zone. Since FEMWATER has separate modules for flow and transport, simulations were run for various combinations like – single porosity flow with equilibrium and non-equilibrium transport model; dual porosity flow with non-equilibrium transport model; and with sorption and ion-exchange reactions to understand the reactive transport process under non-equilibrium condition. Results are shown in two dimensional contour plots as well as one dimensional plot that represents the variations in vertical segment of the domain (at $x = 20^{th}$ m)

for three time periods (600, 1200 and 1825th day). Input data is given in the "dat" file format, which is read by the FEMWATER code. Thereafter, the simulation variable values are stored in the output files at each time step. Numerical values from the output files are presented in contour plots by developing Matlab programming code.

5.4.2.1 Single porosity flow and equilibrium transport (HOSFET)

Spatial and temporal variation of pressure head is solved by mixed form Richards equation in flow module and contaminant transport is solved by advection diffusion equation. Outputs like, velocity and water content for all the time steps from flow simulation and geometrical coordinate details are given as input to the transport simulation along with initial and boundary conditions for contaminant. The pressure head profile and the evolution of concentration profile in the domain at three time steps are shown in Figure 5.4. No changes were observed in the pressure head profile at later times after the initial development. Nevertheless, the concentration plume evolves continuously through time and space. In the unsaturated zone, the plume movement is in vertical direction and towards the water table and once the plume enters the saturated zone it starts moving in the horizontal direction along with the ground water flow.

2D contour plot of pressure head **Pressure distribution plot at vertical segment (x=20m)**

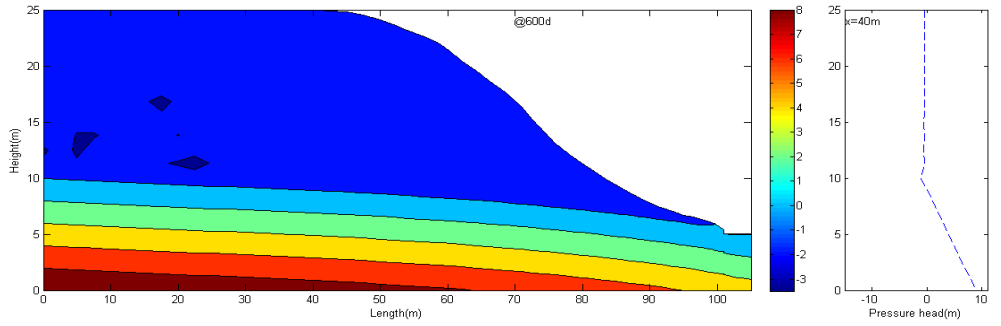

(a1)

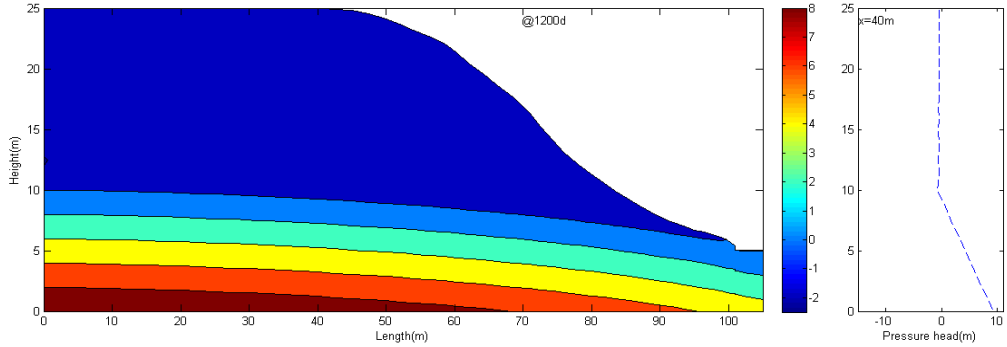

(a2)

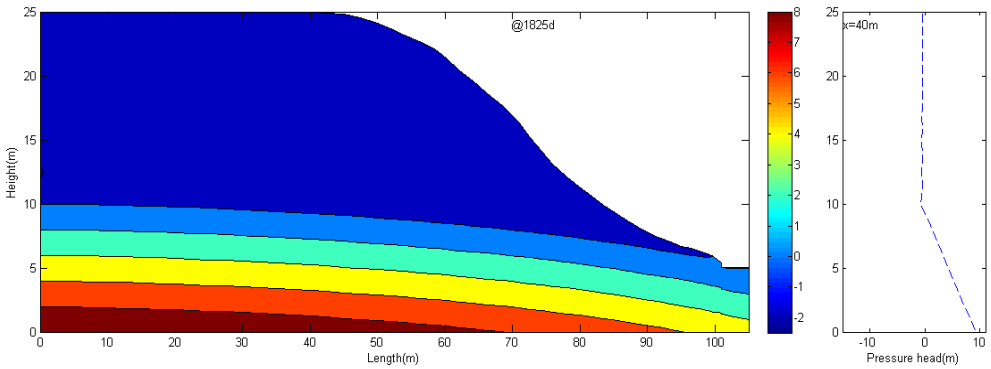

(a3)

Fig.5.4A Pressure head distribution at (a1) 600th day (a2) 1200th day (a3) 1825th day by single porosity flow for homogeneous medium

2D contour plot of ferrous ion concentration | **Concentration plot at vertical segment (x=20m)**

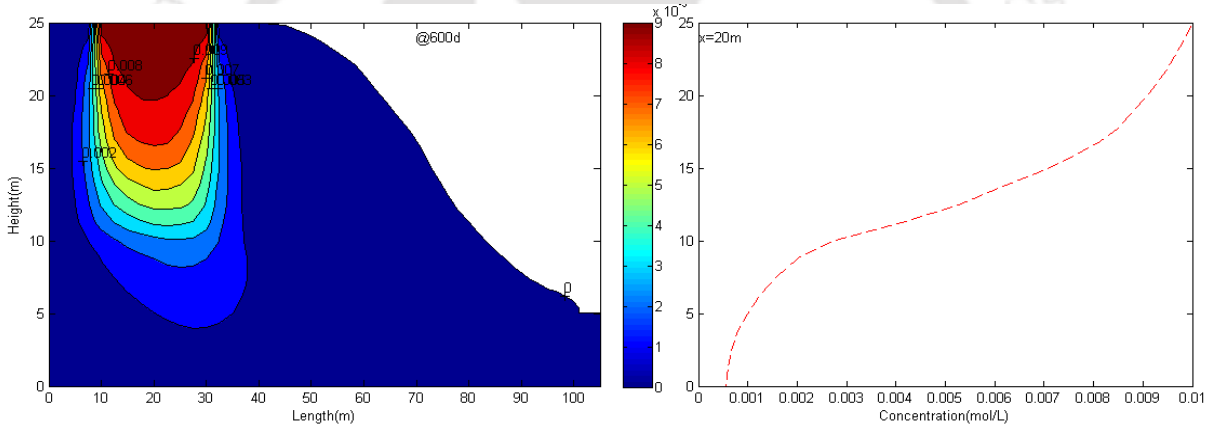

(b1)

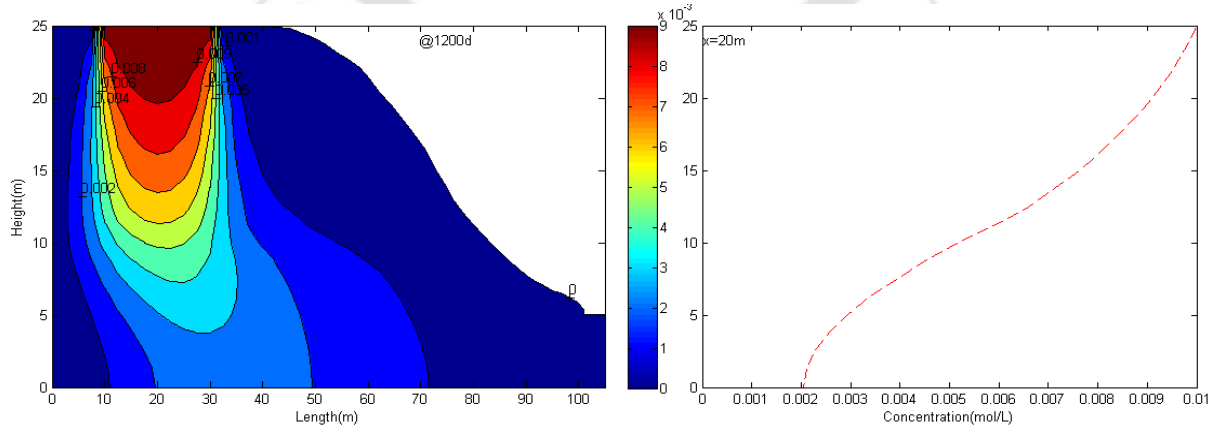

(b2)

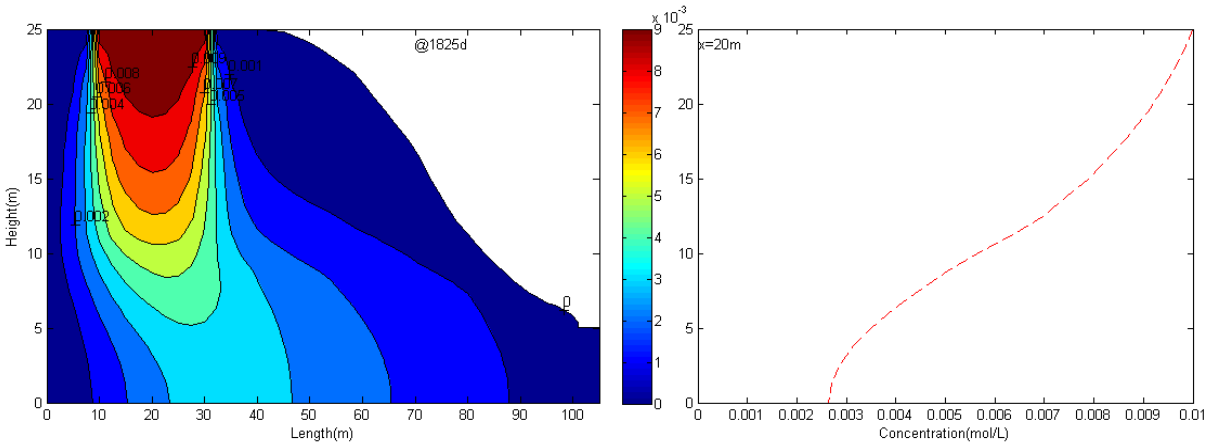

(b3)

Fig.5.4B Concentration profile at (b1) 600th day (b2) 1200th day (b3) 1825th day by single porosity flow and equilibrium transport model for homogeneous medium

5.4.2.2 Single porosity flow and non-equilibrium transport (HOSFNET)

Non-equilibrium contaminant transport can be modelled by two types, this section deals with the type I, where water content value from flow model is splited into mobile and immobile region and it is given as input to the non-equilibrium transport model. In flow module, spatial and temporal variation of pressure head is solved by single porosity mixed form Richards equation and contaminant transport is solved by non-equilibrium model. Chapter 3 explained the addition of mixed form Richards equation and non-equilibrium transport equation to the FEMWATER model. Figure 5.5 shows the concentration profile at three time steps.

2D contour plot of concentration **Concentration plot at vertical segment (x=20m)**

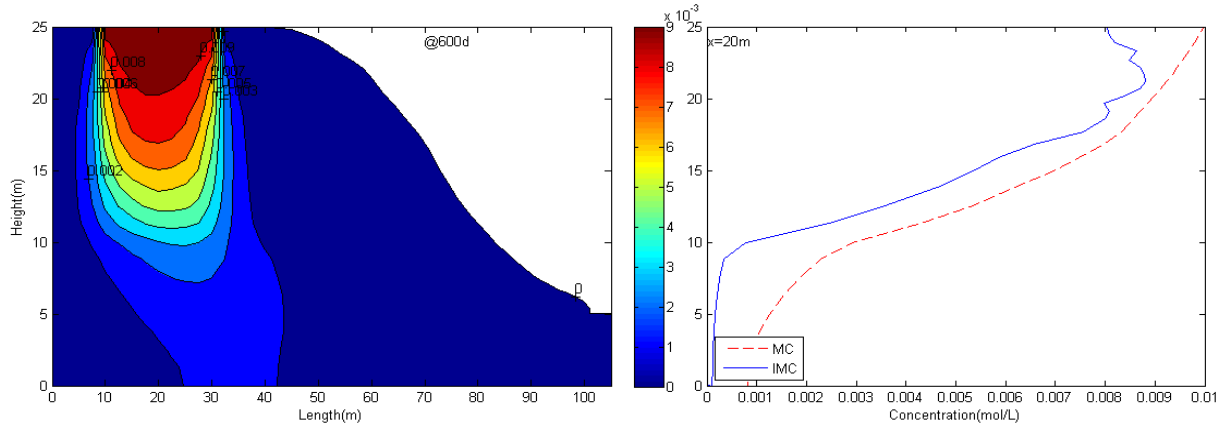

(a)

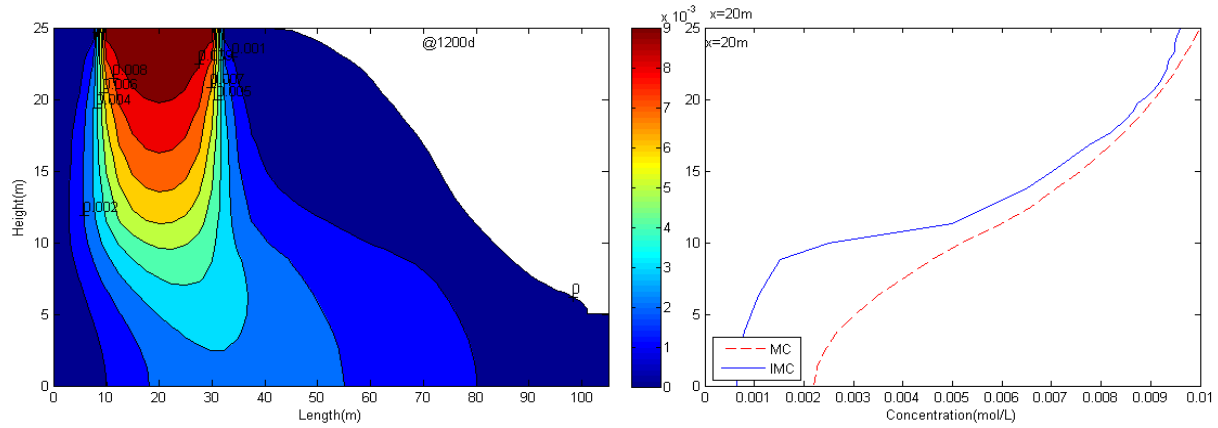

(b)

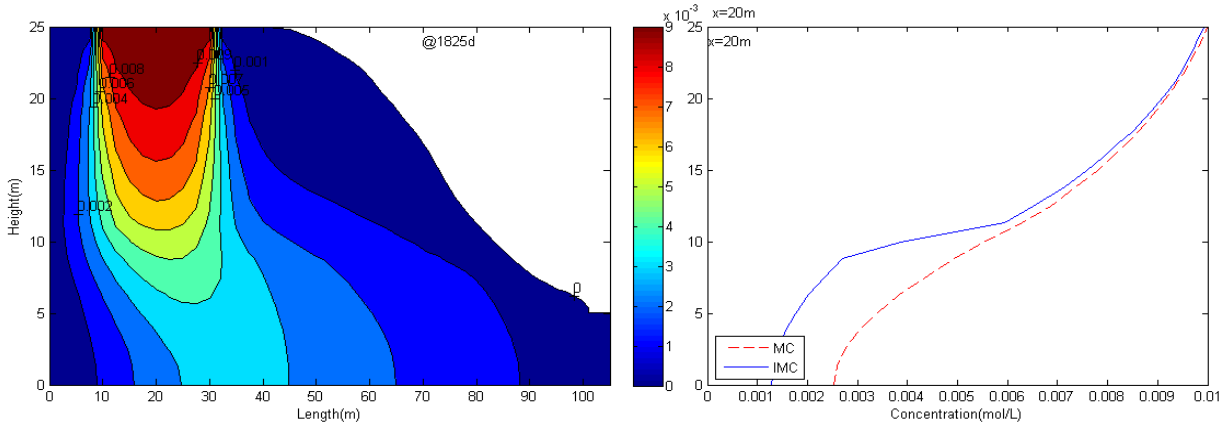

(c)

Fig.5.5 Concentration distribution in the domain by non-equilibrium model at (a) 600th day (b) 1200th day and (c) 1825th day (- - - concentration in mobile water, —— concentration in immobile water)

5.4.2.3 Dual porosity flow and non-equilibrium transport (HODFNET)

In type II non-equilibrium model, the FEMWATER flow model itself is modified to accommodate mobile and immobile zones of liquid and the variations of these liquid zones with respect to pressure (or suction). This model is improvement to the HOSFNET model as it takes values of mobile and immobile water content directly from the flow model instead of splitting the water content into two portions. This model can compute the spatial and temporal variations of pressure head using the dual porosity/mobile-immobile flow module and contaminant concentrations using non-equilibrium solute transport model. Incorporation of dual porosity flow equation to the FEMWATER model is explained in Chapter 3. Figure 5.6 shows the result from type II non-equilibrium model.

2D contour plot of pressure head **Pressure distribution plot at vertical segment (x=20m)**

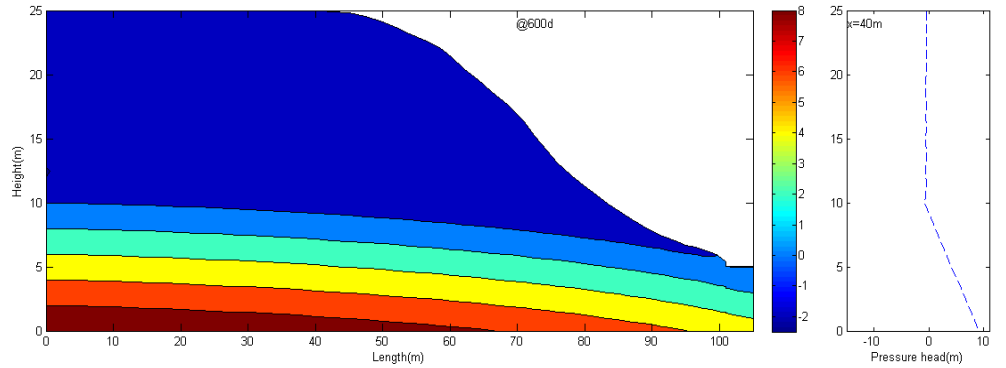

(a1)

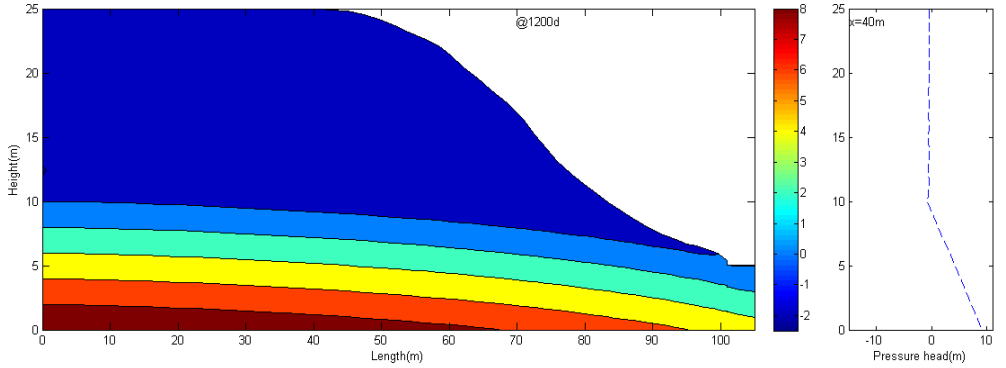

(a2)

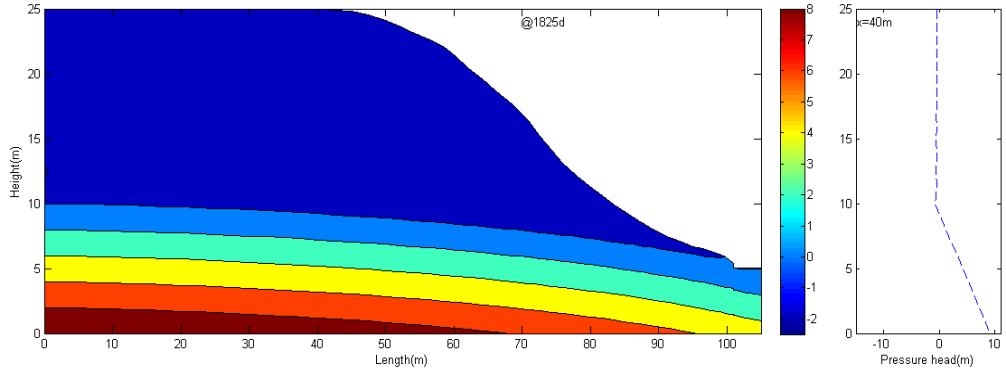

(a3)

Fig.5.6A Pressure head distribution by dual porosity model at (a1) 600th day (a2) 1200th day (a3) 1825th day

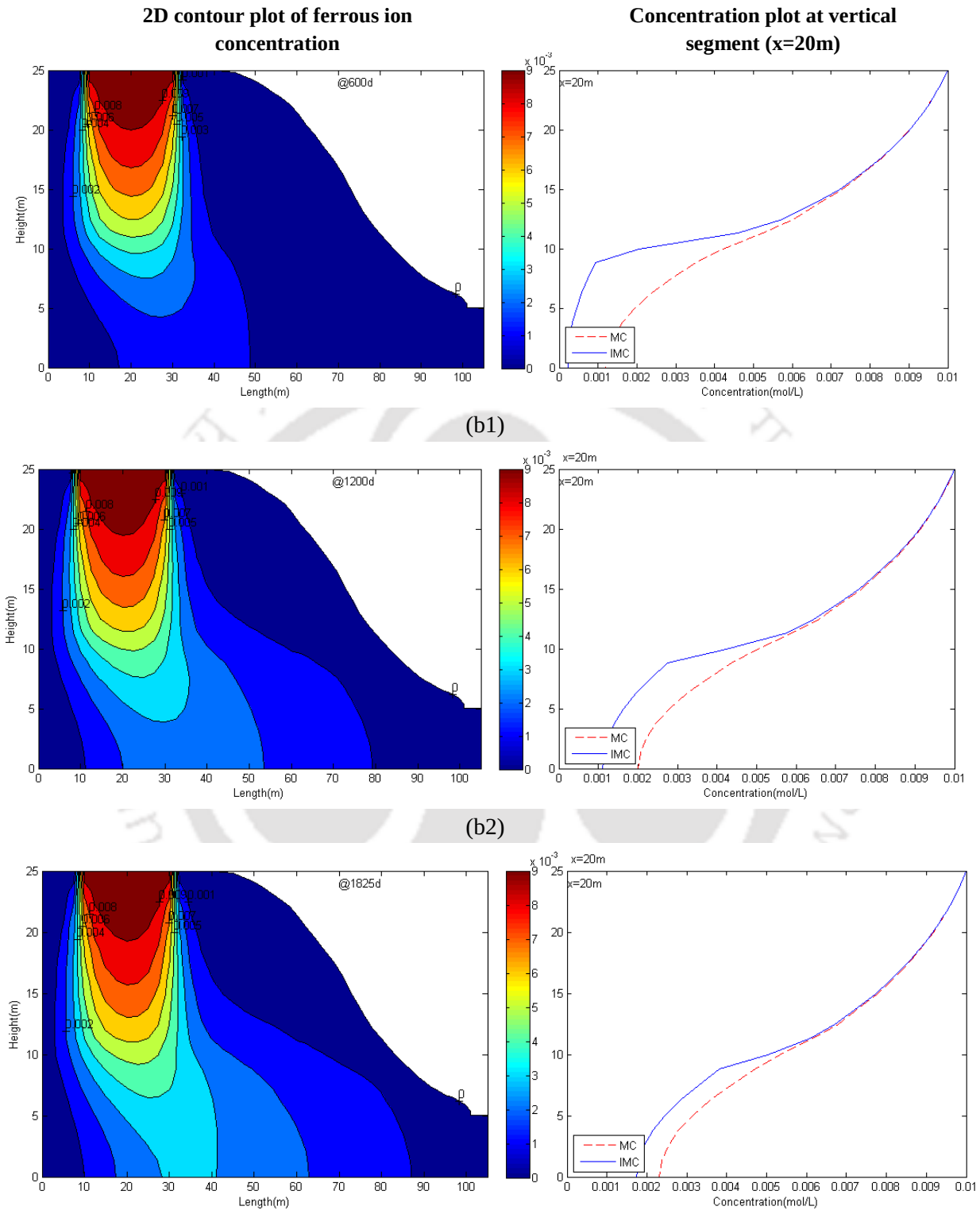

Fig.5.6B Simulated concentration profile by non-equilibrium model at (b1) 600th day (b2) 1200th day (b3) 1825th day

5.4.2.4 Comparison of simulations of non-equilibrium transport models (HOSFNET vs. HODFNET)

To study the impact of mobile-immobile flow on contaminant transport two non-equilibrium model methods, i) single porosity flow - non-equilibrium transport model and ii) dual porosity/mobile-immobile flow - non-equilibrium transport model, are compared in this section. Simulation is done for five years and the results are presented for the time steps of 600, 1200 and 1825th day. Notable differences between the two non-equilibrium simulations are observed (Figure 5.7). At 600th day, more spreading of contaminant in the bottom region (saturated region) is observed in HODFNET model than the HOSFNET model (Figure 5.7 a1 and b1).

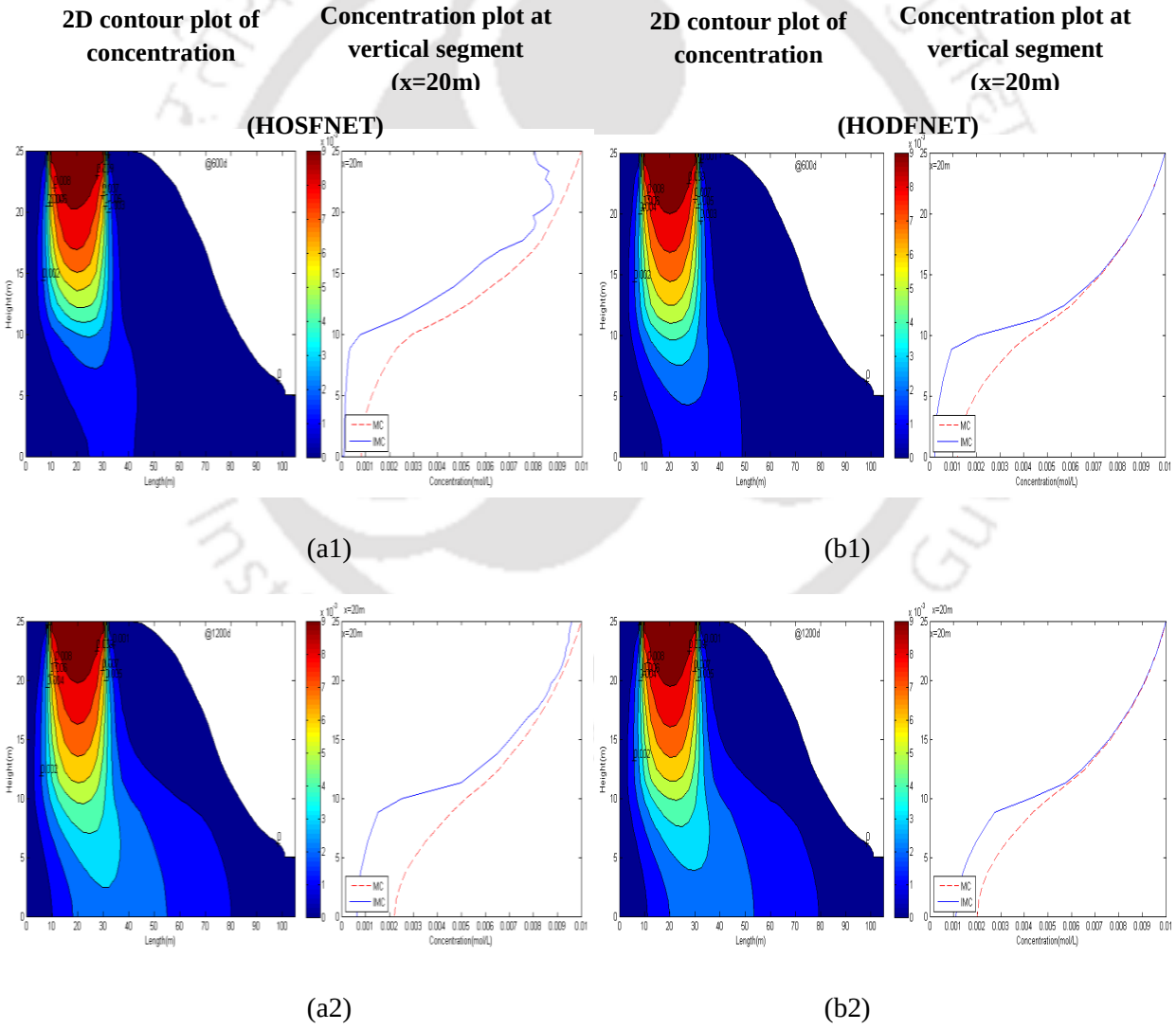

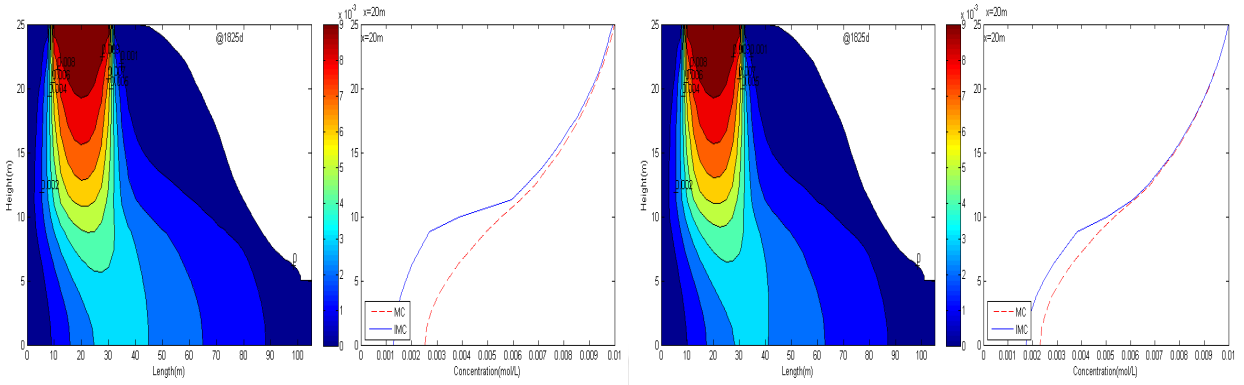

(a3) (b3)

Fig.5.7 Single porosity flow and non-equilibrium concentration profile at (a1) 600th day (a2) 1200th day (a3) 1825th day; dual porosity flow and non-equilibrium concentration profile at (b1) 600th day (b2) 1200th day (b3) 1825th day (- - - concentration in mobile water, —— concentration in immobile water)

In the unsaturated region, that has dense concentration, the differences in contaminant concentrations in simulations from the two non-equilibrium models (HOSFNET and HODFNET) are less. In HODFNET model, the contaminant concentration at 600th day in mobile and immobile zones of unsaturated region is almost same (1D plot of Figure 5.7 b1) due to the rapid transfer of contaminant mass between mobile and immobile region. However, in the HOSFNET model (1D plot of Figure 5.7 a1); the difference in concentrations of the contaminant in mobile and immobile water is large. At 1200th day, there is no difference observed in concentrations of contaminants in mobile and immobile zones of water in unsaturated zone, however, there is a difference in spreading pattern in saturated zone as is evident between two non-equilibrium models. Saturated zone, in HODFNET simulation, transfers more contaminant mass to immobile zone than HOSFNET model as time increases. Difference is observed in spreading pattern of concentration magnitude $\leq$ 0.004 mol/l, especially at later periods of simulation (>1000 day). At initial times (< 600 days) spreading pattern is more in less concentration region of HODFNET model (Figure 5.7 a1 vs. b1) and at later times spreading is more in less concentration region of HOSNFET model (Figure 5.7 a3 vs. b3). At the end of fifth year, reach of contaminant at the downstream is almost same for both the transport simulations. Non-equilibrium transport process enhances the spreading of contaminant in the less concentration region at initial simulation times and due to the process of mass transfer from mobile to immobile water region, contaminant concentration in mobile water decreases at later time steps.

5.4.2.5 Reactive transport and non-equilibrium mass transfer effects on contaminant transport

In this section, the reactive transport in the variably saturated zone is simulated along with the concept of physical non-equilibrium. Sorption and ion-exchange are the two reactive mechanisms considered. Both reactions treated in this study are assumed to be governed by local chemical equilibrium, which assumes that chemical reaction is time independent compared to the physical processes and the forward and backward reactions takes place at that instant of time. As expected HODFNET model advances the concentration front compared to equilibrium reactive transport simulation (Figure 5.10)

5.4.2.6 Single porosity flow and equilibrium transport (advective dispersive model) with sorption reaction (SR-HOSFET)

Transport with default advective-dispersive equation and sorption reaction is simulated to analyse the non-equilibrium effect on reactive transport. Sorption reaction retards the contaminant transport and it depends upon the soil type and specific contaminant type. Compared to conservative transport process, sorption retards the contaminant movement that is evident from the comparison of Figures 5.4B and 5.8.

2D contour plot of concentration **Concentration plot at vertical segment (x=20m)**

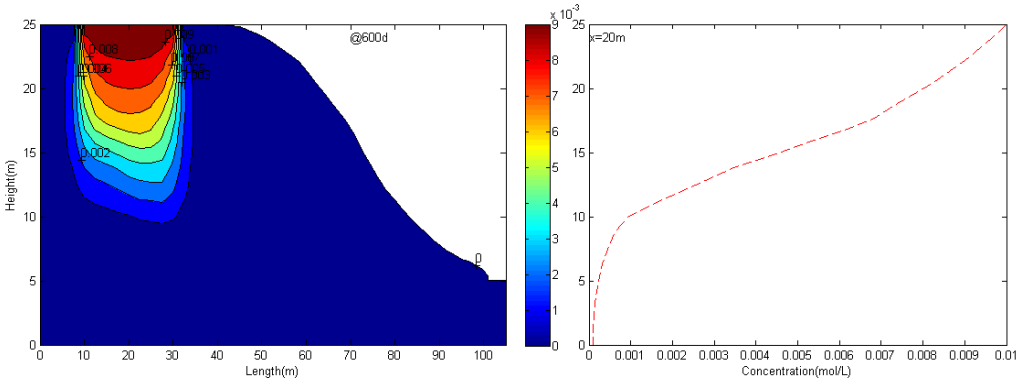

(a)

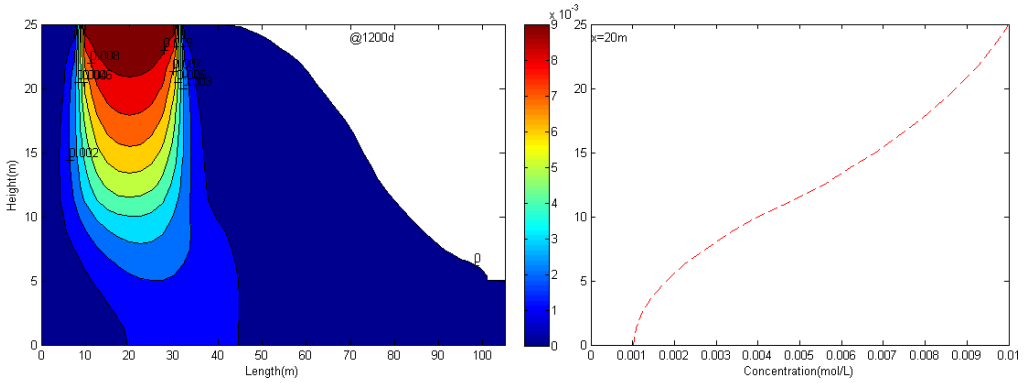

(b)

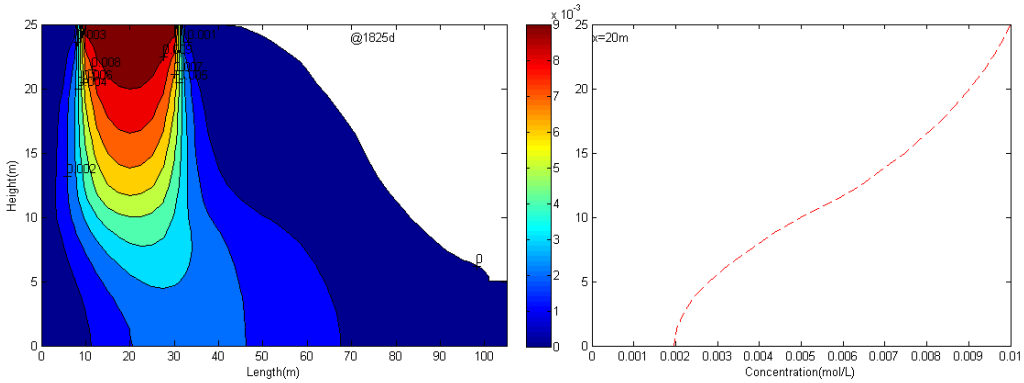

(c)

Fig.5.8 Concentration distribution simulation by single porosity flow and equilibrium transport model with sorption reaction at (a) 600th day (b) 1200th day (c) 1825th day

5.4.2.7 Single porosity flow and non-equilibrium transport with sorption reaction (SR-HOSFNET)

Early arrival of contaminants due to the soil aggregated nature or dead end pores is modeled by non-equilibrium transport models. This section gives the simulation results of physical non-equilibrium transport process along with sorption reaction to study the effects of non-equilibrium mass transfer on the reactive transport. However, single porosity is assumed for water flow through the pores and thereby to solve the flow module. Figure 5.9 shows that mass transfer of contaminant between mobile and immobile zones affect the contaminant transport under reactive conditions as well. Sorption reaction retards the contaminant movement by holding the contaminants on the surface of the solid particles; portion of the contaminant, those are not participating in reaction, tends to move faster due to the non-equilibrium effect so the solute

front advances quickly to the downstream compared to the results of equilibrium reactive transport model.

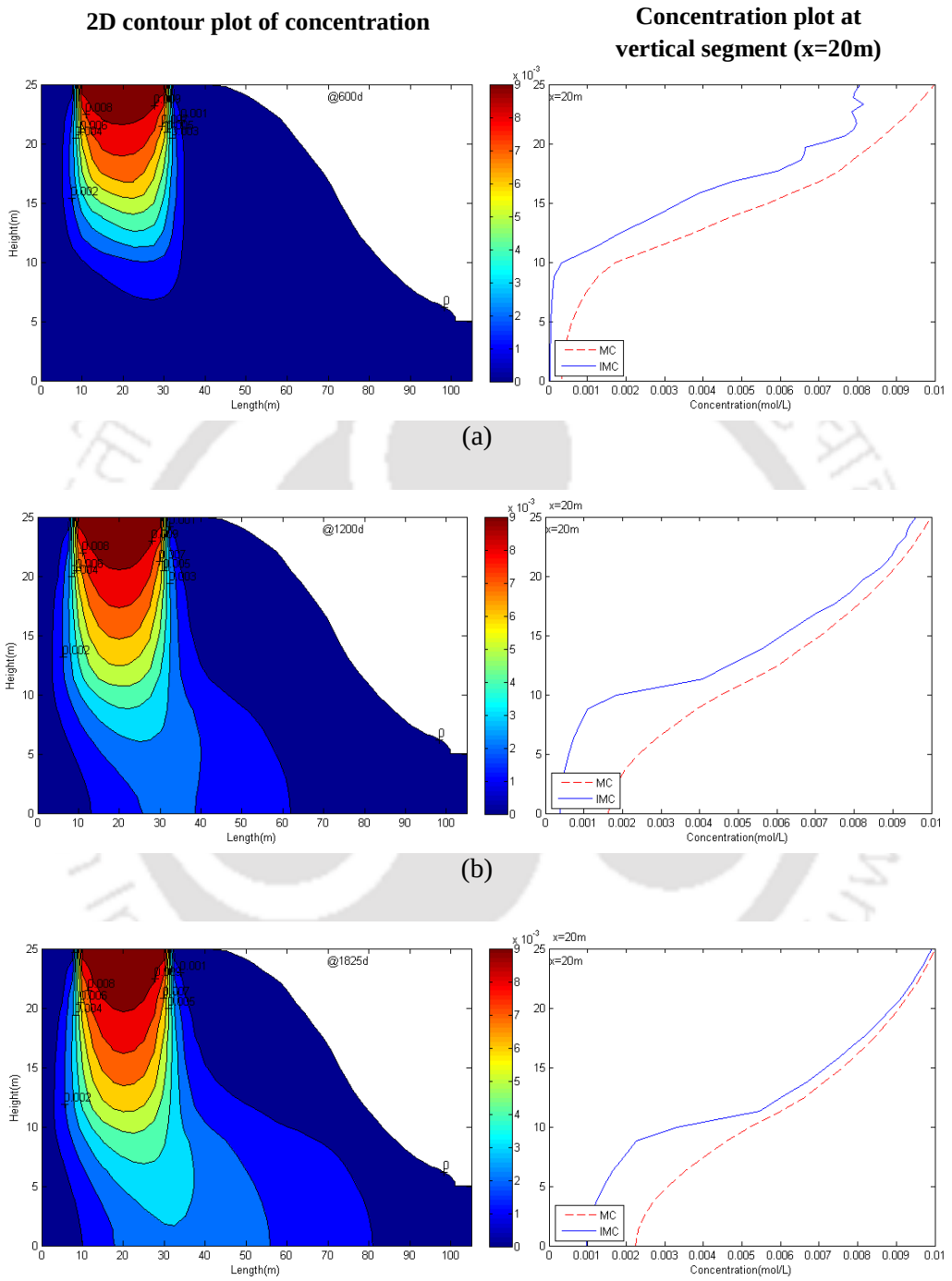

Fig.5.9 Concentration distribution simulation by single porosity flow and non-equilibrium transport model with sorption reaction at (a) 600th day (b) 1200th day (c) 1825th day (- - - concentration in mobile water, —— concentration in immobile water)

5.4.2.8 Dual porosity flow and non-equilibrium transport with sorption reaction (SR-HODFNET)

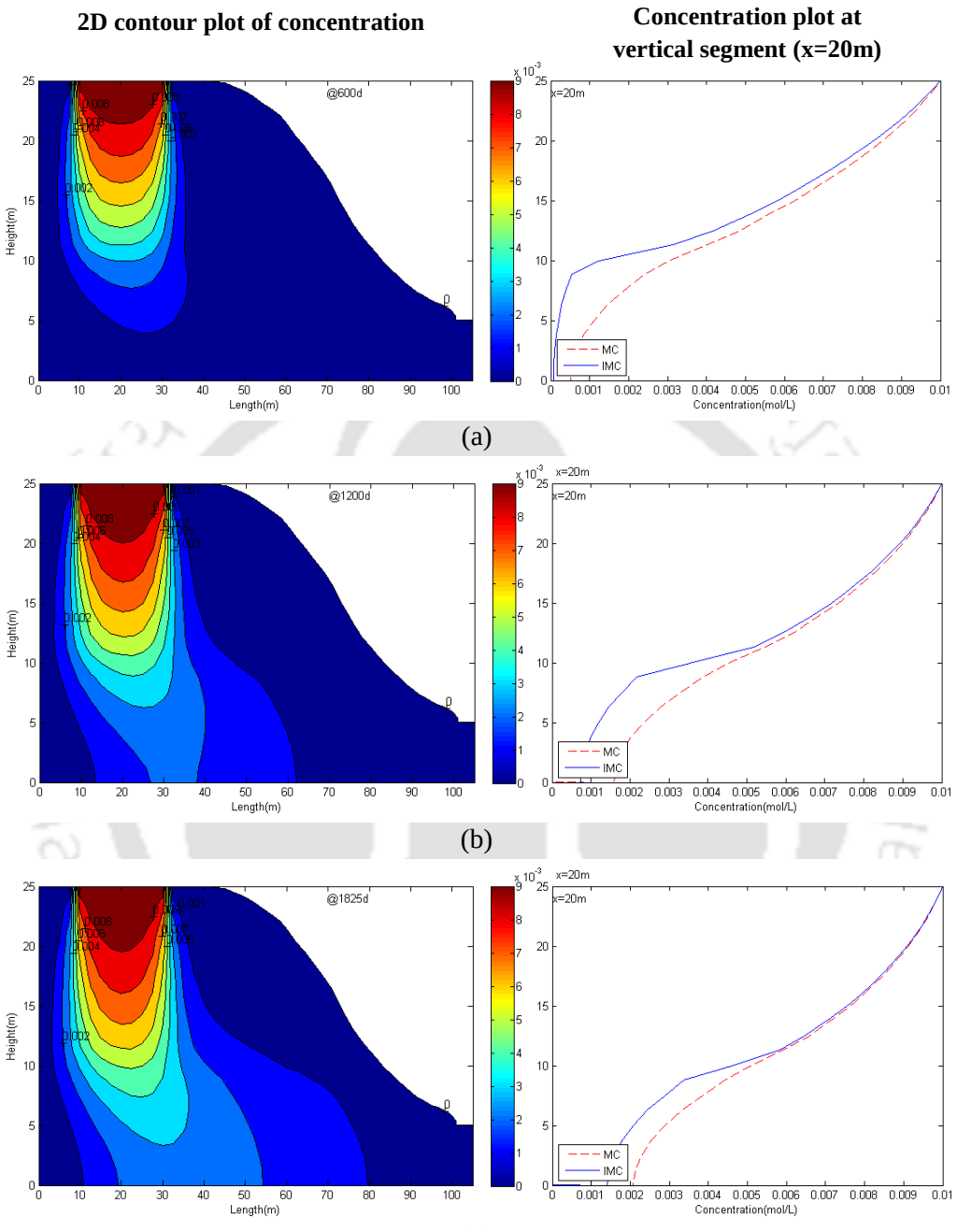

Fig.5.10 Concentration distribution simulation by dual porosity flow and non-equilibrium transport model with sorption reaction at (a) 600th day (b) 1200th day (c) 1825th day (- - - concentration in mobile water, ‑ —— concentration in immobile water)

Figure 5.10 show results from the second type of non-equilibrium model. That is the effect on solute transport, while taking into account the dual porosity in flow module as well as physical

non-equilibrium in solute transport along with the sorption reaction. In this case, as well, the evolution of contaminant plume through the subsurface media is seen to be effected by the dual porosity and by the physical non-equilibrium. The next section explains the difference between the results of SR-HOSFET, SR-HOSFNET, and SR-HODFNET models.

5.4.2.9 Comparison of equilibrium and two non-equilibrium transport models (SR-HOSFET, SR-HOSFNET, and SR-HODFNET) with sorption reaction

Vertical segment concentration distribution of ferrous ion in mobile water from three simulations with sorption reaction is given (in 1D format) in the Figure 5.11. Like in the conservative transport, non-equilibrium transfer process enhances contaminant spreading in the reactive transport too, however, spreading of contaminant is less in reactive transport model compared to conservative transport simulation, due to the retardation action. As seen from the Figure 5.11, contaminant travels a bit slower for the case of equilibrium transport with sorption reaction (dashed line), than in the case of non-equilibrium reactive transport (continuous and starred line). In unsaturated zone there is little difference between the three transport combinations, however, in saturated zone the two non-equilibrium models exhibit similar result but both differ from equilibrium model.

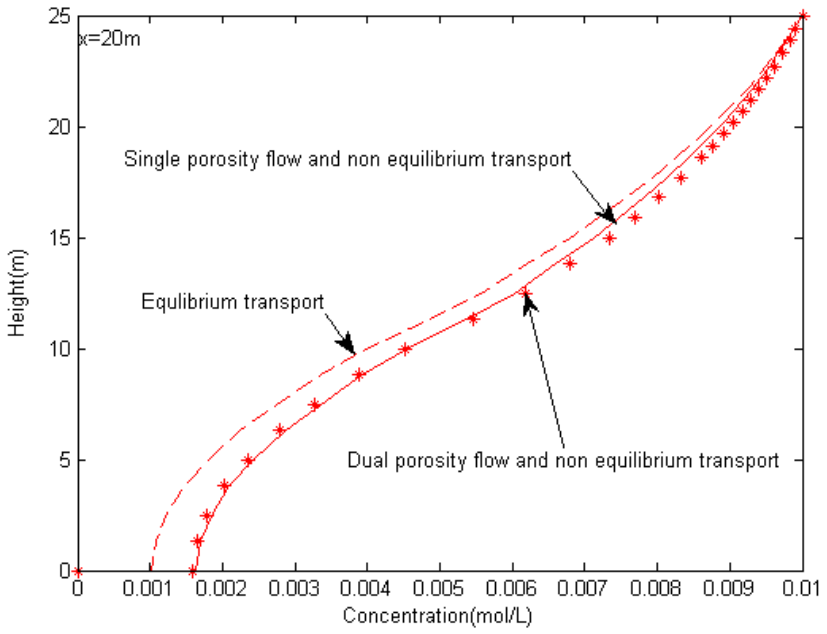

Fig.5.11 Comparison of ferrous ion concentration in mobile water at vertical segment (x=20th m) at 1200th day by equilibrium and non-equilibrium transport model simulation with sorption reaction.

In the equilibrium sorption, the reactions occur instantaneously and thereafter, the contaminants are advected and diffused. Some part of the contaminant mass enters in to immobile region and some part of it participates in sorption reactions. The remaining portion of contaminant in mobile water travels fast due to more speed of water in mobile zone. This velocity increase causes enhanced spreading of contaminant plume in non-equilibrium simulations. As time proceeds, the difference between two non-equilibrium transport simulations decreases for conservative transport and further decreases for reactive transport.

5.4.2.10 Single porosity flow and equilibrium transport with ion exchange reaction (IE-HOSFET)

The incoming contaminants in ionic form, ferrous ion (Fe^{2+}), can be attracted by the opposite charge that is present in the soil or porous media, sodium (Na^{+}). Ion-exchange is also a kind of sorption reaction; however, it replaces the existing ion in the medium which is not considered to be harmful to the environment. This reaction module is included to the FEMWATER model in the modified version. Figure 5.12 shows the result of ion-exchange simulation.

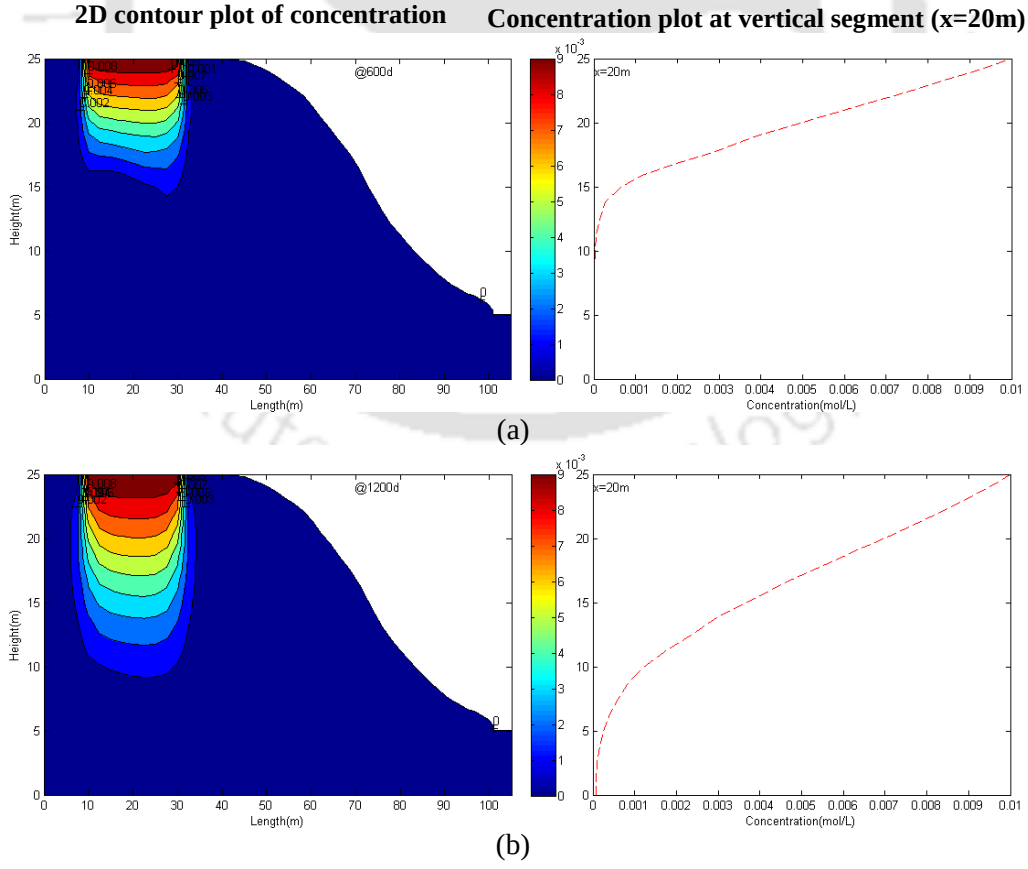

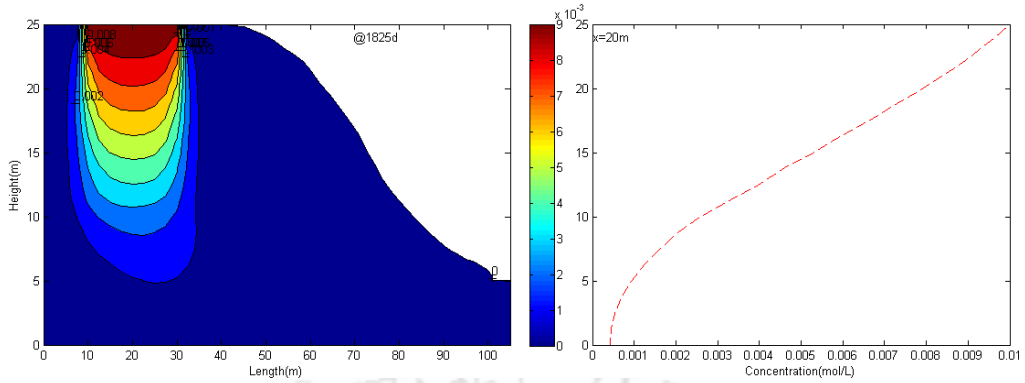

(c)

Fig.5.12 Concentration distribution simulation by single porosity flow and equilibrium transport model with ion-exchange reaction at (a) 600th day (b) 1200th day (c) 1825th day

5.4.2.11 Single porosity flow and non-equilibrium transport with ion exchange reaction (IE-HOSFNET)

This section describes the transport properties of ferrous ion along with non-equilibrium mass transfer and ion-exchange reaction. Water content value is obtained from the single porosity flow model and it is given as input to the transport model by partitioning in to mobile and immobile water, for the purpose of easy understanding this way of representing non-equilibrium is defined as ***first type non-equilibrium***. Nevertheless, the velocity remains the same as single porosity model output, results are shown in Figure 5.13.

2D contour plot of concentration **Concentration plot at vertical segment (x=20m)**

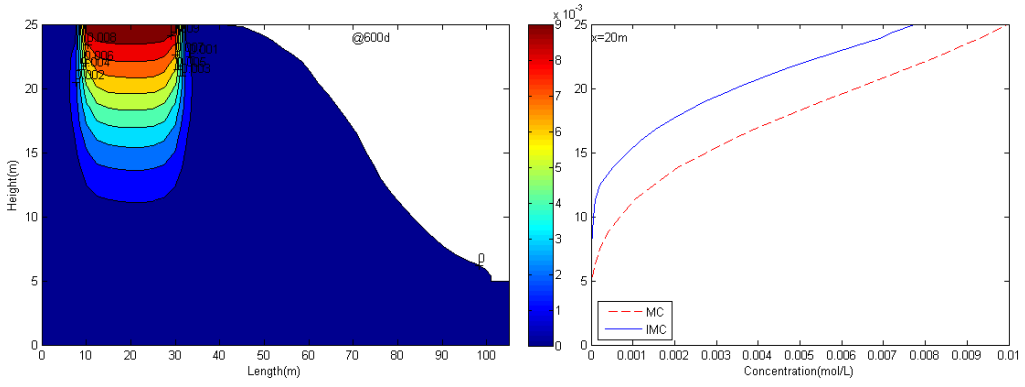

(a)

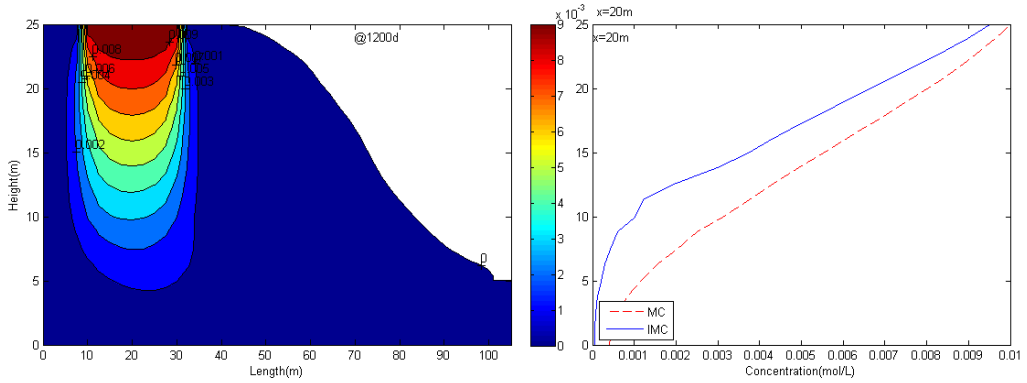

(b)

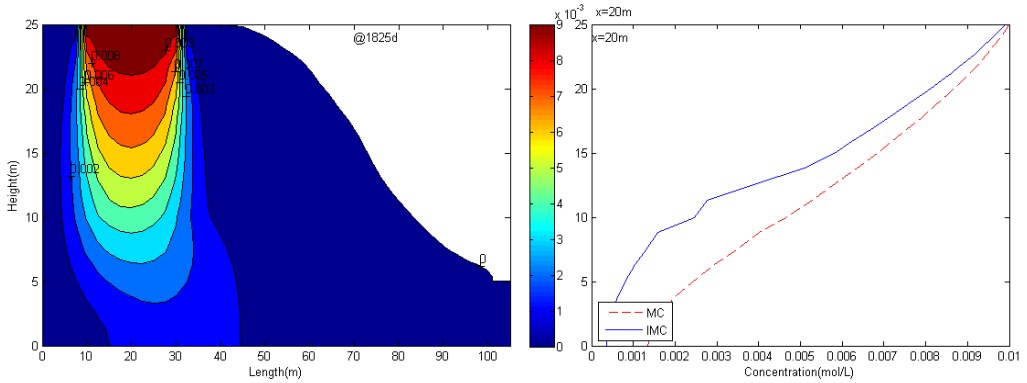

(c)

Fig.5.13 Concentration distribution simulation by single porosity flow and non-equilibrium transport model with ion-exchange reaction at (a) 600th day (b) 1200th day (c) 1825th day (- - - concentration in mobile water, —— concentration in immobile water)

5.4.2.12 Dual porosity flow and non-equilibrium transport with ion exchange reaction (IE-HODFNET)

.

2D contour plot of concentration **Concentration plot at vertical segment (x=20m)**

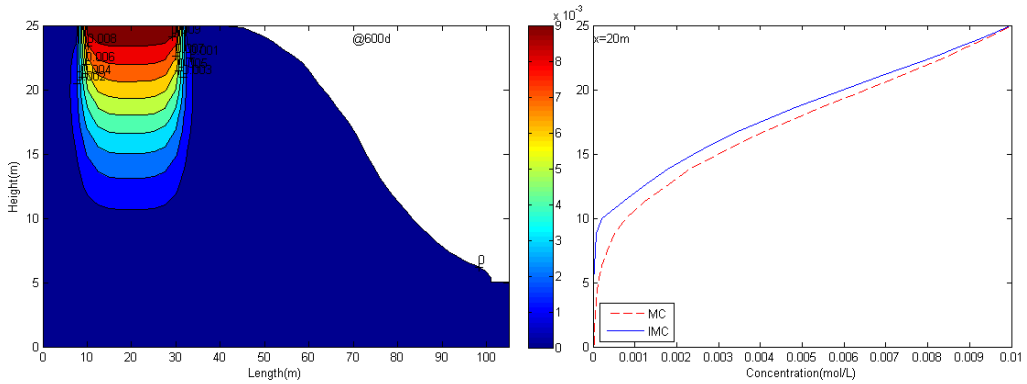

(a)

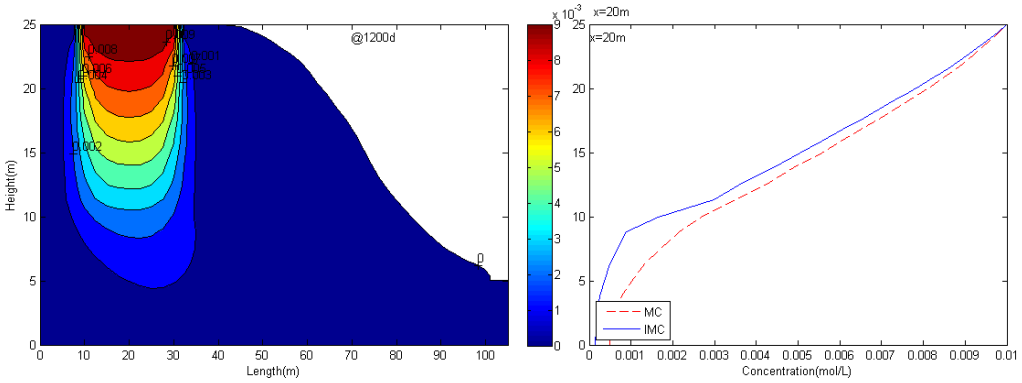

(b)

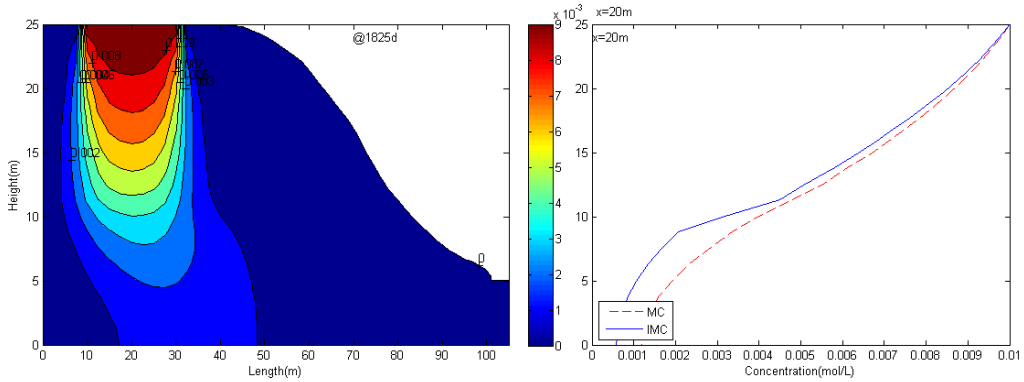

(c)

Fig.5.14 Concentration distribution simulation by dual porosity flow and non-equilibrium transport model with ion-exchange reaction at (a) 600th day (b) 1200th day (c) 1825th day (- - - concentration in mobile water, —— concentration in immobile water)

Second type non-equilibrium model, where mobile and immobile water content value is obtained by dual porosity flow model is applied to study the reactive transport model with ion-exchange reaction and also to study the difference between two types of non-equilibrium model. Ion-exchange reaction is assumed as equilibrium reaction, which occurs quickly than the transport process. Compare to first type non-equilibrium model (IE-HOSFNET), mass exchange between two water regions is more in second type non-equilibrium model (IE-HODFNET), it is shown in Figures 5.14.

5.4.2.13 Comparison of equilibrium and non-equilibrium transport with ion-exchange reaction

As in the case of sorption reaction, non-equilibrium transport with ion-exchange also exhibits quick arrival of contaminants at downstream. However, compared to sorption reaction, non-

equilibrium ion-exchange transport shows much difference between equilibrium and non-equilibrium transport (Figure 5.15). In the case of ion-exchange, the Fe^{2+} ions in the incoming solution are exchanged with the monovalent ions (Na^{+}) present in the soil. The increased advancement of concentration fronts of ferrous ions under non-equilibrium conditions is evident for transport with ion exchange too. Figure 5.15 shows the 1200th day simulation results for three transport simulations, equilibrium and two types of non-equilibrium model, at the vertical segment (x = 20 m) of the two dimensional domain.

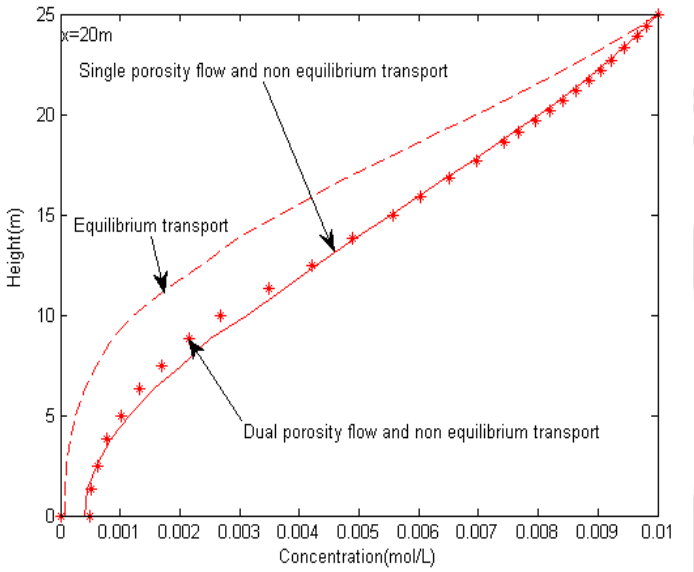

Fig.5.15 Comparison of ferrous ion concentration in mobile water at vertical segment (x=20th m) at 1200th day by equilibrium and non-equilibrium transport model simulation with ion-exchange reaction.

5.4.3 Simulation in heterogeneous medium

Most of the field conditions related to acid mine drainage are not in homogeneous medium. Hence, to simulate the non-equilibrium transport properties for AMD, two types of soils are used to replicate the heterogeneous medium (Figure 5.16). The assumption is; top 10 meter of the domain contains loamy soil and the remaining part of the domain contains the sandy clay loam. The lower part is having less dispersivity and hydraulic conductivity values with different porosity than the top ten meters. Due to the different conductivity and dispersivity, transport characteristic of heterogeneous medium is different from homogeneous medium. During the initial times, the travel of contaminated plume is fast in homogeneous medium compared to heterogeneous medium.

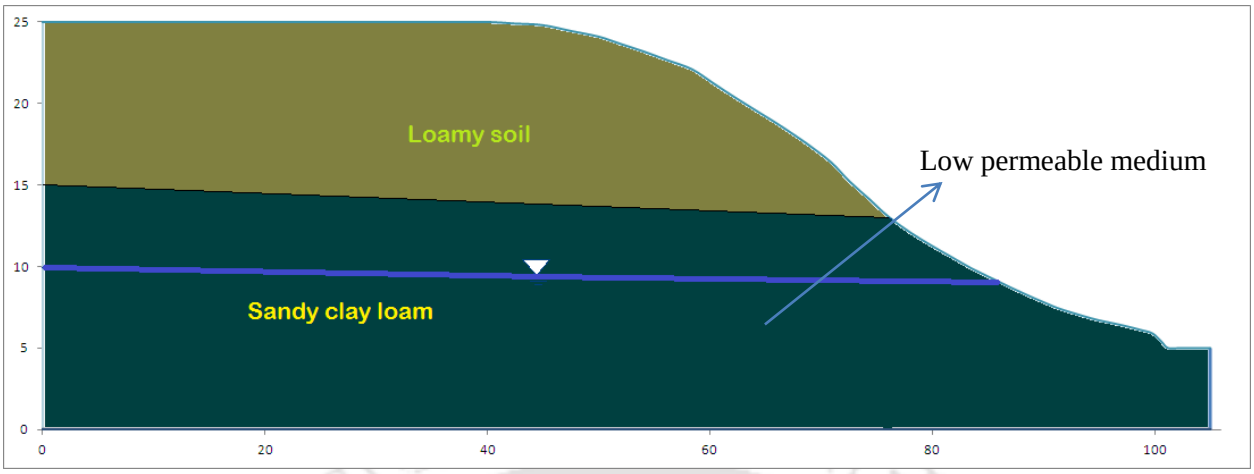

Fig.5.16 Two dimensional vertical cross section of the hypothetical heterogeneous domain

However, at later stages, the plume movement is faster in heterogeneous medium compared to homogenous medium in the top portion of the domain. The transverse spreading in saturated region is much decreased due to less dispersivity and conductivity.

Same initial and boundary conditions are applied as for the homogeneous domain. The vertical left, front, back surface and horizontal bottom of the region are impermeable boundaries. The sloping region on the top right is a variable flow boundary with either zero ponding depth or a net rainfall rate of 0.00139 m/day. The horizontal region on the top is a Cauchy flow boundary with an infiltration rate of 0.0139 m/day. The vertical line and the bottom on the right side are assumed as known head conditions (Dirichlet boundary conditions). Water table is at 12.5 m at the left side and 5 m at right side and initial condition is assumed as hydrostatic pressure head (height of water table – height of nodal points from bottom) at each nodes. Saturated zone is mentioned by the symbol (inverted triangle) in the figure 5.16.

5.4.3.1 Single porosity flow and equilibrium transport (HESFET)

Simulation model in this section is same as the simulation given in the section 5.4.2.1, however, will have two different soil types to represent the heterogeneity. Below figures shows the ferrous ion concentration in the mobile water and their concentrations are expressed in terms of mole per liter. From the simulation results it is observed that low permeable medium severely affects the transport properties and also parameters like dispersivity, mass transfer rate constant, mobile water content, inflow, etc. also affect the transport, results are shown in Figure 5.17.

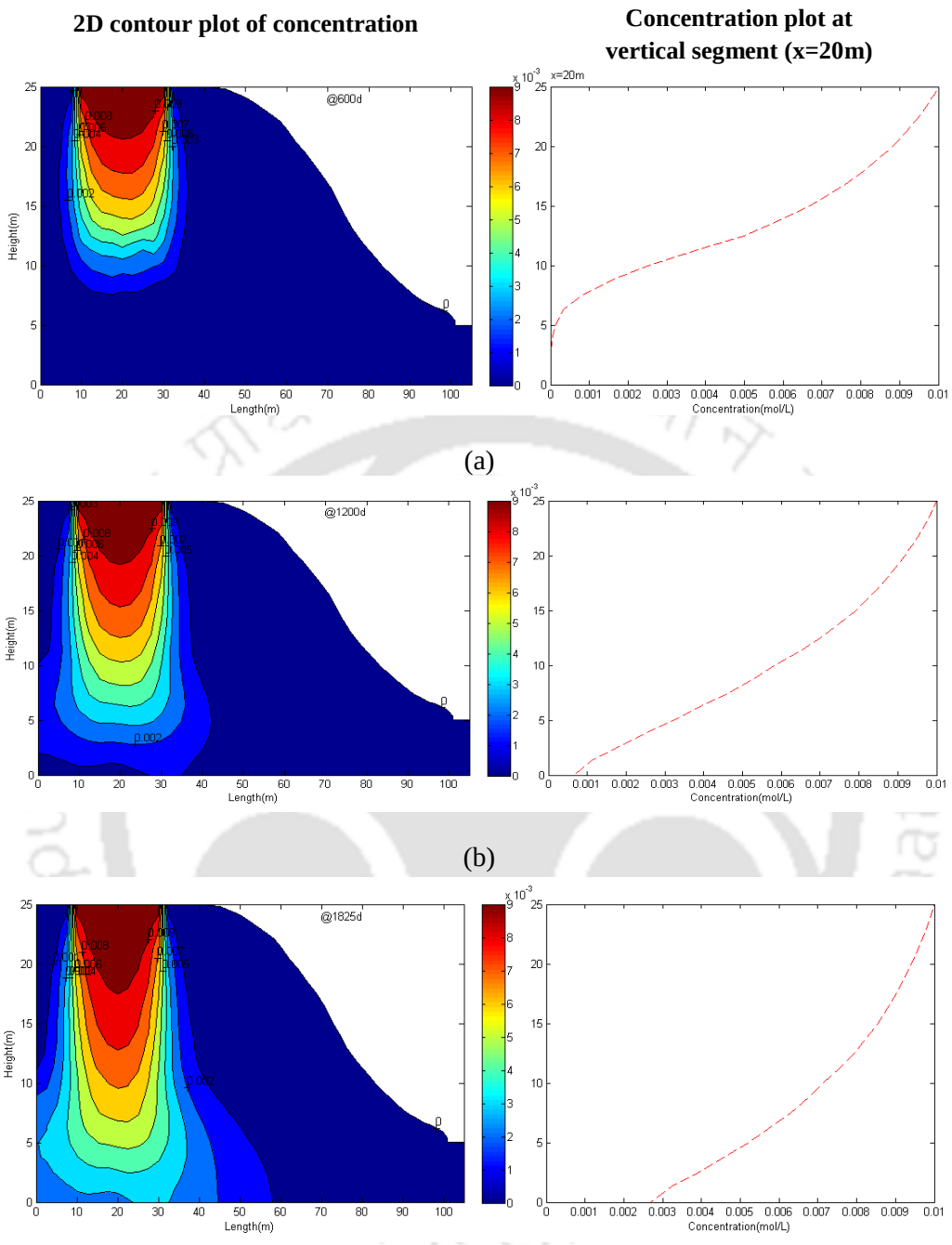

Fig.5.17 Simulation of concentration profile in heterogeneous medium by single porosity flow and equilibrium transport model at (a) 600th day (b) 1200th day (c) 1825th day

5.4.3.2 Comparison of two non-equilibrium models

This section compares the two types of non-equilibrium model results in heterogeneous medium for ferrous ion transport. In both the regions, homogeneous and heterogeneous, transport curve

predicted by type II non-equilibrium model (Dual porosity Flow – Non-Equilibrium Transport = DFNET) shows the quick break through across the particular point and time compared to type I non-equilibrium model (Single porosity Flow – Non-Equilibrium Transport = SFNET); due to the increase in mass transfer in to the immobile water region. When the volumetric water content value becomes less in the pore region it leads to the increase in water flow velocity, this scenario is fully captured by the type II non-equilibrium model, which solves dual porosity flow equation, unlike the type I model. That is why solution front seems advanced in the HEDFNET model outputs, Figures 5.18 b1- b3. In this chapter non-equilibrium model is mentioned in two names as second type non-equilibrium model and type II non-equilibrium model. Both the names are same and this is applicable to names 'type I and first type non-equilibrium model' also.

Concentration plot at vertical segment (x=20m) of the 2D domain

HESFNET **HEDFNET**

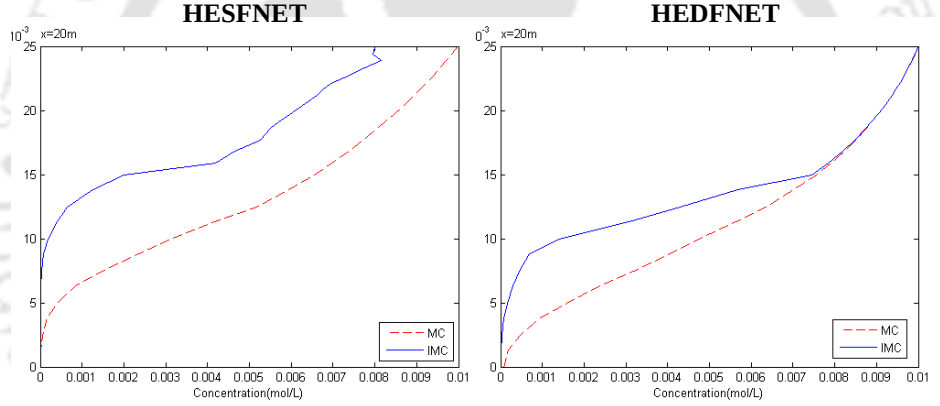

(a1) (b1)

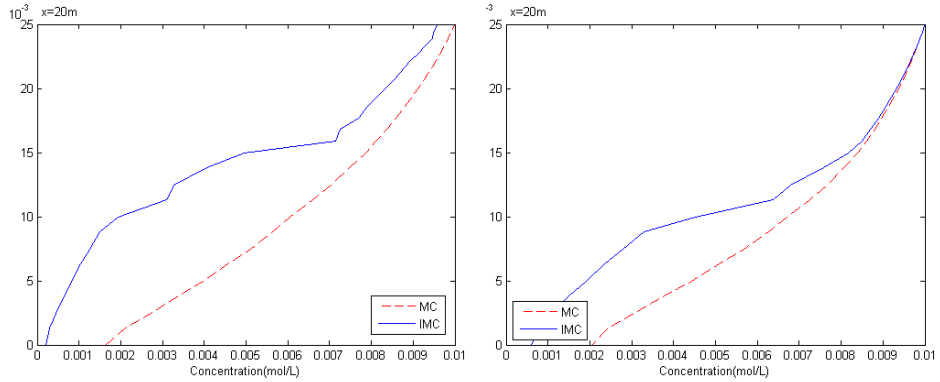

(a2) (b2)

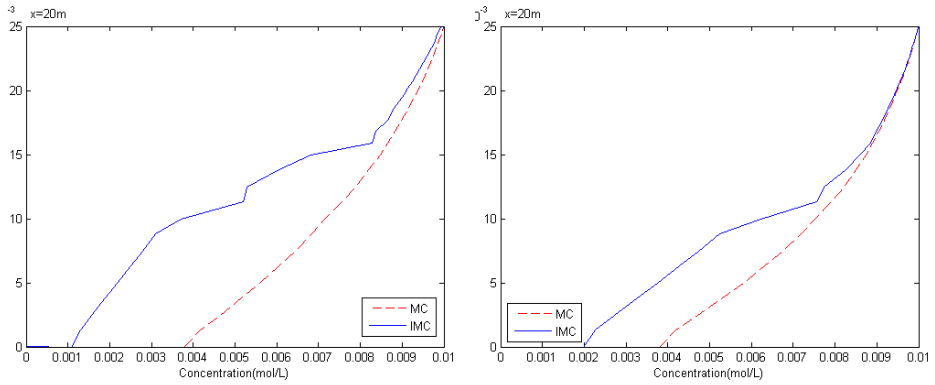

(a3) (b3)

Fig.5.18 Comparison of concentration transport by single porosity flow and non-equilibrium transport model at (a1) 600th day (a2) 1200th day (a3) 1825th day and dual porosity flow and non-equilibrium transport at (b1) 600th day (b2) 1200th day (b3) 1825th day (- - - concentration in mobile water, —— concentration in immobile water)

5.4.3.3 Comparison of non-equilibrium conservative transport in homogeneous and heterogeneous medium

This section compares the results of conservative non-equilibrium transport model for homogeneous and heterogeneous medium. Contaminant spreading pattern in both, saturated and unsaturated, regions are different and the presence of immobile region further affects the contaminant distribution. In the homogeneous medium, mass transferred in to the immobile region is more compared to concentration in immobile water in heterogeneous medium, due to the conductivity and dispersivity nature of the domain. In homogeneous medium at 600th day, low concentration region reaches the bottom of the region (Figure 5.19 a1), but in case of heterogeneous medium plume reaches up to the depth of 17 m only (Figure 5.19 b1) due to less conductivity of the region.

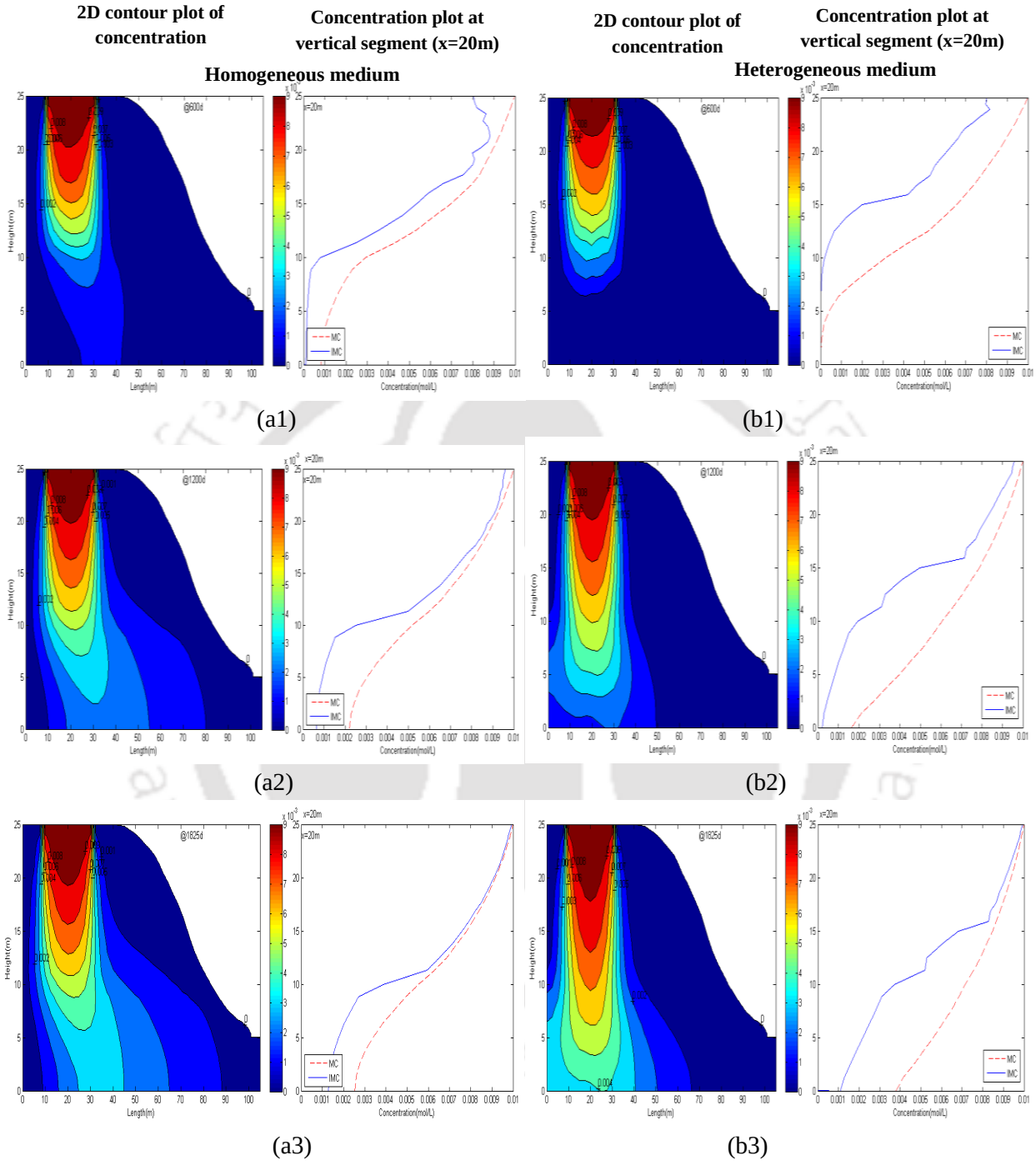

Fig.5.19 Simulation of concentration transport by single porosity flow and non-equilibrium transport in homogeneous model at (a1) 600th day (a2) 1200th day (a3) 1825th day; single porosity flow and non-equilibrium transport profile in heterogeneous medium at (b1) 600th day (b2) 1200th day (b3) 1825th day (- - - concentration in mobile water, —— concentration in immobile water)

5.4.3.4 Comparison of equilibrium and non-equilibrium model simulation with sorption reaction for heterogeneous domain

This section compares the simulated results of equilibrium and non-equilibrium transport models with linear sorption reaction for heterogeneous medium. Like in the case of conservative transport, reactive transport simulation also shows the nature of less transfer of contaminants to the immobile zone due to the less conductive zone. Figure 5.21 shows the liquid concentration distribution at the vertical segment of the domain, which is directly under the leachate entering zone. As the time goes on domain is contaminated due to continuous contaminant inflow and is considered throughout the simulation. As and when the mobile pore water is saturated with contaminant concentration, through diffusion process, contaminant from mobile water enters in to the immobile water. In addition, the contaminant which is in contact with the pore surface participates in the sorption reaction. Figure 5.20 explains the contaminant distribution at 1200th day with sorption reaction for three models.

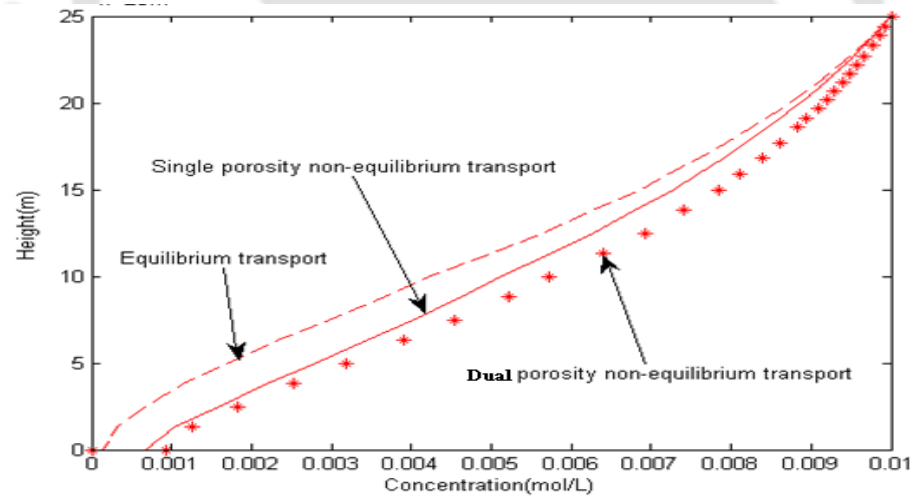

Fig. 5.20 Comparison of ferrous ion concentration in mobile water at vertical segment (x=20th m) at 1200th day by equilibrium and non-equilibrium transport model simulation with sorption reaction in heterogeneous medium.

Concentration plot at vertical segment (x=20m) of the two dimensional domain

Equilibrium model | **Non-Equilibrium model-Type I (SFNET)** | **Non-Equilibrium model-Type II (DFNET)**

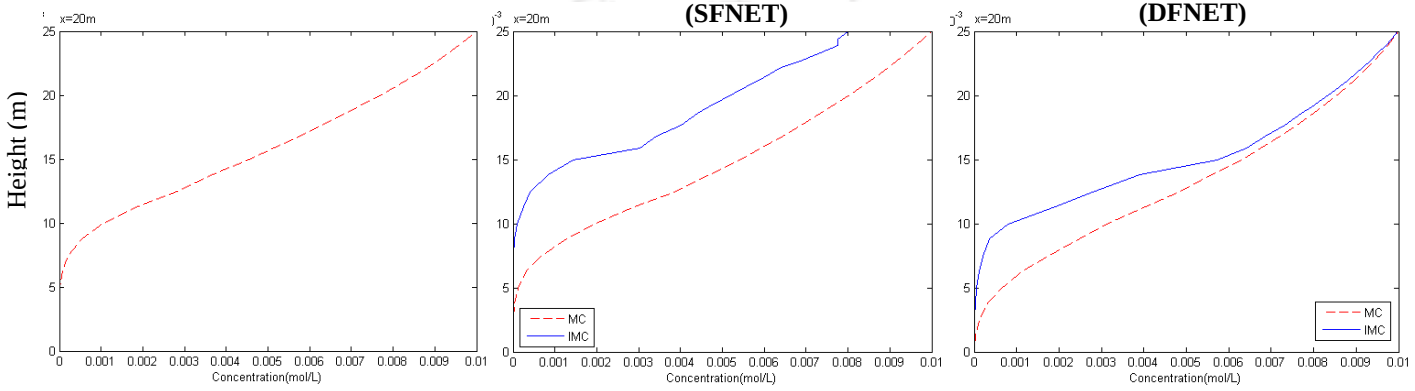

(a1) (b1) (c1)

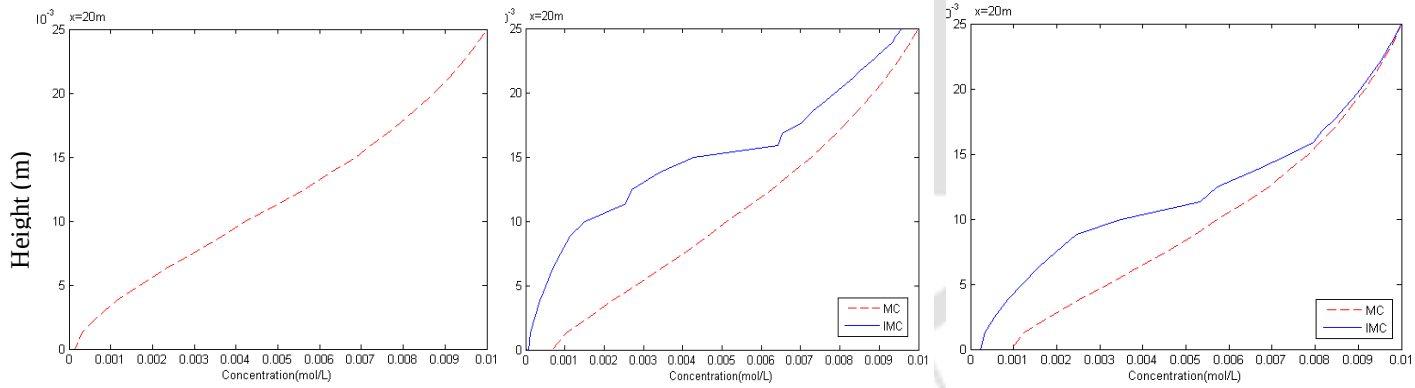

(a2) (b2) (c2)

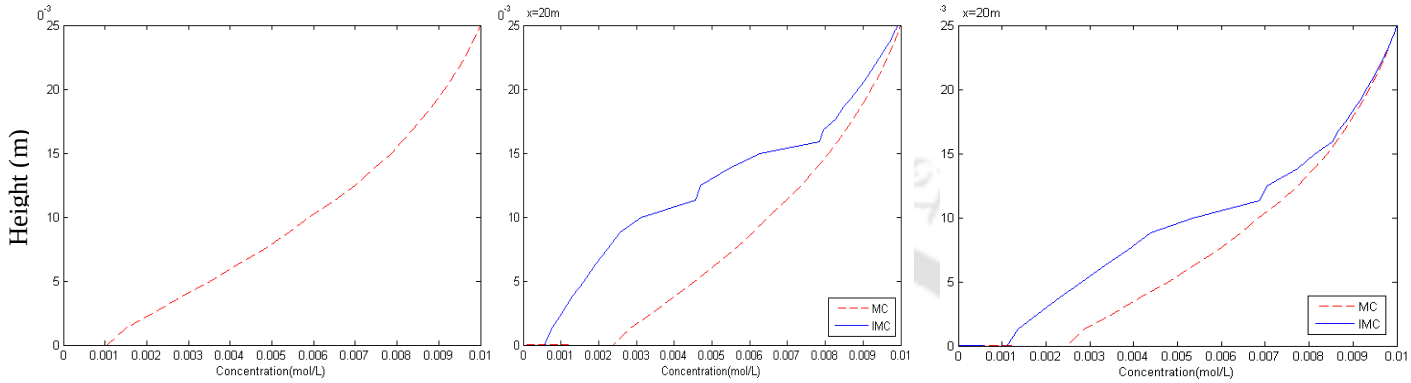

(a3) (b3) (c3)

Fig. 5.21 Simulation in heterogeneous medium by equilibrium model (a1) 600 (a2) 1200 and (a3) 1825th day; single porosity flow and non-equilibrium transport model with sorption reaction at (b1) 600 (b2) 1200 and (b3) 1825th day; dual porosity flow and non-equilibrium transport model with sorption reaction at (c1) 600 (c2) 1200 and (c3) 1825th day (- - - concentration in mobile water, —— concentration in immobile water)

5.4.3.5 Comparison of non-equilibrium transport with sorption reaction in homogeneous and heterogeneous medium

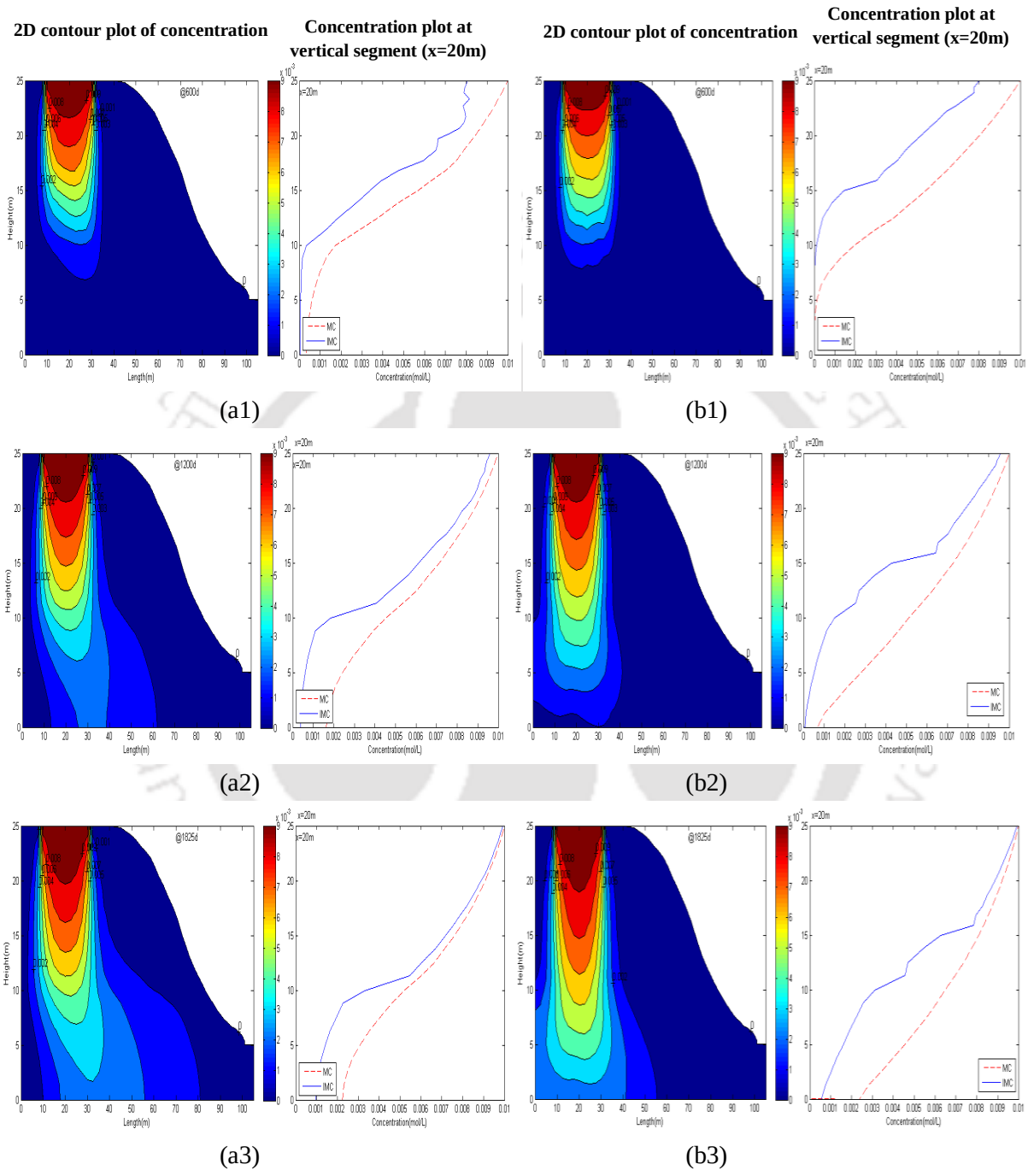

Fig.5.22 Simulated concentration distribution by single porosity flow and non-equilibrium transport model of homogeneous medium with sorption at (a1) 600th day (a2) 1200th day (a3) 1825th day; and of heterogeneous medium with sorption at (b1) 600th day (b2) 1200th day (b3) 1825th day (- - - concentration in mobile water, —— concentration in immobile water)

This section describes the difference between non-equilibrium model results of the homogeneous and heterogeneous medium with sorption reaction. Results shows that considerable difference between concentration in mobile and immobile water is observed in saturated zone at later times, mass transfer in to the immobile region in the saturated zone is very less and those regions are not much effective like unsaturated zones. At the end of the simulation, concentrations in mobile and immobile water in unsaturated zones are nearing equal to each other (Figure 5.22 a3 and b3).

5.4.3.6 Single porosity flow and equilibrium transport with ion exchange reaction (IE-HESFET)

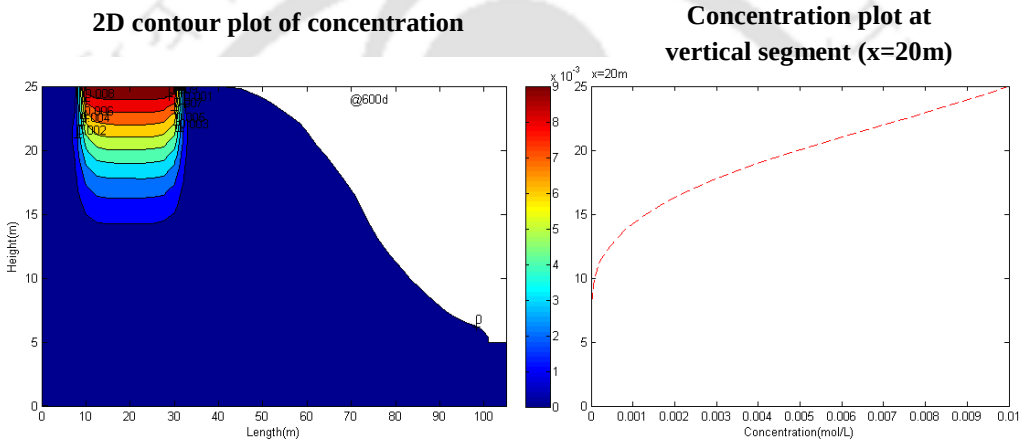

(a)

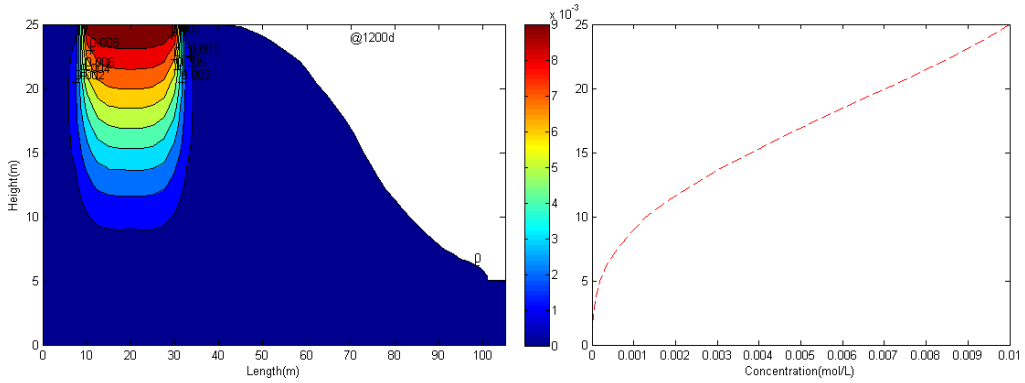

(b)

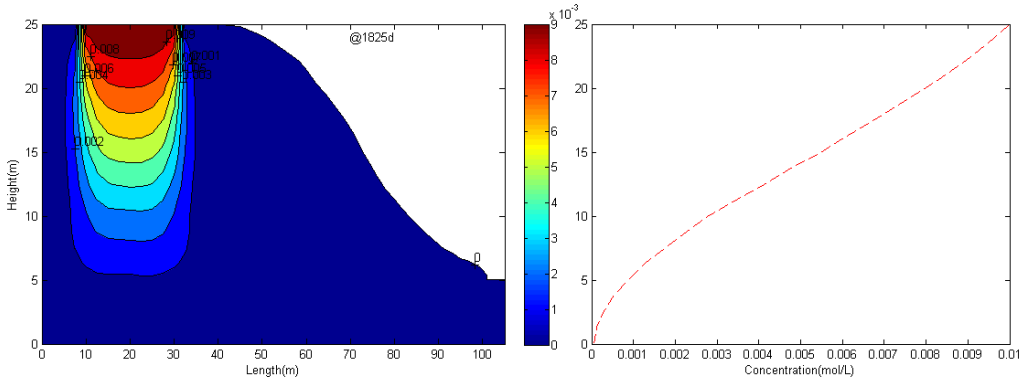

(c)

Fig.5.23 Concentration distribution simulation in heterogeneous medium by single porosity flow and equilibrium transport model with ion-exchange reaction at (a) 600th day (b) 1200th day (c) 1825th day

This section describes the transport of contaminants with ion exchange reaction in heterogeneous domain. The incoming contaminants, ferrous ion (Fe^{2+}), are attracted by the opposite charge that is present in the porous medium, in that way ferrous ion transport got retarded. As shown in Figure 5.23 ion-exchange reaction decreases the concentration in liquid, but those harmful contaminants got exchanged to the porous medium. Since the FEMWATER is single component transport model, contour plot of sodium (Na^{+}) ion that exchanged for ferrous ion is not given.

5.4.3.7 Single porosity flow and non-equilibrium transport with ion exchange reaction (IE-HESFNET)

This section presents the first type non-equilibrium transport model with ion-exchange reaction in heterogeneous medium. The non-equilibrium effects are evident from figures 5.23 and 5.24 though reactions are taking place. Compared to equilibrium model result (Figure 5.23) concentration plumes advances by few meters in non-equilibrium model (figure 5.24). The variation or difference in contaminant spreading of equilibrium and non-equilibrium models are same in the regions of dense concentration (0.009 mol/L) to low concentration (0.001 mol/L) for three time step (600, 1200 and 1825 day) results which are presented. With respect to time spreading difference also same between the models, for example from ADE model at 600th day spreading of contaminant plume reaches up to the depth of 15 m (figure 5.24(a)) and from non-equilibrium model at 600th day spreading of contaminant plume reaches up to the depth of 17.5 m (figure 5.24(a)), around 2 to 2.5 m difference is observed between the model results, more or less other time steps (1200 and 1825 days) results also shows the same difference (around 2m).

Though reactions are taking place effect of non-equilibrium transport is observed, only ferrous ion concentration is presented in the figures since the model is confined to single specie transport, exchanged sodium ion concentration is not given. As given in Selim et al. (1987) improvements were observed in the predictions by two region/mobile-immobile model along with ion-exchange reaction.

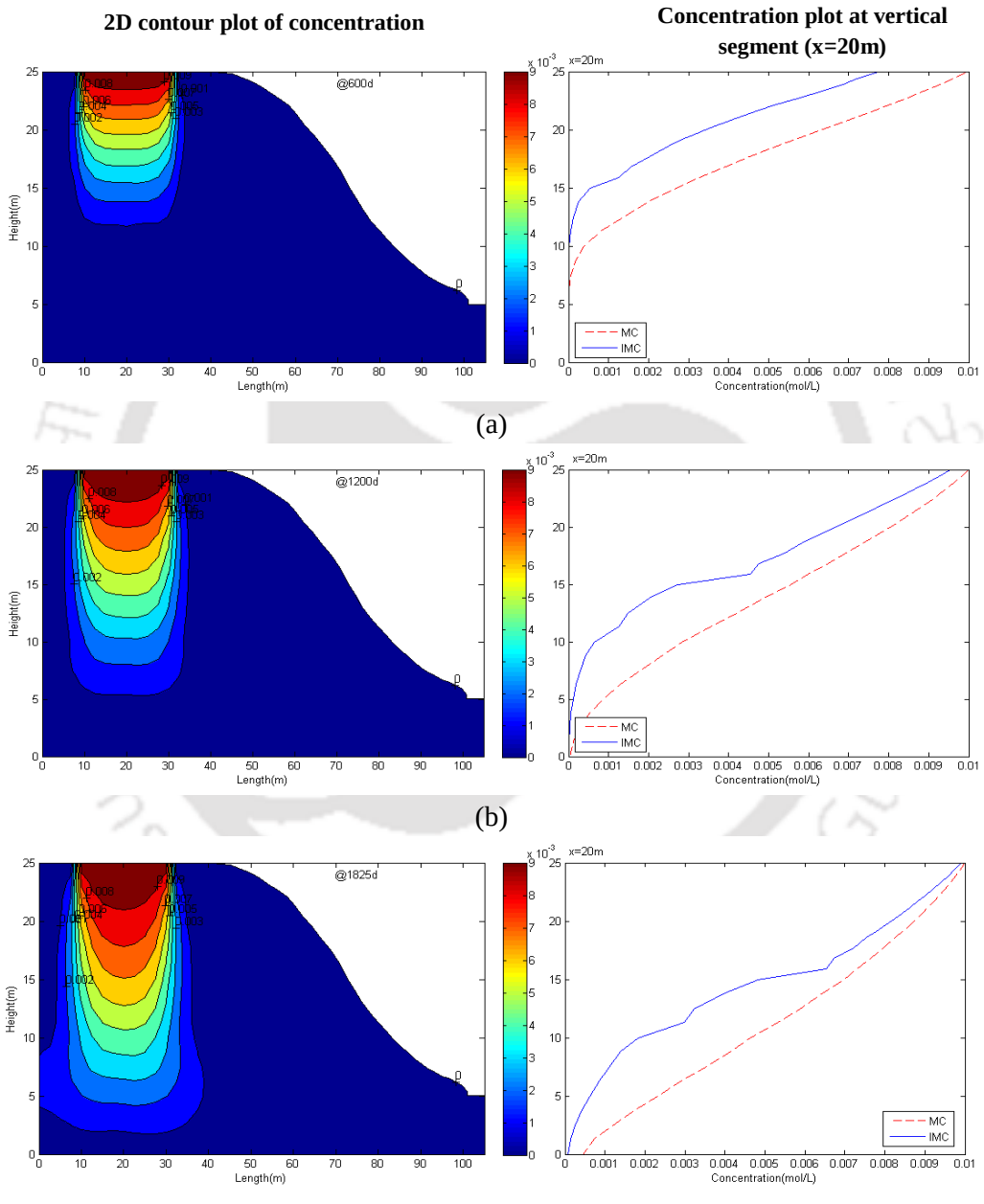

Fig.5.24 Concentration distribution simulation in heterogeneous medium by single porosity flow and non-equilibrium transport model with ion-exchange reaction at (a) 600th day (b) 1200th day (c) 1825th day (- - - concentration in mobile water, —— concentration in immobile water)

5.4.3.8 Dual porosity flow and non-equilibrium transport with ion exchange reaction (IE-HEDFNET)

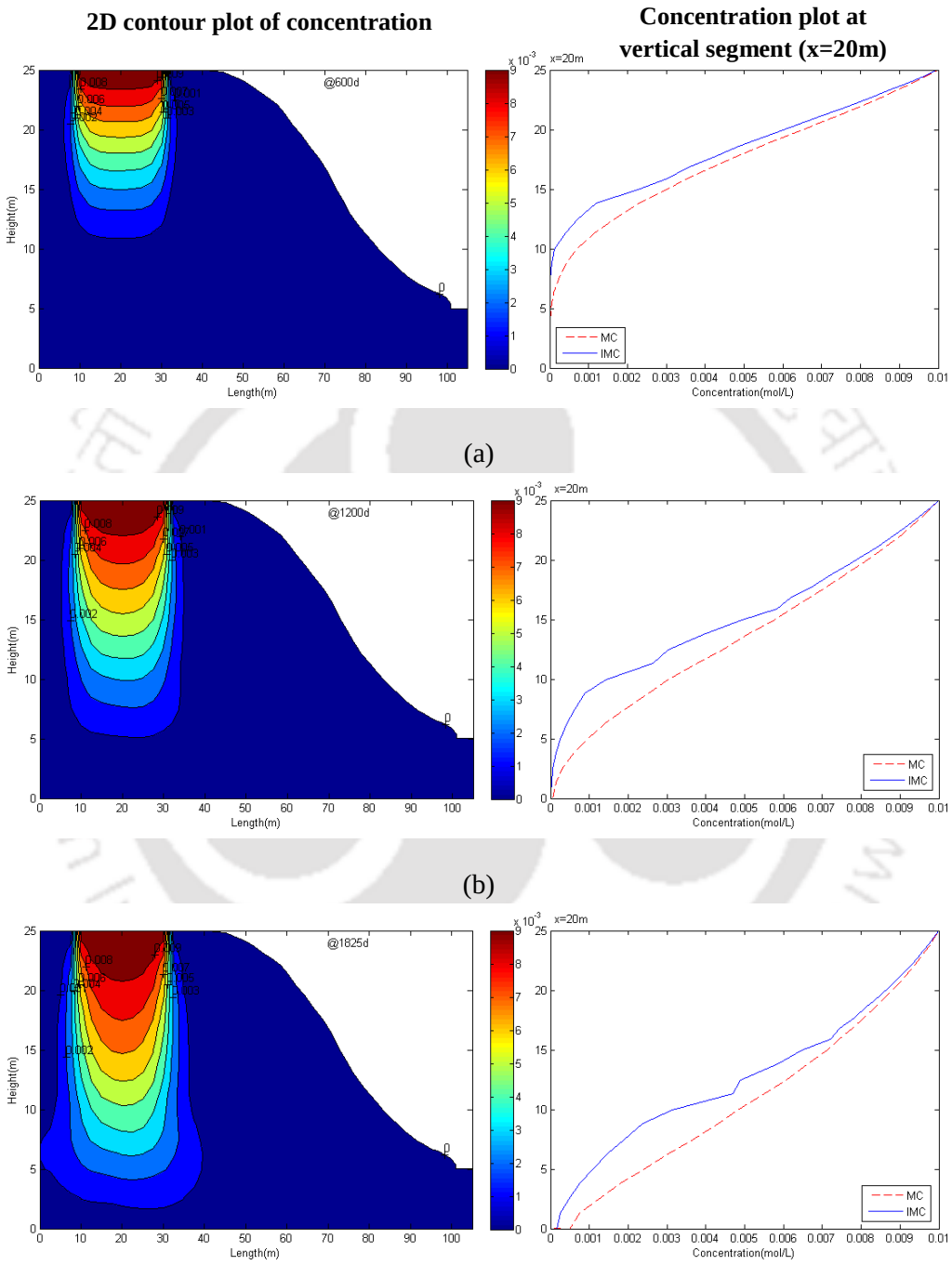

Fig.5.25 Concentration distribution simulation in heterogeneous medium by dual porosity flow and non-equilibrium transport model with ion-exchange reaction at (a) 600th day (b) 1200th day (c) 1825th day (- - - concentration in mobile water, —— concentration in immobile water)

This section gives the second type non-equilibrium transport model results along with ion-exchange reaction for three different time steps (600, 1200 and 1825th day). In the previous section we have seen that non-equilibrium mass transfer not only affects conservative contaminant transport, but also affects reactive transport. This second type non-equilibrium model shows (Figure 5.25) further effect on contaminant present in immobile water region. All the second type non-equilibrium models clearly show that the mass exchange in to the immobile region is more compared to the first type model. Immobile region mass becomes the reason for late arrival of contaminants at later times which causes the tail like region in the output breakthrough curves.

5.4.3.9 Comparison of equilibrium and non-equilibrium transport with ion-exchange reaction

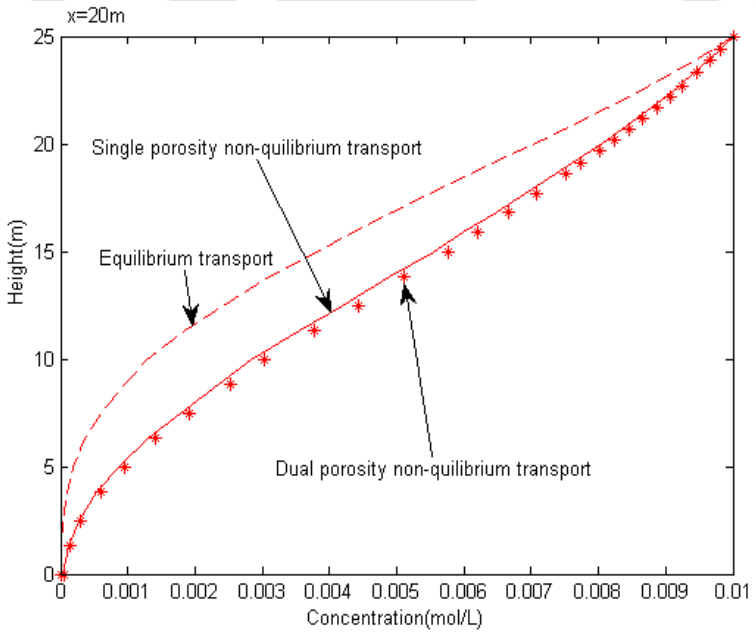

Fig. 5.26 Comparison of ferrous ion concentration in mobile water at vertical segment (x=20th m) at 1200th day by equilibrium and non-equilibrium transport model simulation with ion-exchange reaction in heterogeneous medium.

In this section comparison of the three transport models are presented. Figure 5.26 shows the concentration distribution at 1200th day at the vertical segment (x=20 m) by three transport models. Two types of non-equilibrium transport models show difference in output, in the form of quick arrival, compared to the equilibrium model. Whether in homogeneous or heterogeneous

medium, since the input concentration is continuous there is not much difference is observed between the two non-equilibrium models.

5.4.3.10 Comparison of non-equilibrium transport with ion-exchange reaction in homogeneous and heterogeneous medium

Ion-exchange reaction has much effect on the transport and in the saturated zone it seems to be spread little. Compared to equilibrium transport, non-equilibrium process advances the concentration front for reactive as well as conservative concentration in heterogeneous medium. As in the case of homogeneous medium 0.001 and 0.002mol/l concentration fronts spread more in the saturated zone, 0.009 to 0.003mol/l concentration zones did not spread much, due to the transport in unsaturated zone. One main difference observed between, transport in homogeneous and heterogeneous medium is that transfer of contaminants to immobile water regions. Once the contaminant enters in to the different (less conductivity) region transfer of contaminant mass to immobile region gets decrease in spite of same non-equilibrium parameters.

Less conductivity region starts from the depth of 10 m from the top surface of the domain (height of 15 m from bottom), from where the variation in concentration starts in the immobile water. Slow movement of contaminants take place in the region with less conductivity, this leads to the decrease in mass transfer in to the immobile water region, it is observed in the Figure 5.27. At initial time steps there were no difference observed between the concentration in immobile water of the two domains (homogeneous and heterogeneous), at 600th day concentration difference observed, at the point of 10 m depth from surface, between homogeneous and heterogeneous immobile water region is 0.0004 mol/L.

This difference gets increased as 0.0009 to 0.001 mol/L at later time steps (1200 and 1825th days). Long-time simulations may give different results, also results may change based on the input concentration, soil type, saturation, etc. Concentration in mobile water region shows very little difference (0.0002 mol/L) between homogeneous and heterogeneous domain simulations at the point of 10 m depth. These values are obtained from the vertical segment plot shown in figure 5.27.

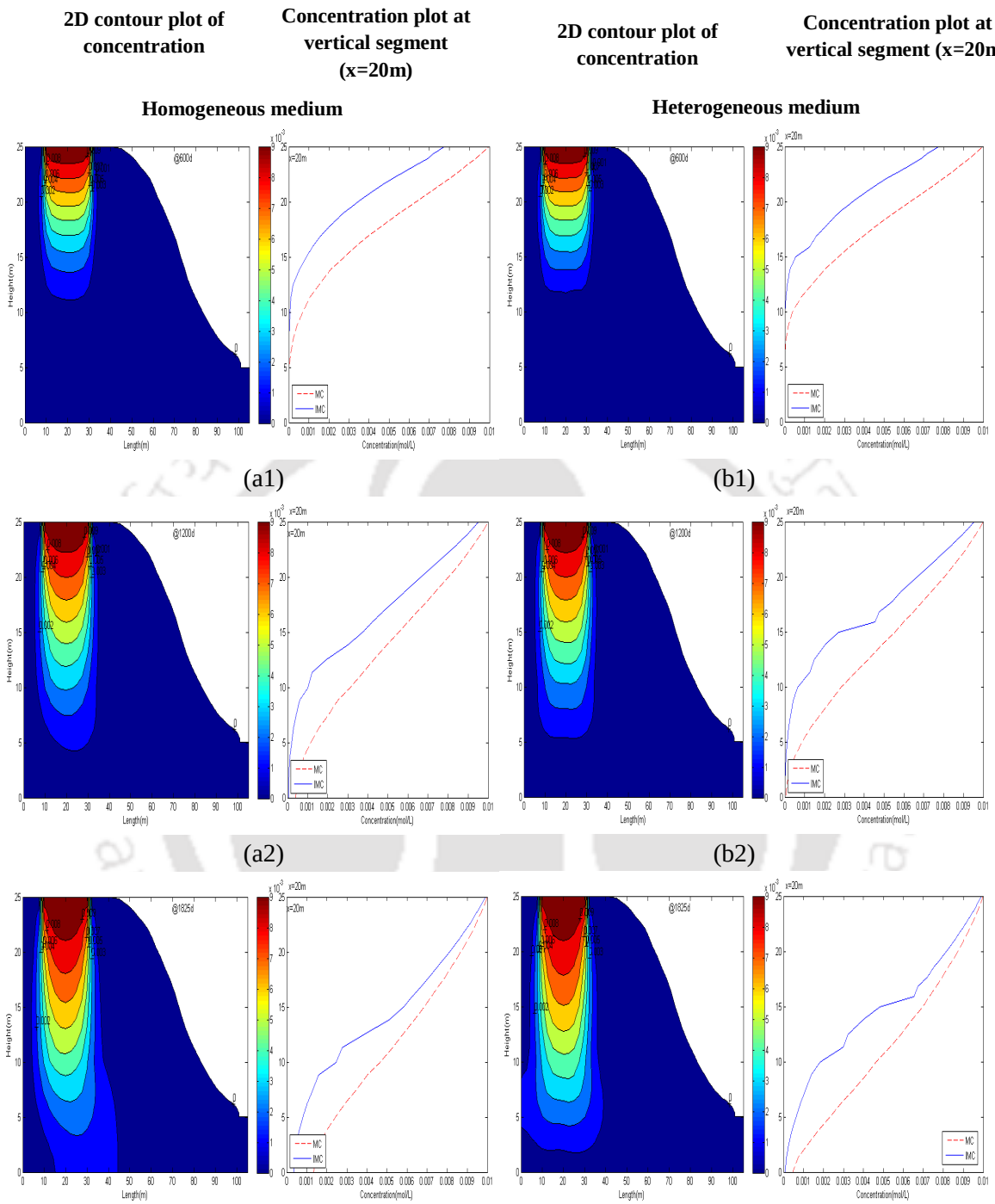

Fig.5.27 Contaminant distribution by single porosity flow and non-equilibrium transport model of homogeneous medium with ion-exchange at (a1) 600th day (a2) 1200th day (a3) 1825th day; and of heterogeneous medium at (b1) 600th day (b2) 1200th day (b3) 1825th day (- - - concentration in mobile water, —— concentration in immobile water)

5.4.4 Effects of mass transfer rate coefficient

Transfer of contaminant mass from mobile water to immobile water, due to concentration gradient, is defined as mass transfer. It is an important characteristic of an unsaturated and aggregated soil and its effect on contaminant transport is simulated by first and second type non-equilibrium transport models. As shown in the Figure 5.28, mass transfer process increases the concentration in immobile water, obviously concentration in mobile water get decreases. Mass transfer is the important process that differentiates the equilibrium and non-equilibrium transport process. Mass transfer is not an empirical value; it is obtained from experimental values by curve fitting methods, so this section explains how this parameter value can impact the transport properties. Mass transfer in to the immobile region is very less when low value (0.000001) is assigned to mass transfer rate constant, if there is no partition in contaminant concentration then the downstream gets maximum concentration plume it is shown in Figure 5.28 (a). Increase in mass transfer rate constant, increases the concentration in immobile water and it lessen the plume concentration which moves to the downstream.

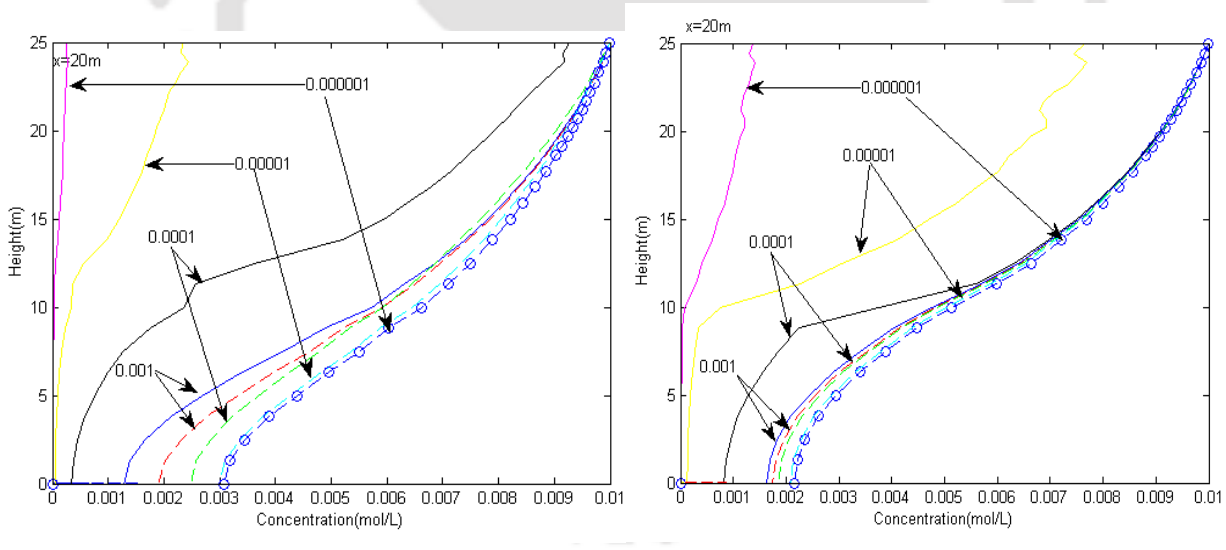

(a) (b)

Fig.5.28 Mass transfer effects by (a) **s**ingle porosity flow and non-equilibrium transport model (first type) and (b) by dual porosity flow and non-equilibrium transport model (second type) (- - - concentration in mobile water, —— concentration in immobile water)

5.4.5 Water content effects

Amount of mobile water content present in the medium may affect the water flow and contaminant mass transport. When mobile water increases eventually immobile water decreases;

it exhibits or resembles the moisture flow properties of single domain flow. Mobile water content variation and its effect on contaminant transport are given in the Figure 5.29. Mobile water content to total water content ratio (f) is one of the important parameter that affects the solute transport (Gaudet et al. 1997). Less amount of mobile water content leads to the quicker transport of contaminant in mobile water. When mobile water content increases situation leads to the equilibrium transport and reaching of contaminants to downstream takes time. Figure 5.29 (a) shows the result from non-equilibrium type I. In unsaturated zone difference between contaminant in mobile and immobile water is observed for small values (0.4 and 0.6) of mobile water content. Increase in the immobile water content leads to the quicker mass transport is observed in the Figure 5.29; dotted red line, contains 0.6 of immobile water content value and 0.4 as mobile water content value, reaches the maximum value at the given space and time.

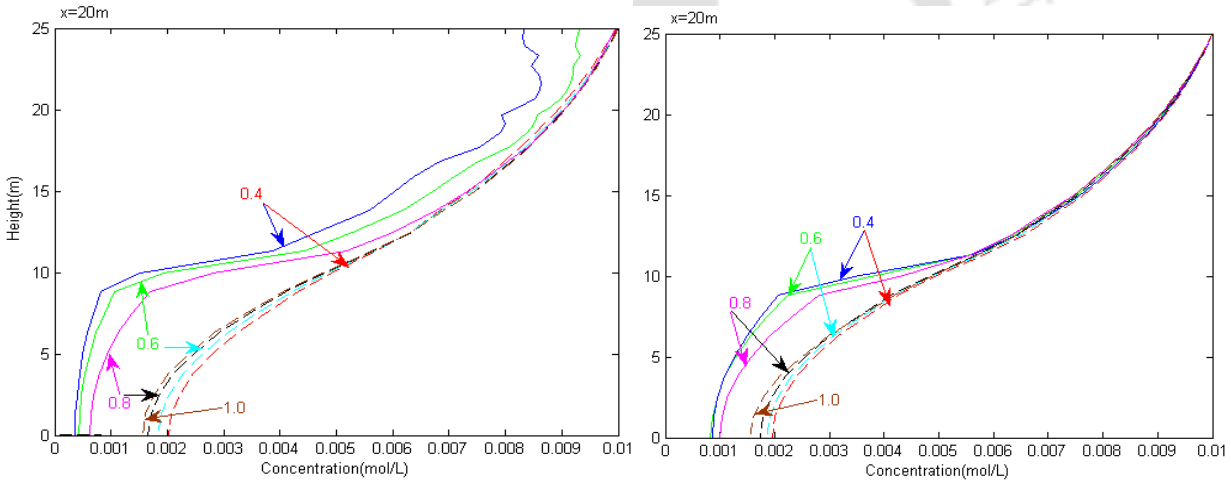

(a) (b)

Fig.5.29 Effects of mobile water content on mass transport in homogeneous medium by (a) **s**ingle porosity flow and non-equilibrium transport model and (b) by dual porosity flow and non-equilibrium transport model (- - - concentration in mobile water, —— concentration in immobile water)

Simulation of type II non-equilibrium transport model shows that mass transfer in to immobile region is more; this leads to the immobile water region to reach the maximum concentration level faster compared to the type I model. In unsaturated zone for all the water content values (0.4, 0.6, 0.8 and 1) concentration in mobile and immobile regions are same, but have differences in concentration value in the saturated zone (Figure 5.29 b).

5.7 Summary

This chapter presents the results produced from the modified FEMWATER model, which was applied to the hypothetical domain to study the impact of physical non-equilibrium on the AMD (ferrous ion) reactive transport. Three models applied to the domain to solve concentration distribution, are (i) equilibrium model/advection-dispersion equation, (ii) single porosity flow – non-equilibrium transport model (first type), where water content value obtained from flow model (Richards equation) is splitted in to mobile and immobile water content and given in to non-equilibrium transport model, and (iii) dual porosity flow – non-equilibrium transport model (second type), where water content value obtained as mobile and immobile water content from dual porosity flow model and given in to non-equilibrium transport model. These models were applied to study conservative and reactive solute transport properties in homogeneous and heterogeneous medium along with set of assumptions. In both the mediums, homogeneous and heterogeneous, non-equilibrium transport models show the signs of quick transfer of contaminants to the downstream than equilibrium model. In heterogeneous medium spreading of contaminants in the low conductivity region is limited though the non-equilibrium parameters are same. Sorption and ion-exchange reactions were considered to represent the reactive transport of ferrous ion, and still non-equilibrium mass transfer have effects on the transport properties. Solute front from advection-dispersion transport model along with reaction arrives late at observing point, where quick arrival of solute front is observed by non-equilibrium models at observing point. Ion-exchange reaction strongly retards the contaminant among sorption and ion-exchange reactions, under both equilibrium and non-equilibrium conditions. Second type non-equilibrium model simulates natural mass transfer process unlike the first type model, which properly could not capture the velocity details of mobile-immobile flow. It is evident in the mass transfer nature and arrival time of solute front at down streams. Mobile water content to total water content ratio (f) and mass transfer rate constant (Γ_w and Γ_c) are the parameters which affect transport properties, especially high immobile water content causes quick arrival of solute front at the downstream. Effects of other chemical parameters were not studied since this study focuses on the non-interactive solute transport with less interactive surface reactions. Further future studies will focus on the multispecies reactive transport, since AMD involves with deep interactive reactions with multiple solutes is dissolved form.

CHAPTER 6

CONCLUSIONS AND SCOPE FOR FUTURE WORK

This chapter presents the summary and conclusions from the whole research work and limitations of the model. The scope for further research is also presented in this final chapter.

6.1 Summary

Acid mine drainage (AMD) is known as the drainage water, from mines and mine waste, resulting from natural oxidation of sulphide minerals (Pyrite, Pyrrhotite, Marcasite, Galena, etc.), which are exposed to air and moisture. AMD may emerge from underground mines, as runoff from open pit mines, as effluent/leachate from waste/burden rock dumps and ore stockpiles, mill tailings, etc. It is characterized by high TDS, low pH, and elevated concentrations of iron, sulfate and other metals. Low pH water has the risk of leaching heavy metals from mine surroundings and during the time of flooding these metals may enter in to water bodies. Heavy metals pose severe threat to the aquatic species, plants, humans and microbes in soil as well. The pollution of surface and subsurface water due to AMD is a huge concern to the society and necessary steps are needed.

Modeling is an important tool that can be used to understand hydrological or geo chemical processes by interpreting the experimental results as well as by making predictions. Though experiments are base to carry out modeling it is not possible to conduct experiments to observe long term results. In such cases, models can be used to predict various processes. The actual conditions of acid mine drainage contaminant problems are vast and highly complex and rarely a numerical or computational model will be able to incorporate all the field conditions, while performing the simulation. The conventional solute transport models of earlier years use the simple advection diffusion equation to simulate the contaminant movement in subsurface. Presence of complexities in fluid flow as well as mass transfer due to the velocity differences and existence of dead end pores in the medium affect the simulation results (Gaudet et al. 1977 and Van Genuchten et al. 1977). Hence, the numerical models on contaminant transport related to AMD involves in incorporating different acceptable features and various mass transfer phenomena to simulate more or less the field situation and to make the model prediction more accurate.

There are only very few studies available on reactive transport of AMD with non-equilibrium transport processes. Inclusion of these complexities in to the transport model may potentially provide more insights on the transport processes involved in the subsurface environment. In addition, the non-equilibrium transport models may provide more accurate simulation outputs that can aid in designing remedial or preventive measures. The FORTRAN based source code of

US-EPA developed finite-element model FEMWATER, which was originally devoid of modules on non-equilibrium solute transport, is henceforth modified, in this thesis, to analyse the reactive transport of AMD in the subsurface environment. Since this work is focused on the non-equilibrium mass transfer effects, emphasis was given to the mass transfers of both the liquid and solute between the mobile and immobile water regions.

FEMWATER contains two modules, 3DFEMWATER and 3DLEWASTE. The transport module, 3DLEWASTE was modified to handle the non-equilibrium solute mass transport and the flow module 3DFEMWATER was modified to accommodate liquid mass transfer between the mobile and immobile regions. Two approaches of physical non-equilibrium transport were followed, i) Single porosity Flow and Non-Equilibrium Transport (SFNET) simulation (first type non-equilibrium), and ii) Dual porosity Flow and Non-Equilibrium Transport simulation (DFNET) (second type non-equilibrium). Ion exchange reaction was added to the model; and model was updated to handle multicomponent but without any interactions between the components. Following the modification of FEMWATER model and its validation, parameter analysis study was done and then the modified FEMWATER model was applied to the hypothetical domain to study the impact of physical non-equilibrium on the AMD (ferrous ion) reactive transport. These models were applied to study conservative and reactive solute transport properties in homogeneous and heterogeneous medium along with set of assumptions.

6.2 Conclusions from the simulation run

The modified code was successfully validated with literature data and applied to simulate AMD transport in the variably saturated subsurface zone. Based on the simulations, following conclusions are drawn,

- Difference in contaminant (ferrous ion) spreading pattern is observed between the conventional equilibrium and physical non-equilibrium models. Mainly the advancement of solute front in the direction of water flow is observed for non-equilibrium simulation results with respect to equilibrium simulation result.
- Difference in contaminant spreading pattern is also observed between first and second type non-equilibrium models. Due to the addition of time dependent water mass transfer between mobile and immobile zones in the flow model in the second type non-equilibrium models,

the advancement of the contaminant plume front is more evident than the conventional physical non-equilibrium transport models.

- It is observed that at initial time (600th day) less concentration contour (0.001 mol/l) spreads more in the saturated zone, under non-equilibrium condition with conservative and reaction transport. At later time (1825th day) spreading of less concentration contours (0.001, 0.002 and 0.003 mol/l) decreased under non-equilibrium condition due to mass transfer from mobile region to immobile region.
- Second type non-equilibrium model simulates natural mass transfer process unlike the first type model, which properly could not capture the velocity details of mobile-immobile flow. It is evident in the mass transfer nature and arrival time of solute front at down streams.
- Little difference is observed in contaminant spreading pattern of homogeneous and heterogeneous domain simulations, especially in the immobile water zone. Transfer of contaminant mass to immobile region is more in homogeneous medium but in the heterogeneous medium mass transfer to immobile region decreases, particularly in the less conductivity zone.
- Non-equilibrium transport model does exhibit its properties on the reactive transport too. Though sorption and ion-exchange reactions limit the contaminant transport in subsurface region, mobile-immobile flow advances solute front a bit further. Ion-exchange reaction exhibit strong action against spreading. Compare to sorption, the ion-exchange reaction is less affected by non-equilibrium process and in conservative case transport is much affected by non-equilibrium process and enhances the prediction accuracy.
- Mainly two parameters i) f - mobile water content to total water content ratio and ii) Γ - mass transfer rate constant, which affect contaminant transport properties, especially high immobile water content causes quick arrival of solute front at the downstream.

6.3 Limitations and future scope

Model simulations were run with various assumptions and simple surface reactions to analyse the effects on non-equilibrium on reactive transport, those assumptions may be the limitations of the model, are:

- Single specie transport model.
- Simple surface reactions (sorption and ion-exchange).

- Mass transfer, due to soil property, between the mobile and immobile water region has linear relation.
- Hypothetical model domain
- Isothermal and near neutral pH conditions

There is lot of scope for future research on geochemical studies of mine water transport and possible studies that can be undertaken are

- ✓ Inclusion of multispecies reactive module to analyse the subsurface transport properties of heavy metals under the mobile-immobile flow condition.
- ✓ Including the parameter for degradation of mine water due to bacterial activity
- ✓ Including the relationship between the reactions and pH

Appendix - A

This section gives the details of the equations in the third chapter; especially derivation of equation 3.8 from equation 3.7,

$$\int N_i \left[\frac{\partial\left(\theta_j N_j\right)}{\partial t} - \vec{\nabla}\cdot\left[K\left(h\right)\left(h_j \vec{\nabla} N_j + \vec{\nabla} z\right)\right] - q \right] dR = 0 \tag{3.7}$$

$$\int N_i \frac{\partial\left(\theta_j N_j\right)}{\partial t} dR - \int N_i \vec{\nabla}\cdot\left[K\left(h\right)\left(h_j \vec{\nabla} N_j + \vec{\nabla} z\right)\right] dR - \int N_i q dR = 0 \tag{3.7a}$$

Integration by parts, a special rule, is available for integrating products of two functions; it can be applied on the first term on the right hand side of the above equation,

$$\int u dv = uv - \int v du \tag{3.7b}$$

$$\int N_i \left(\vec{\nabla}\cdot\left[K\left(h\right)\left(h_j \vec{\nabla} N_j + \vec{\nabla} z\right)\right]\right) dR = \int K\left(h\right)\nabla N_i \left(h_j \nabla N_j + \nabla z\right) dR - \int N_i n \cdot K\left(h\right)\left(h_j \nabla N_j + \nabla z\right) dB \tag{3.7c}$$

$$\int K\left(h\right)\nabla N_i \left(h_j \nabla N_j + \nabla z\right) dR = \int \nabla N_i K\left(h\right)\nabla N_j dR\, h_j - \int N_i n \cdot K\left(h\right)\left(h_j \nabla N_j + \nabla z\right) dB + \int K\left(h\right)\nabla N_i \left(\nabla z\right) dR \tag{3.7e}$$

$$\int N_i N_j dR \frac{d\theta_j}{dt} + \int \nabla N_i K\left(h\right)\nabla N_j dR\, h_j - \int N_i n \cdot K\left(h\right)\left(h_j \nabla N_j + \nabla z\right) dB + \int K\left(h\right)\nabla N_i \left(\nabla z\right) dR - \int N_i q dR = 0 \tag{3.8}$$

Appendix – B

Derivation of contaminant transport equation with concentration in mobile and immobile water and with variable immobile water content (equation 3.71). Let's assume that there is no decay and no additional source terms for contaminant conservation, i.e. $Q = \lambda = 0$, thus mass conservation for water and contaminant is given by

$$\frac{\partial \theta_m}{\partial t} + \frac{\partial \theta_{im}}{\partial t} = -\nabla \cdot V + q$$

$$\frac{\partial M}{\partial t} = -\nabla \cdot \left(\theta_m D \nabla C_m\right) - \nabla \cdot \left(C_m V\right)$$

where M is the mass of contaminant that is split between mobile and immobile water and sorption sites that are in contact with either the mobile or immobile liquid and given by

$$M = \theta_m C_m + \theta_{im} C_{im} + \rho_b f k_d C_m + \rho_b \left(1 - f\right) k_d C_{im}$$

and M becomes

$$M = \left[\theta_m + \rho_b f k_d\right] C_m + \left[\theta_m + \rho_b \left(1 - f\right) k_d\right] C_{im}$$

Thus $\partial M / \partial t$ is given by

$$\frac{\partial M}{\partial t} = \left[\theta_m + \rho_b f k_d\right] \frac{\partial C_m}{\partial t} + C_m \frac{\partial \theta_m}{\partial t} + \left[\theta_{im} + \rho_b \left(1 - f\right) k_d\right] \frac{\partial C_{im}}{\partial t} + C_{im} \frac{\partial \theta_{im}}{\partial t}$$

Substitute for $\partial M / \partial t$ into the contaminant conservation equation and using and noting that $\nabla \cdot \left(C_m V\right) = C_m \nabla \cdot V + V \cdot \nabla C_m$ gives

$$\left[\theta_m + \rho_b f k_d\right] \frac{\partial C_m}{\partial t} + \left[\theta_{im} + \rho_b \left(1 - f\right) k_d\right] \frac{\partial C_{im}}{\partial t} + C_m \left\{\frac{\partial \theta_m}{\partial t} + \nabla \cdot V\right\} + C_{im} \frac{\partial \theta_{im}}{\partial t} = \nabla \cdot \left(\theta_m D \nabla C_m\right) - V \cdot \left(\nabla C_m\right)$$

$$\frac{\partial \theta_m}{\partial t} + \nabla \cdot V = q - \frac{\partial \theta_{im}}{\partial t}$$

and we finally have

$$\left[\theta_m + \rho_b f k_d\right] \frac{\partial C_m}{\partial t} + \left[\theta_{im} + \rho_b \left(1 - f\right) k_d\right] \frac{\partial C_{im}}{\partial t} + \left(C_{im} - C_m\right) \frac{\partial \theta_{im}}{\partial t} + q C_m = \nabla \cdot \left(\theta_m D \nabla C_m\right) - V \cdot \left(\nabla C_m\right) \qquad (3.71)$$

and the final equation for describing the contaminant distribution with changes in mobile and immobile water is given by

$$\left(\theta_{\mathrm{m}}+\rho_b f\frac{d\bar{c}}{dC}\right)\frac{\partial C_{\mathrm{m}}}{\partial t}+\left[\theta_{\mathrm{im}}+\rho_b\left(1-f\right)\frac{d\bar{c}}{dC}\right]\frac{\partial C_{\mathrm{im}}}{\partial t}-\frac{\partial\theta_{im}}{\partial t}C_m=\vec{\nabla}\cdot\left(\theta_{\mathrm{m}}D_{\mathrm{m}}\vec{\nabla}C_m\right)-V\cdot\vec{\nabla}C_m+QC_{in}-QC_m$$

The term $C_{im}\ (\partial\theta_{im}/\partial t)$ is added into the following equation

$$\left[\theta_{\mathrm{im}}+\rho_b\left(1-f\right)\frac{d\bar{c}}{dC}\right]\frac{\partial C_{\mathrm{im}}}{\partial t}=\Gamma_c\left(C_m-C_{im}\right)-\frac{\partial\theta_{\mathrm{im}}}{\partial t}C_{im}$$

$$\left[\theta_{\mathrm{im}}+\rho_b\left(1-f\right)\frac{d\bar{c}}{dC}\right]\frac{\partial C_{\mathrm{im}}}{\partial t}=\Gamma_c\left(C_m-C_{im}\right)-QC_{im} \qquad (3.72)$$

REFERENCES

1. Abdelghani, F. B., Simon, R., Aubertin, M., Molson, J., and Therrien, R. 2009. Modeling water flow and transport of contaminants from mine wastes stored in open pits within fractured rock. GEOHALIFAX, 62nd Canadian Geotechnical Conference and 10th joint CGS/IAH-CNC Groundwater conference, 20-24th September, BC, Canada.

2. Abdul-Wahab, S. A., and Marikar, F. A. 2012. The environmental impact of gold mines: pollution by heavy metals. Central European Journal of Engineering, 2(2), 304-313.

3. Abrosimova, N., Gaskova, O., Loshkareva, A., Edelev, A., and Bortnikova, S. 2015. Assessment of the acid mine drainage potential of waste rocks at the Ak-Sug porphyry Cu–Mo deposit. Journal of Geochemical Exploration, 157, 1-14.

4. Alimi-Ichola. I., and Gaidi. L. 2006. Influence of the unsaturated zone of soil layer on the solute migration. Engineering Geology, 85(1-2), 2-8.

5. Ardejani, F. Z., Singh, R., Marandi, R., and Baffi, E. 2007. A three dimensional finite volume model for acid mine drainage simulation in opencast mine backfill. IWMA Symposium: Water in Mining Environments, 27th-31stMay, Cagliari, Italy.

6. Baviskar, S., and Heimovaara, T. 2014. Addressing preferential flow in landfills by finite difference and marker-in-cell method. International Conference on Heat Transfer and Fluid Flow, Prague, Czech Republic, 11th -12th August, 127-1 to 127-10.

7. Bell, F. G., and Donnelly, L. J. 2006. Mining and its impact on the environment. Taylor & Francis, 387-420.

8. Berezina, O. A., Maksimovich, N. G., and Pyankov, S. V. 2018. Hydroecological characteristic of coal-mining regions with crucial anthropogenic load (in the case study of the Yaiva river basin). IOP Conf. Series: Earth and Environmental Science 107, 012001.

9. Bernardes de Souza, C. M., and Mansur, M. B. 2011. Modelling of acid mine drainage (amd) in columns. Brazilian Journal of Chemical Engineering, 28(3), 425 - 432.

10. Bibby, R. 1981. Mass transport of solutes in dual-porosity media. Water Resources Research, 17(4) 1075-1081.

11. Blodau, C. 2006. A review of acidity generation and consumption in acidic coal mine lakes and their watersheds. Science of The Total Environment, 369(1-3), 307-332.

12. Blowes, D. W., Ptacek, C. J., Jambor, J. L., and Weisener, C, G. 2003. The geochemistry of acid mine drainage. Treatise on Geochemistry, 9, 149-204.

13. Bond, W. J., and Wierenga, P. J. 1990. Immobile water during solute transport in unsaturated sand columns. Water Resources Research, 26(10), 2475-2481.

14. Booth, C. J. 2002. The effects on longwall mining on overlying aquifers. In: Younger PL, Robbins NS (Eds.), 2002 Mine Water Hydrology and Geochemistry. Geological Society, London, Special Publication, 198: 17—45.

15. Bresler, E. 1973. Simultaneous transport of solutes and water under transient unsaturated flow conditions. Water Resources Research, 9(4), 975-986.

16. Bwapwa, J. K. 2018. A review of acid mine drainage in a water-scarce country: Case of South Africa. Environmental Management and Sustainable Development, 7(1), 1 – 20.

17. Bussiere, B., Chapuis, R. P., and Aubertin, M. 2003. Unsaturated flow modeling for exposed and covered tailings dams. Montreal ICOLD Conference.

18. Celia, M. A., Bouloutas, E. T., and Zarba, R. L. 1990. A general mass-conservative numerical solution for the unsaturated flow equation. Water Resources Research, 26(7), 1483-1496.

19. Chen, A., Lin, C., Lu, W., Wu, Y., Ma, Y., Li, J., and Zhu, L. 2007. Well water contaminated by acidic mine water from the Dabaoshan mine, south China: Chemistry and toxicity. Chemosphere, 70, 248-255.

20. Chon, H., Kim, J., and Choi, S. 1999. Hydrogeochemical characteristics of Acid Mine Drainage around the abandoned Youngdong coal mine in Korea. Resource Geology, 49(2), 113-120.

21. Coats, K. H., and Smith, B. D. 1964. Dead end pore volume and dispersion in porous media. Society of Petroleum Engineering, 4(1), 73-84.

22. Corapcioglu, M. (1994). Advances in porous media, Volume 2. Elsevier.

23. Cornell, R. M., Giovanoli, R., and Schneider, W. 1989. Review of the hydrolysis of iron (III) and the crystallization of amorphous iron (III) hydroxide hydrate. Journal of Chemical Technology and Biotechnology, 46(2), 115-134.

24. Costa, J. L., and Prunty, L. 2006. Solute transport in fine sandy loam soil under different flow rates. Agricultural Water Management, 83(1-2), 111–118.

25. Coumans, Catherine and Nettleton, G. 2000. The Philippines: Centuries of Mining. Forest Peoples Programme, Philippine Indigenous Peoples Links and World Rainforest Movement. Undermining the Forest. Published by Netherlands Committee for IUCN, The World Conservation Union, 56-70.

26. Council, G. W. 1994. Solute dispersion in groundwater: The synergistic effect of heterogeneity and hydraulic gradient variability. M.Sc. Thesis, MIT.

27. Crawford, J. 1999. Geochemical modelling – a review of current capabilities and future directions. SNV Report 262, Swedish Environmental Protection Agency, Sweden.

28. de Smedt, F. 1981. Solute transfer through unsaturated porous media. Studies in Environmental Science, 17, 1011-1016.

29. de Smedt, F., and Wierenga, P. J. 1979. A generalized solution for solute flow in soils with mobile and immobile water. Water Resources Research, 15(5), 1137-1141.

30. de Smedt, F., and Wierenga, P. J. 1979. Mass transfer in porous media with immobile water. Journal of Hydrology, 41(1-2), 59-67.

31. de Vasconcellos, C. A. B., and Amorim, J. C. C. 2001. Numerical simulation of unsaturated flow in porous media using a mass-conservative model. Proceedings of COBEM, Fluid Mechanics, 8, 139-148.

32. Dold, B. 2010. Basic concepts in environmental geochemistry of sulfidic mine-waste management, Waste Management, Er Sunil Kumar (Ed.), InTech, DOI: 10.5772/8458. Available from: https://www.intechopen.com/books/waste-management/

33. Dou, W., and Jin, Y. C. 1996. Analytical solution of the solute transport equation for the binary homovalent ion exchange in groundwater. Journal of Hydrology, 180(1–4), 139–153.

34. Duguid, J. O., and Reeves, M. 1976. Material transport through porous media: a finite element Galerkin model. ORNL-4928, United States.

35. Elango, L., Stagnitti, F., Gnanasundar, D., Rajmohan, N., Salzman, S., LeBlanc, M. and Hill, J. 2004. A Review of Recent Solute Transport Models and a Case Study. Chapter 5 of Environmental Sciences and Environmental Computing. Vol. II (P. Zannetti, Editor). Published by The EnviroComp Institute, UK

36. Elberling, B., Nicholson, R. V., and Scharer, J. M. 1994. A combined kinetic and diffusion model for pyrite oxidation in tailings: a change in controls with time. Journal of Hydrology, 157(1-4), 47-60.

37. Engdahl, N. B. 2009. Heterogeneity effects on flow and transport within a shallow fluvial aquifer. M.Sc Thesis, University Of New Mexico.

38. Equeenuddin, Sk. Md., Tripathy, S., Sahoo, P. K., and Panigrahi, M. K. 2013. Metal behavior in sediment associated with acid mine drainage stream: Role of pH. Journal of Geochemical Exploration, 124, 230-237.

39. Field, S. M., and Leij, F. J. 2014. Combined physical and chemical non-equilibrium transport model for solution conduits. Journal of Contaminant Hydrology, 157, 37-46.

40. Finfrock, S. H. 1994. Modelling groundwater contamination for the Hanford environmental disposal facility (WHC-SA-2665-FP). United States.

41. Foster-Reid, G. H. 1994. Variability of hydraulic conductivity and sorption in a heterogeneous aquifer. M.Sc. Thesis, MIT.

42. Fromm, V. V., and Kalashnikov, G. V. 1982. Effect of mine water on rock deformation in coal mines. International Journal of Mine Water, 1(3), 43-49.

43. Gaikwad, R. W., Sapkal, R. S., and Sapkal, V. S. 2010. Removal of Copper ions from Acid Mine Drainage waste water using ion exchange technique: Factorial design analysis. Journal of Water Resources and Protection, 2, 984-989.

44. Gao, H., Butler, A., Wheater, H., and Vesovic, V. 2001. Chemically reactive multicomponent transport simulation in soil and groundwater: 1. Model development and evaluation. Environmental Geology, 41, 274-279.

45. Gao, H., Vesovic, V., Butler, A., and Wheater, H. 2001. Chemically reactive multicomponent transport simulation in soil and groundwater: 2. Model demonstration. Environmental Geology, 41, 280-284.

46. Gaudet, J. P., Jegat, H., Vachaud, G., and Wierenga, P. J. 1977. Solute transfer, with exchange between mobile and stagnant water, through unsaturated sand. Soil Science Society of America Journal - SSSAJ, 41, 665-671.

47. Gerke, H. H., Molson, J. W., and Frind, E. O. 1988. Modeling the effect of chemical heterogeneity on acidification and solute leaching in overburden mine spoils. Journal of Hydrology, 209 (1998), 166–185.

48. Grove, D. B., and Stollenwerk, K. G. 1984. Computer model of one-dimensional equilibrium-controlled sorption processes: U.S. Geological Survey Water-Resources Investigations Report 84-4059, 7-37.

49. Handayani, H. E., Ibrahim, E., Ngudiantoro, Ridho, M. R., and Yazid, M. 2016. The effects of acid mine drainage (AMD) on the internal and the external environment in the open coal mining activities. International Journal of Chemical and Environmental Engineering, 7(1), 60-63.

50. Hanna, G. P., Jr., Lucas, J. R., Randles, C. I., Smith, E. E., and Brant, R, A. 1963. Acid mine drainage research potentialities. Water Environment Federation. 35(3), 275-296.

51. Hardyanto, W., and Merkel, B. 2007. Introducing probability and uncertainty in groundwater modeling with FEMWATER-LHS. Journal of Hydrology, 332, 206-213.

52. Hariprasad, K. S., Mohan Kumar, M. S., and Sekhar, M. 2001. Modeling flow through unsaturated zones: Sensitivity to unsaturated soil properties. Sadhana, 26(6), 517–528.

53. Hatfield, K., Burris, D. R., and Wolfe, N. L. 1996. Analytical model for heterogeneous reactions in mixed porous media. Journal of Environmental Engineering, 122, 676-684.

54. Hoffert, J. R. 1947. Acid mine drainage. Industrial and Engeering Chemistry, 39(5), 642-646.

55. Hou, L., Hu, B. X., Qi, Z., and Yang, H. 2018. Evaluating equilibrium and non-equilibrium transport of ammonium in a loam soil column. Hydrological Processes, 32, 80-92.

56. Jacobs, J. A., Lehr, J. H., and Testa, S. M. 2014. Acid mine drainage, rock drainage, and acid sulfate soils: causes, assessment, prediction, prevention, and remediation. John Wiley and Sons, pp 254.

57. Jarvis, N. J. 2007. A review of non-equilibrium water flow and solute transport in soil macropores: principles, controlling factors and consequences for water quality. European Journal of Soil Science, 58(3), 523–546.

58. Jamal, A., Dhar, B. B., and Ratan, S. 1991. Acid mine drainage control in an opencast coal mine. Mine Water and the Environment, 10, 1-16.

59. Johnson, D. B. and Hallberg, K. B. 2005. Acid mine drainage remediation options: a review. Science of the Total Environment, 338, 3-14.

60. Kartha, S. A., and Srivastava, R. 2008. Effect of immobile water content on contaminant transport in unsaturated zone. Journal of Hydro-environment Research, 1, 206-215.

61. Kartha, S.A., and Srivastava, R. 2012. Slow and fast transport in heap leaching of precious metals. Transport in Porous Media, 94(3), 707-727.

62. Karthikeyan, M., Tan, T. S., Phoon, K. K., 2001. Numerical oscillation in seepage analysis of unsaturated soils. Canadian Geotechnical Journal, 38, 639–651.

63. Khan, A. 2014. Ion exchange- A treatment option for acid mine drainage. Master thesis, Norwegian university of Science and Technology.

64. Kim, S., and Corapcioglu, M. Y. 2002. Contaminant transport in dual-porosity media with dissolved organic matter and bacteria present as mobile colloids. Journal of Contaminant Hydrology, 59, 267-289.

65. Kim, S., Lee, H., and Park, J. 2012. Simulation of seawater intrusion range in coastal aquifer using FEMWATER model for disaster information. Marine Georesources and Geotechnology, 30, 210-221.

66. Kruse, N. A. S., Younger, P. L., and Kutija, V. 2006. Computational methods for acid mine drainage management: Simulation of hydrogeochemical processes in abandoned underground coal mines. Journal American Society of Mining and Reclamation. 10.21000/JASMR06020966.

67. Kumari, S., Udayabhanu, G., and Prasad, B. 2010. Studies on environmental impact of acid mine drainage generation and its treatment: An appraisal. International Journal of Environmental Protection, 30(11), 953-967.

68. Kumar, C. P. 2012. Numerical model parameters for simulation of contaminant transport. International Journal of Scientific Research and Reviews, 1(3), 45-63.

69. Lafleur, D. W., and Raven, K. G. 1990. Calibration and validation of FEMWATER/FEMWASTE. Project No. 5.121.1, Atomic Energy Control Board, Ottawa, Ontario, 1-136.

70. Lei, L., Song, C., Xie, X., Li, Y., and Wang, F. 2010. Acid mine drainage and heavy metal contamination in groundwater of metal sulfide mine at arid territory (BS mine, Western Australia). Transaction of Nonferrous Metals Society of China, 20(8), 1488-1493.

71. Leij, F. J., and Bradford, S. A. 2009. Combined physical and chemical nonequilibrium transport model: analytical solution, moments and application to colloids. Journal of Contaminant Hydrology, 110, 87-99.

72. Lofts, S., Tipping, E., and Hamilton-Taylor, J. 2008. The chemical speciation of Fe (III) in freshwaters. Aquatic Geochemistry, 14(4), 337-358.

73. Lin, H. J., Deliman, P., and Martin, W. D. 1995. FEMWATER usability for the EPA master and wellhead protection research programs. United States Environmental Protection Agency, technical report HL-95-5, 1-87.

74. Marcus, J. J., 1997. Mining environmental handbook. Effects of mining on the environment and American environmental controls on mining. Imperial College Press, ISBN 1-86094-029-3.

75. Mayer, K. U., Benner, S. G., and Blowes, D. W. 1999. The reactive transport model MIN3P: Application to acid mine drainage generation and treatment-Nickel Rim mine site, In Proc.: Sudbury'99, Conference on Mining and the Environment, Subdry, Ontario, Canada.

76. Mcnab Jr, W. W. 1997. Simulation of reactive geochemical transport in groundwater using a semi-analytical screening model. Computers and Geosciences, 23(8), 869-882.

77. Merkal, B. J., and Planer-Friedrich, B. 2008. Groundwater Geochemistry: A practical guide to modeling of natural and contaminated aquatic systems, Springer-Verlag Berlin Heidelberg.

78. Moeng, K. 2018. Community perceptions on the health risks of acid mine drainage: the environmental justice struggles of communities near mining fields. Environment, Development and Sustainability, 1–22.

79. Mohanasundaram, S., Suresh Kumar, G., and Narasimhan, B. 2013. Numerical modeling of fluid flow through unsaturated zone using a dual porosity approach. ISH Journal of Hydraulic Engineering, 19(2), 97-110.

80. Molson, J., Aubertin, M., Bussiere, B., and Benzaazoua, M. 2008. Geochemical transport modelling of drainage from experimental mine tailings cells covered by capillary barriers, Applied Geochemistry, 23(1), 1-24.

81. Molson, J., Aubertin, M., and Bussiere, B. 2012. Reactive transport modeling of acid mine drainage within discretely fractured porous media: plume evolution from a surface source zone. Environmental Modeling and Software, 38, 259-270.

82. Molson, J. W., Fala, O., Aubertin, M., and Bussiere, B. 2005. Numerical simulations of pyrite oxidation and acid mine drainage in unsaturated waste rock piles. Journal of Contaminant Hydrology, 78, 343-371.

83. Narasimhan, T. N., White, A. F., and Tokunaga, T. 1986. Groundwater contamination from an inactive uranium mill tailings pile 2. Application of a dynamic mixing model. Water Resources Research, 22(13), 1820-1834.

84. Nengovhela, N. R., Strydom, C. A., Maree, J. P., and Greben, H. A. 2004. Chemical and biological oxidation of iron in acid mine water. Mine Water and the Environment, 23(2), 76-80.

85. Noosai, N., Vijayan, V., and Kengskool, K. 2014. Model application for acid mine drainage treatment processes. International Journal of Energy and Environment, 5(6), 693-700.

86. Nordstrom, D. K. 1982. Aqueous pyrite oxidation and the consequent formation of secondary iron minerals. Soil Science Society of America, 10, 37-56.

87. Palihakkara, C. R., Dassanayake, S., Jayawardena, C., and Senanayake, I. P. 2018. Floating wetland treatment of acid mine drainage using Eichhornia crassipes (water Hyacinth). Journal of Health and Pollution, 8(17), 14-18.

88. Pang, L., and Close, M. E. 1999. Non-equilibrium transport of Cd in alluvial gravels. Journal of Contaminant Hydrology, 36(1-2), 185-206.

89. Pang, L., Close, M., and Noonan, M. 1998. Rhodamine WT and bacillus subtilis transport through an alluvial gravel aquifer. Groundwater, 36(1), 112-122.

90. Paul, H., Larry, D. R., David, L. C., and Edward, M. E. 1971. Kinetics of hydrolysis of ferric ion in dilute aqueous solution. The Journal of Physical Chemistry, 75(7), 929-932.

91. Rao, P. S. C., Rolston, D. E., Jessup, R. E., and Davidson, J. M. 1980. Transport in aggregated porous media: Theoretical and experimental evaluation. Soil Science Society of America Journal, 44, 1139-1146.

92. Rawat, S. N., and Singh, G. 1982. Occurrence of acid mine drainage in northeastern coal mines in India. Symposium on surface mining hydrology, sedimentology and reclamation, University of Kentucky, Lexington, Kentucky, December 5 – 10.

93. Rawat, S. N., and Singh, G. 1982. The role of micro-organisms in the formation of acid mine drainage in the north eastern coal field of India. International Journal of Mine Water, (2), 29-36.

94. Rose, A. L., and Waite, T. D. 2003. Kinetics of hydrolysis and precipitation of ferric iron in seawater. Environmental Science and Technology, 37(17), 3897-3903.

95. Ross, P. J., and Smettem, R. J. 2000. A simple treatment of physical non-equilibrium water flow in soils. Soil Science Society of America Journal, 64, 1926-1930.

96. Rubin, J., and James, R. V. 1973. Dispersion-affected transport of reacting solutes in saturated porous media: Galerkin method applied to equilibrium-controlled exchange in unidirectional steady water flow. Water Resources Research, 9(5), 1332-1356.

97. Runchal, A. K., and Sagar, B. 1991. PORFLOW: A model for fluid flow, heat, and mass transport in multifluid, multiphase fractured or porous media: User's manual version: 2.39, Analytic and Computation Research, Inc, LOSAngeles, CA.

98. Sahoo, P. K., Tripathy, S., Equeenuddin, Sk.Md., and Panigrahi, M. K. 2012. Geochemical characteristics of coal mine discharge vis-à-vis behavior of rare earth elements at Jaintia Hills coalfield, northeastern India. Journal of Geochemical Exploration, 112, 235-243.

99. Salomons, W., and Forstner, U. 1988. Environmental Management of Solid Waste Dredged Material and Mine Tailings, 24-43.

100. Schoen, R., Gaudet, J. P., and Bariac, T. 1999. Preferential flow and solute transport in a large lysimeter, under controlled boundary conditions. Journal of Hydrology, 215(1-4), 70-81.

101. Selim, H.M., Schulin, R., and Fluhler, H. 1987. Transport of ion exchange of calcium and magnesium in an aggregated soil. Soil Science Society of America Journal, 51, 876-884.

102. Simunek, J., Jarvis, N. J., van Genuchten, M. Th., and Gärdenäs, A. 2003. Review and comparison of models for describing non-equilibrium and preferential flow and transport in the vadose zone. Journal of Hydrology, 272(1-4), 14-35.

103. Simunek, J., and van Genuchten, M. Th. 2008. Modeling non-equilibrium flow and transport processes using HYDRUS. Vadose Zone Journal, 7, 782-797.

104. Simunek, J., Wendroth, O., Wypler, N., and van Genuchten, M. T. 2001. Non-equilibrium water flow characterized by means of upward infiltration experiments. European Journal of Soil Science, 52, 13-24.

105. Singh, G. 1987. Mine water quality deterioration due to acid mine drainage. International Journal of Mine Water, 6(1), 49-61.

106. Singh, G. 2008. Chemical, microbiological and ecological aspects of Acid mine drainage and its control aspects. Chapter 9 of Environmental science and technology in India, Daya Publishing House, 63-81.

107. Singh, G., and Bhatnagar, M. 1988. Inhibition of bacterial activity in acid mine drainage. International Journal of Mine Water, 7(4), 13-26.

108. Singh, G., and Rawat, N. S. 1985. Removal of trace elements from acid mine drainage. International Journal of Mine Water, 4(1), 17-23.

109. Skauge, A., Pourmohammadi, S., Vik, B., and Spildo, K. 2006. Dispersion measurements used in special core analysis of carbonates. International Symposium of the Society of Core Analysts, Trondheim, Norway 12-16 September.

110. Stefansson, A. 2007. Iron (III) hydrolysis and solubility at 25^0C. Environmental Science and Technology, 41(17), 6117-6123.

111. Stumm, W., and Morgan, J. J. 1996. Aquatic chemistry: Chemical equilibria and rates in natural waters, 3rd edition, John Wiley & Sons, Inc.

112. Sudicky, E. A., Cherry, J. A., and Frind, E. O. 1983. Migration of contaminants in groundwater at a landfill: A case study: 4. A natural-gradient dispersion test. Journal of Hydrology, 63(1-2), 81-108.

113. U.S. Environmental Protection Agency (USEPA), 1994. Technical Document: Acid Mine Drainage Prediction. EPA Publication Number: 530-R-94-036.

114. Valocchi, A. J. 1984. Describing the Transport of Ion-Exchanging Contaminants Using an Effective K_d Approach. Water Resources Research, 20 (4), 499-503.

115. van Genuchten, M.Th. 1980. A closed form equation for predicting the hydraulic conductivity of unsaturated soils. Soil Science Society of America Journal, 44, 892-898.

116. van Genuchten, M. Th. 1982. A comparison of numerical solutions one-dimensional unsaturated- saturated flow and mass transport equations. Advances in Water Resources, 5(1), 47-55.

117. van Genuchten, M. Th., and Jirka Simunek, 2004. Integrated modeling of vadose-zone flow and transport processes. Volume 6, Unsaturated-zone Modeling: Progress, Challenges and Applications.

118. van Genuchten, M.Th., and Wierenga, P.J. 1976. Mass transfer studies in sorbing porous media: I Analytical solutions. Soil Science Society of America Journal, 40, 473-480.

119. van Genuchten, M.Th., and Wierenga, P.J. 1977. Mass transfer studies in sorbing porous media: II Experimental evaluation with tritium (^3H_2O). Soil Science Society of America Journal, 41, 272-278.

120. Vauclin, M., Khanji, D. and Vachaud, G. 1979. Experimental and numerical study of a transient, two-dimensional unsaturated-saturated water table recharge problem. Water Resour. Res., 15(5): 1089-1101.

121. Vereecan, H. 1995.The effect of soil heterogeneity and hysteresis on solute transport: a numerical experiment. Ecological Modeling 77, 273-288.

122. Vereecken, H., and Nitzsche, O. 2002. Modeling sorption and exchange processes in column experiments and large scale field studies. Mine Water and the Environment, 21, 15-23.

123. Vyawahre, A., and Rai, S. 2016. Acid Mine Drainage: A case study of an Indian coal mine. International Journal of Scientific Research in Science, Engineering and Technology, 2(2), 1297-1301.

124. Walter, A. L., Frind, E. O., Blowes, D. W., Ptacek, C. J., and Molson, J. W. 1994. Modeling of multicomponent reactive transport in groundwater 2. Metal mobility in aquifers impacted by acidic mine tailings discharge. Water Resources Research, 30, 3149-3158.

125. Wang, L. K., Chen, J. P., Hung, Y., and Shammas, N. K., 2009. Heavy metals in the Environment, CRC press, 27-33.

126. Webb, J. A., and Sasowsky, I. D. 1994. The interaction of acid mine drainage with a carbonate terrane: evidence from the Obey River, north-central Tennesse. Journal of Hydrology. Volume 161, Issues 1-4, Pages 327-346.

127. Wierenga, P.J., and Van Genuchten, M.Th. 1989. Solute transport through small and large unsaturated soil columns. 27(1), 35-42.

128. Williamson, M. A., Kirby, C. S., and Rimstidt, J. D. 2006. Iron dynamics in Acid Mine Drainage. Journal American Society of Mining and Reclamation, 2411-2423.

129. Worch, E. 2003. Modeling the solute under non-equilibrium conditions on the basis of mass transfer equations. Journal of Contaminant Hydrology, 68(1-2), 97-120.

130. Wunderly, M. D., Blowes, D. W., Frind, E. O., Ptacek, C. J., and Al, T. A. 1995. A multicomponent reactive transport model incorporating kinetically controlled pyrite oxidation. Conference on Mining and the Environment, Sudbury, Ontario, May 28th-June 1st.

131. Xu, T., White, S. P., Pruess, K., and Brimhall, G. H. 2000. Modeling of pyrite oxidation in saturated and unsaturated subsurface flow systems. Transport in Porous Media, 39, 25-56.

132. Yeh, G.T. 2000. Computational subsurface hydrology Reactions, Transport and Fate, Kulwer Academic Publishers.

133. Yeh, G.T. 2008. Numerical Modeling of Coupled Fluid Flow and Thermal and Reactive Biogeochemical Transport in Porous and Fractured Media. Computational Geosciences, 14(1), 149-170.

134. Yeh, G. T., Fang, Y., Zhang, F., Sun, J., Li, Y., Li, M. H., and Siegel, M. D. 2010. Numerical modeling of coupled fluid flow and thermal and reactive biogeochemical transport in porous and fractured media. Computational Geosciences, 14(1), 149-170.

135. Yeh, G. T., Sharp-Hansen, S., Lester, B., Strobl, R., and Scarbrough, J. 1992. 3DFEMWATER/3DLEWASTE: numerical codes for delineating wellhead protection areas in agricultural regions based on the assimilative capacity criterion. U.S. Environmental Protection Agency, Washington, D.C., EPA/600/R-92/223. (https://www.epa.gov/ceam/3dfemwater3dlewaste)

136. Yeh, G.T., Sun, J., Philip, M.J., William, D.B., Ming-Hsu, L., Malcom, D.S. and Yilin, F. 2004. HYDROGEOCHEM 5.0: A three-dimensional model of coupled fluid flow, thermal transport, and hydrogeochemical transport through variably saturated conditions: Version 5.0.

137. Yeh, G. T., and Huff, D. D. 1983. FEWA: A finite element model of water flow through aquifers. ORNL-5976. Oak Ridge National Laboratory, Oak Ridge, Tennessee, 1-113.

138. Yeh, G. T., and Huff, D. D. 1985. FEMA: A finite element model of material transport through aquifers. ORNL-6063. Oak Ridge National Laboratory, Oak Ridge, Tennessee, 1-88.

139. Yeh, G. T., and Ward, D. S. 1981. FEMWASTE: A Finite-Element Model of waste transport through saturated- unsaturated porous media. ORNL-5601. Oak Ridge National Laboratory, Oak Ridge, Tennessee, 1-66.

140. Younger, P. L., and Wolkersdorfer, C. 2004. Mining impacts on the fresh water environment: Technical and managerial guidelines for catchment scale management. Mine Water and the Environment, 23, S2-S80.

141. Zheng, C., and Bennett, G. D., 2002. Applied contaminant transport modelling. Wiley Interscience publishers.

142. Zysset, A., Stauffer, F., and Dracos, T. 1994. Modelling of chemically reactive groundwater transport. Water Resources Research, 30(7), 2217-2228.

List of Publications from this Thesis Work

1. Someswaran R., Kartha S. A. (2017). "Unsaturated Physical Non-equilibrium Contaminant Transport Modeling Using Modified FEMWATER". In: Saha A., Das D., Srivastava R., Panigrahi P., Muralidhar K. (eds) Fluid Mechanics and Fluid Power – Contemporary Research. Lecture Notes in Mechanical Engineering. Springer, New Delhi, 1163-1170.

International conferences

2. Someswaran, R., and Kartha, S. A. (2017). "Analysis of Contaminant Transport in the Saturated Aquifer under the Condition of Heterogeneity and Non-equilibrium Mass Transfer". International Conference on Modeling of Environmental and Water Resources Systems, Harcourt Butler Technical University (HBTU), Kanpur, 24th –26th March 2017.
3. Someswaran, R., and Kartha, S. A. (2015). "Non-equilibrium reactive transport modeling of Acid Mine Drainage in subsurface water". 36th IAHR World Congress, The Hague, the Netherlands, 28th June – 03rd July 2015.
4. Someswaran, R. and Kartha, S. A. (2013). "Reactive Solute Transport Modeling of Acid Mine Drainage to Unconfined Groundwater Aquifers". 40th International Association of Hydrogeologists Congress (IAH 2013), Perth Convention and Exhibition Centre, Perth, Australia, 15th – 20th September 2013.

National conference

5. Someswaran, R. and Kartha, S. A. (2014). "Analysis of Effects of Heterogeneity on Transport of Acid Mine Drainage". National Conference on Water and its Sustainability in Mining and Other Environment: Vision 2050 (WSME 2014), ISM Dhanbad, 28th - 29th March 2014, 299-307.